NUMERICAL SOLUTIONS TO THE VISCOUS SHOCK-LAYER BLUNT-BODY PROBLEM WITH INERT GAS INJECTION

by

Robert E. Whitehead

Thesis submitted to the Graduate Faculty of the

Virginia Polytechnic Institute and State University

in partial fulfillment of the requirements for the degree of

DOCTOR OF PHILOSOPHY

in

Engineering Mechanics

APPROVED:

Dr. R.T. Davis, Committee Chairman

Prof. F.J. Maher

Dr. D.T. Mook

Dr. J.E. Kaiser

Dr. F.R. DeJarnette

Dr. D. Frederick, Department Head

Date

August, 1970

Blacksburg, Virginia

ACKNOWLEDGEMENTS

The author wishes to express his sincere gratitude to his committee chairman, Dr. R.T. Davis, whose patience and guidance made this thesis possible. The author also thanks the remainder of his committee, Prof. F.J. Maher, Dr. D.T. Mook, Dr. J.E. Kaiser, and Dr. F.R. DeJarnette, for their assistance and criticism of this work. Appreciation also goes to Dr. C.H. Lewis whose willing assistance in obtaining information on the problem was very valuable. Finally, thanks are due to Sandia Corporation who sponsored the project under which this research was carried out.

TABLE OF CONTENTS

LIST OF TABLES AND FIGURES

NOMENCLATURE

a^*	Body nose radius of curvature.
a_i, a_{ij}, a_{ijk}	Coefficients in G function defined by equation (3.17).
c_i	Mass concentration of i^{th} species, $\frac{\rho}{\bar{\rho}}$.
$(c_p)_i$	Constant pressure specific heat of i^{th} species, $\frac{(c^*_p)_i}{c^*_{p\infty}}$.
$\bar{c}_p$	Constant pressure specific heat of mixture, $\sum c_i (c_p)_i$.
c_f	Skin friction coefficient, $2\tau^*_w/\rho^*_\infty U^{*2}_\infty$, defined by equation (2.21).
D_{IA}	Binary diffusion coefficient, $D^*_{IA}/U^*_\infty a^*$.
F_o	Maxwellian velocity distribution function defined by equation (3.6).
F_G	Perturbed velocity distribution function defined by equation (3.1).
G	Function of molecular velocities defined by equation (3.8b).
h	Static enthalpy, h^*/U^{*2}_∞.
H	Total enthalpy, H^*/U^{*2}_∞.
$\bar{H}$	Shock normalized total enthalpy defined by equation (2.11h).
j_i	Concentration diffusion flux component normal to body surface defined by equation (2.5).

K	Thermal conductivity, $K^*/\mu^*(U_\infty^{*2}/c_{p\infty}^*)c_{p\infty}^*$.
$\bar{K}$	Shock normalized thermal conductivity defined by equation (2.11ℓ).
$\dot{m}$	Injectant mass flow rate/unit area defined by equation (6.1).
$\dot{M}$	Total injectant mass flow rate defined by equation (6.2).
M_i	Molecular weight of i^{th} species.
$\bar{M}$	Molecular weight of mixture defined by equation (2.10).
n	Coordinate measured normal to body, n^*/a^*, see Figure 1.
N	Number density of gas molecules, number of molecules/volume.
P	Pressure, $P^*/\rho_\infty^* U_\infty^{*2}$.
$\bar{P}$	Shock normalized pressure defined by equation (2.11e).
q_w	Heat transfer at body surface, $q_w^*/\rho_\infty^* U_\infty^{*3}$, defined by equation (2.22).
Q_1, Q_2, Q_3	Transformed molecular velocities defined by equation (3.4).
r	Radius measured from the axis of symmetry to a point on the body surface, r^*/a^*, see Figure 1.
R	Universal gas constant.
$\bar{R}$	Gas constant, $R/\bar{M}$.
Re	Reynolds number, $\frac{\rho^* u^* a^*}{\mu^*}$.
s	Coordinate measured along body surface, s^*/a^*, see Figure 1.
T_∞^*	Free stream temperature.
T	Temperature, $T^*/(U_\infty^{*2}/c_{p\infty}^*)$.

$\bar{t}$	Shock normalized temperature defined by equation (2.11g).
U_∞^*	Free stream velocity.
U^*	Molecular velocity relative to macroscopic velocity in s-direction.
u	Velocity component in s-direction, u^*/U_∞^*.
$\bar{u}$	Shock normalized velocity component defined by equation (2.11c).
V^*	Molecular velocity relative to macroscopic velocity in n-direction.
v	Velocity component in n-direction, v^*/U_∞^*.
$\bar{v}$	Shock normalized velocity component defined by equation (2.11d).
W^*	Molecular velocity normal to s-n plane.
α	Shock angle, see Figure 1.
α_t	Thermal accommodation coefficient, taken to be 1.
$\alpha_1,\alpha_2,\alpha_3,\alpha_4$	Coefficients in equation (2.12).
β	Angle defined in Figure 1.
γ	Ratio of specific heats.
δ	Injection coefficient defined as the ratio of the injection area to the total surface area.
ϵ	Perturbation parameter, $[\mu^*(\frac{U_\infty^{*2}}{c_{p\infty}^*})/\rho_\infty^* U_\infty^* a^*]^{1/2}$.
η	Shock normalized coordinate normal to body defined by equation (2.11a).
θ	Fraction of incident molecules diffusely reflected from body.

κ Body surface curvature, $\kappa^* a^*$, see Figure 1.

μ Coefficient of viscosity, $\mu^*/\mu^*(U_\infty^{*2}/c_{p\infty}^*)$.

$\bar{\mu}$ Shock normalized viscosity defined by equation (2.11k).

ξ Coordinate tangent to body surface defined by equation (2.11b).

ρ_∞^* Free stream density.

ρ Density, ρ^*/ρ_∞^*.

$\bar{\rho}$ Shock normalized density defined by equation (2.11f).

ϕ Body angle defined in Figure 1.

Subscripts

A Refers to air species.

I Refers to injected species.

i i^{th} species.

n $\frac{\partial}{\partial n}$.

sh Value behind shock.

s.p. Stagnation point.

s $\frac{\partial}{\partial s}$.

w Wall values.

η $\frac{\partial}{\partial \eta}$.

ξ $\frac{\partial}{\partial \xi}$.

∞ Free stream conditions.

Superscripts

-	Shock normalized values.
*	Dimensional quantities.

I. INTRODUCTION AND REVIEW OF THE LITERATURE

Mass transfer across a body surface in hypersonic flow has attracted considerable interest because of the resulting reduction in heat transfer and wall shear stress. This mass transfer may arise by injection or ablation which may be simulated by injection. Most theoretical studies of the problem have centered around solutions to the laminar boundary-layer equations with mass transfer across the body surface. Both air into air and foreign gas injection studies have been made.

Jaffe, Lind, and Smith (1967) numerically investigated solutions to the laminar boundary-layer equations with the discontinuous injection of helium, air, argon, and carbon dioxide into equilibrium air for flow past slender cones at hypersonic conditions. Moore and Lee (1967) investigated discontinuous injection of helium, argon, and xenon into the laminar boundary layer along the surface of a sharp cone. They viewed air as a reacting seven-component gas mixture in chemical non-equilibrium. Inger and Sayano (1969) did an approximate boundary-layer solution using the Kármán-Pohlhausen integral method for both continuous and discontinuous injection of air into air along a hemispherically blunted cone. They approximately accounted for the interaction of the blown boundary layer with the inviscid stream, which was not done by Moore and Lee (1967). Lewis, Adams, and Gilley (1968) numerically solved the laminar boundary-layer equations with injections of helium and argon into air for a spherically blunted cone

and interacted the boundary-layer solution with an inviscid blunt-body solution using an iteration scheme. Numerous other authors (see Chen, Aroesty, and Mobley (1967), for example) have done theoretical calculations for stagnation-region solutions with mass transfer.

The experimental data available for the conditions discussed above is meager. Pappas and Lee (1969) experimentally investigated the problem that was investigated theoretically by Lewis, Adams, and Gilley (1968) and compared with their results.

Davis (1970a) has developed a method for solving a set of laminar, hypersonic, viscous shock-layer equations for a chemically-reacting binary mixture and applied the method to the problem of hypersonic flow of oxygen atoms and molecules past a blunt body. The method is essentially the same as that developed by Davis (1970b) for the hypersonic blunt-body problem for a one-component gas. The equations solved by Davis (1970a,b) are valid to second order in the inverse square root of a Reynolds number throughout the entire shock-layer. Thus he is able to find solutions for the entire shock layer by solving only one set of equations.

The idea of using the method developed by Davis (1970a) to study the mass transfer problem is appealing for several reasons. First, solutions may be found for Reynolds numbers lower than those for which boundary-layer theory is valid. Also, by finding solutions for the entire shock layer, the necessity of having to determine the effect of the blown boundary layer on the inviscid flow is eliminated since this effect is included as part of the viscous shock-layer solution.

The aim of the work done here, therefore, is to study the effect of inert-gas injection on the heat transfer and wall shear stress for a blunt body in hypersonic flow by solving a set of viscous shock-layer equations by a method similar to that developed by Davis (1970a). A set of equations for a binary mixture valid in the entire shock layer to second order in the inverse square root of a Reynolds number is found. These equations are similar to those given by Davis (1970a) except that they are for a non-reacting binary mixture and allow for mass transfer at the body surface. A set of "slip-flow" boundary conditions which take into account mass transfer at the body surface is derived and used in the solution to the problem.

A study is made of the effect of mass injection on the heat transfer and wall shear stress under re-entry conditions. Solutions are found for conditions at altitudes from 300,000 ft. to 100,000 ft at a free-stream velocity of 20,000 fps. In all cases the body geometry is a hyperboloid asymptotic to a cone of total interior angle of 45°. Solutions are found for the injection of argon, helium, and air into air. Both "equilibrium" and "frozen" air models are used for the air species and solutions are found for each case. A mass injection rate that decays exponentially from the stagnation point is used and different total mass transfer rates are used. Comparisons are made for different injection rates, different injectants, and for cases for both equilibrium and frozen air models.

II. FORMULATION OF THE GOVERNING EQUATIONS

The full conservation equations for non-equilibrium flows of mixtures are presented by Bird, Stewart, and Lightfoot (1966). Davis (1970a) has formulated the laminar hypersonic viscous shock-layer equations for axisymmetric non-equilibrium flows of mixtures from these equations. These shock-layer equations are formulated in exactly the same manner as the viscous shock-layer equations for a one-component gas presented by Davis (1970b). In order to derive the viscous shock-layer equations, the equations given by Bird, Stewart, and Lightfoot (1966) are written in a boundary-layer coordinate system, Figure 1, and non-dimensionalized by variables which are of order one in the boundary layer. The same set of equations is written in variables of order one in the inviscid region outside the boundary layer. Terms are kept in each set of equations up to second order in the inverse square root of a Reynolds number. The two sets of equations are combined in such a way that one set of equations valid to second order in the entire shock layer is found. It is found that the continuity and momentum equations for a mixture are the same as the equations for a one-component gas. There are additional terms in the energy equation for a mixture and a conservation-of-species equation not found for a one-component gas is required for the mixture.

The equations presented below are very similar to those formulated by Davis (1970a) except that the chemical production terms have been omitted and the energy equation is presented in terms of both

temperature and total enthalpy. Also, mass transfer is permitted at the body surface when the continuity equation is integrated. The equations are non-dimensionalized as noted in the nomenclature. The appropriate equations, therefore, for hypersonic axisymmetric flows of mixtures valid to second order in the inverse square root of a Reynolds number without chemical reactions but allowing concentration diffusion are:

Continuity Equation

$$[(r + n\cos\phi)\rho u]_s + [(1 + \kappa n)(r + n\cos\phi)\rho v]_n = 0, \qquad (2.1)$$

s-Momentum Equation

$$\rho\left[u\frac{u_s}{1 + \kappa n} + vu_n + \frac{\kappa}{1 + \kappa n}uv\right] + \frac{P_s}{1 + \kappa n} =$$

$$\frac{\varepsilon^2}{(1 + \kappa n)^2(r + n\cos\phi)}[(1 + \kappa n)^2(r + n\cos\phi)\tau]_n , \qquad (2.2a)$$

where

$$\tau = \mu\left(u_n - \frac{\kappa u}{1 + \kappa n}\right) , \qquad (2.2b)$$

n-Momentum Equation

$$\rho\left[u\frac{v_s}{1 + \kappa n} + vv_n - \frac{\kappa}{1 + \kappa n}u^2\right] + P_n = 0 , \qquad (2.3a)$$

which becomes if the thin shock-layer approximation is made,

$$P_n = \frac{\kappa}{1 + \kappa n} \rho u^2 , \tag{2.3b}$$

Energy Equation

$$\rho \bar{c}_p \left(u \frac{T_s}{1 + \kappa n} + v T_n\right) - \left(u \frac{P_s}{1 + \kappa n} + v P_n\right) =$$

$$\frac{\varepsilon^2}{(1 + \kappa n)(r + n \cos\phi)} \left[(1 + \kappa n)(r + n \cos\phi) K T_n\right]_n + \frac{\varepsilon^2}{\mu} \tau^2$$

$$-\Sigma c_{p_i} j_i T_n , \tag{2.4}$$

where for a multi-component mixture, j_i is given by Bird, Stewart, and Lightfoot (1966). For a binary mixture the concentration diffusion flux reduces to the following:

$$j_i = -\rho D_{IA} (c_i)_n , \tag{2.5}$$

where the subscript I denotes the injected gas and A specifies the air species.

The energy equation written in terms of total enthalpy becomes,

$$\frac{\rho u}{1+\kappa n} H_s + \rho v H_n =$$

$$\frac{\varepsilon^2}{(1+\kappa n)(r+n\cos\phi)} \left[(1+\kappa n)(r+n\cos\phi)\frac{K}{\bar{c}_p}(H_n - uu_n - vv_n - \sum h_i (c_i)_n)\right]_n$$

$$+ \frac{\varepsilon^2}{(1+\kappa n)(r+n\cos\phi)} \left[(1+\kappa n)(r+n\cos\phi)\, u\tau\right]_n - \sum (h_i)_n j_i$$

$$- \sum \frac{h_i}{(1+\kappa n)(r+n\cos\phi)} \left[(1+\kappa n)(r+n\cos\phi) j_i\right]_n, \qquad (2.6)$$

Species Equation

$$\frac{\rho u}{1+\kappa n} (c_i)_s + \rho v (c_i)_n = -(j_i)_n - \left(\frac{\kappa}{1+\kappa n} + \frac{\cos\phi}{r+n\cos\phi}\right) j_i . \qquad (2.7)$$

The number of independent equations specified by the species equation (2.7) is one less than the number of species. Therefore, an additional relation between the species is required. This relation is,

$$\sum c_i = 1 . \qquad (2.8)$$

Assuming that the fluid is a mixture of perfect gases and using the law of partial pressures, the equation of state is as follows:

$$p = \frac{\rho R T}{\bar{M} c_p^*} , \qquad (2.9)$$

where

$$\bar{M} = \frac{1}{\sum c_i / M_i} . \qquad (2.10)$$

The above equations are parabolic in nature if the thin shock-layer form of the n-momentum equation (2.3b) is used and are very similar to the compressible boundary-layer equations for flows of mixtures (see Hayes and Probstein (1959) or Fay and Riddell (1958) for example). These equations can be solved readily by an implicit finite-difference scheme developed by Davis (1970b) that is similar to the method developed by Blottner and Flügge-Lotz (1963) for solving the compressible boundary-layer equations.

It is both convenient and helpful in the numerical computations to normalize the independent and dependent variables with their local values at the shock. This permits the taking of a constant number of increments in the independent normal variable in the finite-difference grid between the body and the shock. It also eliminates the need to add grid points in the normal direction as the computation proceeds downstream from the stagnation point. The continuity equation in these transformed variables can be used to determine the shock position directly in the finite-difference solution.

The transformed independent and dependent variables are:

$$\eta = \frac{n}{n_{sh}} , \tag{2.11a}$$

$$\xi = s , \tag{2.11b}$$

$$\bar{u} = \frac{u}{u_{sh}} , \tag{2.11c}$$

$$\bar{v} = \frac{v}{v_{sh}} , \tag{2.11d}$$

$$\bar{p} = \frac{p}{p_{sh}} , \tag{2.11e}$$

$$\bar{\rho} = \frac{\rho}{\rho_{sh}} , \tag{2.11f}$$

$$\bar{t} = \frac{T}{T_{sh}} , \tag{2.11g}$$

$$\bar{H} = \frac{H}{H_{sh}} , \tag{2.11h}$$

$$\bar{\mu} = \frac{\mu}{\mu_{sh}} , \tag{2.11k}$$

and

$$\bar{K} = \frac{K}{K_{sh}} . \tag{2.11ℓ}$$

The necessary transformations for the differential quantities are:

$$\frac{\partial}{\partial s} = \frac{\partial}{\partial \xi} - \frac{n'_{sh}}{n_{sh}} \frac{\partial}{\partial \eta} , \tag{2.11m}$$

$$\frac{\partial}{\partial n} = \frac{1}{n_{sh}} \frac{\partial}{\partial \eta} , \tag{2.11n}$$

and

$$\frac{\partial^2}{\partial n^2} = \frac{1}{n_{sh}^2} \frac{\partial^2}{\partial \eta^2} , \tag{2.11p}$$

where

$$n'_{sh} = \frac{dn_{sh}}{d\xi} . \tag{2.11q}$$

Transforming the species, s-momentum, and energy equations in terms of the new variables results in equations that can be put into the following standard form for a parabolic partial differential equation:

$$\frac{\partial^2 w}{\partial \eta^2} + \alpha_1 \frac{\partial w}{\partial \eta} + \alpha_2 w + \alpha_3 + \alpha_4 \frac{\partial w}{\partial \xi} = 0 \ , \tag{2.12}$$

where w equals c_i in the species equation, $\bar{u}$ in the s-momentum equation, and $\bar{t}$ or $\bar{H}$ in the energy equation. Using equations (2.5) and (2.8) and reducing the governing equations to the case of a binary mixture, the coefficients in these equations are as follows:

s-Momentum Equation

$$\alpha_1 = \frac{\rho_{sh}\, u_{sh}\, n'_{sh}}{\varepsilon^2\, \mu_{sh}} \frac{n_{sh}}{1 + \kappa n_{sh}\, \eta} \frac{\bar{\bar{\rho}}\bar{u}\eta}{\bar{\mu}} - \frac{\rho_{sh}\, v_{sh}\, n_{sh}}{\varepsilon^2\, \mu_{sh}} \frac{\bar{\bar{\rho}}\bar{v}}{\bar{\mu}} + \frac{\bar{\mu}_\eta}{\bar{\mu}} + \frac{\kappa n_{sh}}{1 + \kappa n_{sh}\, \eta}$$

$$+ \frac{\cos\phi\, n_{sh}}{r + n_{sh}\, \eta \cos\phi} \ , \tag{2.13a}$$

$$\alpha_2 = - \frac{\rho_{sh}\, u'_{sh}\, n_{sh}}{\varepsilon^2\, \mu_{sh}} \frac{n_{sh}}{1 + \kappa n_{sh}\, \eta} \frac{\bar{\bar{\rho}}\bar{u}}{\bar{\mu}} - \frac{\rho_{sh}\, v_{sh}\, n_{sh}}{\varepsilon^2\, \mu_{sh}} \frac{\kappa n_{sh}}{1 + \kappa n_{sh}\, \eta} \frac{\bar{\bar{\rho}}\bar{v}}{\bar{\mu}}$$

$$- \frac{\kappa n_{sh}}{1 + \kappa n_{sh}\, \eta} \frac{\bar{\mu}_\eta}{\bar{\mu}} - \left(\frac{\kappa n_{sh}}{1 + \kappa n_{sh}\, \eta} + \frac{\cos\phi\, n_{sh}}{r + n_{sh} \cos\phi}\right) \frac{\kappa n_{sh}}{1 + \kappa n_{sh}\, \eta} \ , \tag{2.13b}$$

$$\alpha_3 = - \frac{P_{sh}\, n_{sh}}{\varepsilon^2 \mu_{sh}} \frac{n_{sh}}{1 + \kappa n_{sh}\, \eta} \frac{1}{\bar{\mu} u_{sh}} \left(\bar{P}_\xi - \frac{n'_{sh}}{n_{sh}} \eta \bar{P}_\eta + \frac{P'_{sh}}{P_{sh}} \bar{P}\right), \tag{2.13c}$$

and

$$\alpha_4 = - \frac{\rho_{sh}\, u_{sh}\, n_{sh}}{\varepsilon^2\, \mu_{sh}} \frac{n_{sh}}{1 + \kappa n_{sh}\, \eta} \frac{\bar{\bar{\rho}}\bar{\bar{u}}}{\bar{\mu}} ; \tag{2.13d}$$

Energy Equation

in terms of temperature,

$$\alpha_1 = \frac{\kappa n_{sh}}{1 + \kappa n_{sh}\, \eta} + \frac{n_{sh} \cos \phi}{r + n_{sh}\, \eta \cos \phi} + \frac{\bar{K}_\eta}{\bar{K}} + \frac{\rho_{sh}\, u_{sh}\, \bar{c}_p}{\varepsilon^2\, K_{sh}\, \bar{K}} \frac{n_{sh}}{1 + \kappa n_{sh}\, \eta} n'_{sh} \eta \bar{\bar{\rho}}\bar{\bar{u}}$$

$$- \frac{\rho_{sh}\, v_{sh}\, n_{sh}\, \bar{c}_p}{\varepsilon^2\, K_{sh}\, \bar{K}} \bar{\bar{\rho}}\bar{\bar{v}} + \frac{\rho_{sh}\, \bar{\rho} D_{IA}}{\varepsilon^2\, K_{sh}\, \bar{K}} [(c_p)_I - (c_p)_A](c_I)_\eta , \tag{2.14a}$$

$$\alpha_2 = - \frac{\rho_{sh}\, u_{sh}\, n_{sh}\, \bar{c}_p}{\varepsilon^2\, K_{sh}\, \bar{K}} \frac{n_{sh}}{1 + \kappa n_{sh}\, \eta} \frac{T'_{sh}}{T_{sh}} \bar{\bar{\rho}}\bar{\bar{u}} , \tag{2.14b}$$

$$\alpha_3 = \frac{P_{sh}\, u_{sh}\, n_{sh}}{\varepsilon^2\, K_{sh}\, \bar{K}\, T_{sh}} \left[\frac{n_{sh}\, \bar{u}}{1 + \kappa n_{sh}\, \eta} \left(\bar{P}_\xi + \frac{P'_{sh}}{P_{sh}} \bar{P} - \frac{n'_{sh}}{n_{sh}} \eta \bar{P}_\eta\right) + \frac{v_{sh}}{u_{sh}} \bar{v}\, \bar{P}_\eta\right]$$

$$+ \frac{u_{sh}^2\, \mu_{sh}}{K_{sh}\, T_{sh}} \frac{\bar{\mu}}{\bar{K}} \left(\bar{u}_\eta - \frac{\kappa n_{sh}\, \bar{u}}{1 + \kappa n_{sh}\, \eta}\right)^2 , \tag{2.14c}$$

$$\alpha_4 = -\frac{\rho_{sh}\, u_{sh}\, n_{sh}\, \bar{c}_p}{\varepsilon^2\, K_{sh}} \frac{n_{sh}}{1 + \kappa n_{sh}\, \eta} \frac{\bar{\bar{\rho u}}}{\bar{K}} \; ; \tag{2.14d}$$

or in terms of total enthalpy,

$$\alpha_1 = \frac{n_{sh}\, \kappa}{1 + \kappa n_{sh}\, \eta} + \frac{n_{sh} \cos \phi}{r + n_{sh}\, \eta \cos \phi} + \frac{\bar{c}_p}{\bar{K}} \left(\frac{\bar{K}}{\bar{c}_p}\right)_\eta - \frac{\rho_{sh}\, v_{sh}\, n_{sh} \bar{c}_p}{\varepsilon^2\, K_{sh}} \frac{\bar{\bar{\rho v}}}{\bar{K}}$$

$$+ \frac{\rho_{sh}\, u_{sh}\, \bar{c}_p}{\varepsilon^2\, K_{sh}} \frac{n_{sh}}{1 + \kappa n_{sh}\, \eta} \frac{\bar{\bar{\rho u}}}{\bar{K}}\, n'_{sh}\eta \; , \tag{2.15a}$$

$$\alpha_2 = -\frac{\rho_{sh}\, u_{sh}\, n_{sh}\, \bar{c}_p}{\varepsilon^2\, K_{sh}} \frac{n_{sh}}{1 + \kappa n_{sh}\, \eta} \frac{H'_{sh}}{H_{sh}} \frac{\bar{\bar{\rho u}}}{\bar{K}} \; , \tag{2.15b}$$

$$\alpha_3 = \frac{\bar{c}_p\, u_{sh}^2}{H_{sh}\, K_{sh}\, \bar{K}} \left(\mu_{sh}\, \bar{\mu} - \frac{\bar{K}\, K_{sh}}{\bar{c}_p}\right) \bar{\bar{u}\bar{u}}_{\eta\eta} + \bar{\bar{u}}_\eta^2 + \left(\frac{\kappa n_{sh}}{1 + \kappa n_{sh}\, \eta}\right.$$

$$\left. + \frac{n_{sh} \cos \phi}{r + n_{sh}\, \eta \cos \phi}\right) \bar{\bar{u}\bar{u}}_\eta \Big\} + \frac{\bar{c}_p\, u_{sh}^2}{H_{sh}\, K_{sh}\, \bar{K}} \bar{\bar{u}\bar{u}}_\eta \left\{\mu_{sh}\, \bar{\mu}_\eta - K_{sh} \left(\frac{\bar{K}}{\bar{c}_p}\right)_\eta\right\}$$

$$- \frac{\bar{c}_p\, u_{sh}^2}{H_{sh}\, K_{sh}\, \bar{K}} \left[\frac{2\kappa n_{sh}\, \mu_{sh}}{1 + \kappa n_{sh}\, \eta} \bar{\bar{\mu u u}} + \frac{n_{sh}\, \kappa}{1 + \kappa n_{sh}\, \eta} \frac{n_{sh} \cos \phi}{r + n_{sh}\eta \cos \phi} \mu_{sh}\, \bar{\bar{\mu u}}^2\right.$$

$$\left. + \frac{n_{sh}\, \kappa \mu_{sh}}{1 + \kappa n_{sh}\, \eta} \bar{u}^2\, \bar{\mu}_\eta\right] + \frac{\bar{c}_p}{H_{sh}\, K_{sh}\, \bar{K}} \left[\left(\frac{\rho D_{IA}}{\varepsilon^2} - \frac{K_{sh}\, \bar{K}}{\bar{c}_p}\right) \left\{\left[(h_I - h_A)(c_I)_\eta\right]_\eta\right.\right.$$

$$+ \left(\frac{n_{sh}\,\kappa}{1+\kappa n_{sh}\,\eta} + \frac{n_{sh}\cos\phi}{r + n_{sh}\,\eta\cos\phi}\right)(h_I - h_A)(c_I)_\eta\} + (h_I - h_A)(c_I)\left\{\left(\frac{\rho D_{IA}}{\varepsilon^2}\right)_\eta\right.$$

$$\left. - K_{sh}\left(\frac{\bar{K}}{\bar{c}_p}\right)_\eta\right\}] - \frac{v_{sh}^2}{H_{sh}}\left[\overline{\overline{vv}}_{\eta\eta} + \bar{v}_\eta^2 + \frac{\bar{c}_p}{\bar{K}}\,\overline{\overline{vv}}_\eta\left(\frac{\bar{K}}{\bar{c}_p}\right)_\eta + \overline{\overline{vv}}_\eta\left(\frac{n_{sh}\,\kappa}{1+\kappa n_{sh}\,\eta}\right.\right.$$

$$\left.\left. + \frac{n_{sh}\cos\phi}{r + n_{sh}\,\eta\cos\phi}\right)\right], \tag{2.15c}$$

$$\alpha_4 = -\frac{\bar{c}_p}{K_{sh}\,\bar{K}}\,\frac{\rho_{sh}\,u_{sh}\,\overline{\overline{\rho u}}}{\varepsilon^2}\,\frac{n_{sh}^2}{1+\kappa n_{sh}\eta}\,; \tag{2.15d}$$

Species Equation

$$\alpha_1 = \frac{\rho_{sh}\,u_{sh}\,n_{sh}\,n'_{sh}}{(1+\kappa n_{sh}\,\eta)\rho D_{IA}}\,\overline{\overline{\rho u}}_\eta - \rho_{sh}\,v_{sh}\,n_{sh}\,\frac{\overline{\overline{\rho u}}}{\rho D_{IA}}$$

$$+ \left(\frac{\kappa n_{sh}}{1+\kappa n_{sh}\,\eta} + \frac{\cos\phi\; n_{sh}}{r + n_{sh}\,\eta\cos\phi}\right) + \frac{(\rho D_{IA})_\eta}{\rho D_{IA}}\,, \tag{2.16a}$$

$$\alpha_2 = 0\,, \tag{2.16b}$$

$$\alpha_3 = 0\,, \tag{2.16c}$$

$$\alpha_4 = -\frac{n_{sh}^2\,\rho_{sh}\,u_{sh}}{1+\kappa n_{sh}\,\eta}\,\frac{\overline{\overline{\rho u}}}{\rho D_{IA}}\,. \tag{2.16d}$$

The continuity and n-momentum equations in the transformed variables are as follows:

Continuity Equation

$$[n_{sh}(r + n_{sh}\,\eta\cos\phi)\rho_{sh}\,u_{sh}\,\bar{\bar{\rho}}\bar{\bar{u}}]_{\xi} +$$

$$[(r + n_{sh}\,\eta\cos\phi)\{(1 + \kappa n_{sh}\,\eta)\rho_{sh}\,v_{sh}\,\bar{\bar{\rho}}\bar{\bar{v}} - n'_{sh}\,\rho_{sh}\,u_{sh}\,\bar{\bar{\rho}}\bar{\bar{u}}\eta\}]_{\eta} = 0 \ , \tag{2.17}$$

n-Momentum Equation

$$\frac{\bar{\bar{\rho}}\bar{\bar{u}}}{1 + \kappa n_{sh}\,\eta}\left(\bar{v}_{\xi} - \frac{n'_{sh}}{n_{sh}}\,\eta\bar{v}_{\eta} + \frac{v'_{sh}}{v_{sh}}\,\bar{v}\right) + \frac{v_{sh}}{u_{sh}}\,\frac{\bar{\bar{\rho}}\bar{\bar{v}}}{n_{sh}}\,\bar{v}_{\eta} - \frac{\kappa}{1 + \kappa n_{sh}\,\eta}\,\frac{u_{sh}}{v_{sh}}\,\bar{\bar{\rho}}\bar{\bar{u}}^2$$

$$+ \frac{P_{sh}}{\rho_{sh}\,u_{sh}\,v_{sh}\,n_{sh}}\,\bar{P}_{\eta} = 0 \ , \tag{2.18a}$$

or making the thin shock-layer approximation, the n-momentum equation becomes

$$\bar{P}_{\eta} = \frac{\kappa}{1 + n_{sh}\,\eta}\,\frac{\rho_{sh}\,u_{sh}^2\,n_{sh}}{P_{sh}}\,\bar{\bar{\rho}}\bar{\bar{u}}^2 \ . \tag{2.18b}$$

The transformed equation of state is

$$\bar{P} = \frac{(\bar{M})_{sh}}{\bar{M}}\,\bar{\bar{\rho}}\bar{\bar{t}} \ . \tag{2.19}$$

The continuity equation (2.17) can be integrated from the body ($\eta = 0$) to the shock ($\eta = 1$) while holding ξ constant to give an equation for the total mass conservation. If mass injection at the body surface is permitted, the resulting equation is

$$\frac{dM}{d\xi} = r[(1 + \frac{n_{sh}\cos\phi}{r})\{n'_{sh}\,\rho_{sh}\,u_{sh} - (1 + \kappa n_{sh})\rho_{sh}\,v_{sh}\} + \rho_{sh}\,v_{sh}\,\bar{\rho}_w\,\bar{v}_w] \ , \qquad (2.20a)$$

where

$$M = \int_0^1 n_{sh}\, r(1 + \frac{n_{sh}\,\eta\cos\phi}{r})\rho_{sh}\,u_{sh}\,\bar{\rho}\bar{u}\,d\eta \ . \qquad (2.20b)$$

This form of the continuity equation (2.20) can be used in the numerical scheme to determine the shock location.

The shear stress and heat transfer must also be modified to account for mass injection at the body surface. The dimensionless shear stress and heat transfer at the body surface for the injection case are given by:

$$c_f = \frac{2\varepsilon^2}{n_{sh}}\,\mu_{sh}\,u_{sh}\,\bar{\mu}\,(\frac{\partial\bar{u}}{\partial\eta} - \kappa n_{sh}\,\bar{u}) - 2\rho_{sh}\,v_{sh}\,u_{sh}\,\bar{\rho}_w\,\bar{v}_w\,\bar{u} \ , \qquad (2.21)$$

and

$$q_w = - \frac{\varepsilon^2 \mu_{sh} T_{sh}}{\sigma n_{sh}} \bar{\mu}\bar{t}_\eta - \frac{\varepsilon^2 \mu_{sh} u_{sh}^2}{n_{sh}} \bar{\mu}\bar{u}\bar{u}_\eta$$

$$- T_{sh} \rho_{sh} v_{sh} \left(1 - \frac{\bar{R}}{(c_p^*)_\infty}\right)(\bar{t}_w - \bar{t})\bar{\rho}_w \bar{v}_w - P_{sh} v_{sh} \bar{P}(\bar{v}_w - \bar{v})$$

$$- \rho D_{IA}(h_I - h_A)(c_I)_\eta \, . \qquad (2.22)$$

These expressions are derived in detail by Whitehead and Davis (1969).

The viscous shock-layer equations as presented are in a form applicable to the problem being considered here. They are also in a form that can be readily solved numerically with the proper boundary conditions and suitable fluid properties. These conditions and properties will be investigated in detail in the next two chapters.

III. FORMULATION OF THE BOUNDARY CONDITIONS

Boundary conditions are given below for conditions at both the shock and body surface. The slip-flow boundary conditions at the body surface are derived by Whitehead and Davis (1969) but are presented again in detail here.

Conditions at the Body Surface

The slip-flow boundary conditions for low-Reynolds-number flow past a solid surface are well known. They have been derived in the literature by various authors (see Patterson (1956) and Shidlovskiy (1967), for example) and applied to flow problems with low to moderate Reynolds numbers by various other authors (see Davis (1970a,b), Street (1960), and Can Dyke (1961), for example). These boundary conditions assume an impermeable surface and zero macroscopic velocity normal to the surface. They also assume that the mean free path, ℓ, although small, is large enough so that there is no interaction between incident and reflected molecules at the surface. Patterson (1956) and Shidlovskiy (1967) have assumed a near Maxwellian distribution function in the Knudsen layer. Some authors (see Kogan (1969), for example) have criticized their approach and suggest more rigorous approaches; however, their results differ little from those of the less refined approach used by Patterson (1956) and Shidlovskiy (1967).

To investigate low to moderate Reynolds number flow with mass injection at the boundary, it is necessary to consider boundary con-

ditions with mass transport across the surface. The derivation performed here essentially follows that given by Shidlovskiy (1967), but allows for the transport of mass across a porous surface. For engineering purposes, this method should produce results of sufficient accuracy, as in the no-injection case. The detailed derivation is made for a one-component gas; that is, the free stream and injected gases are of the same species. How to modify these conditions to the case of a foreign gas being injected into the free-stream species will be discussed later.

To allow mass transport, a model must be chosen to simulate the condition of the body surface. It is assumed in this derivation that molecules reflect both diffusely and specularly from the solid surface. When the boundary conditions are used in the problem solution, only diffuse reflection is considered as this most nearly approximates what is observed physically. In addition, incident molecules are allowed to penetrate the porous surface and be reflected with the injected gas.

The specular reflection is handled exactly as by Shidlovskiy (1967) where the number of specularly reflected molecules is proportional to $(1 - \theta)$. The number of diffusely reflected molecules is proportional to θ, but these molecules are subdivided into those that reflect diffusely from the solid portion of the surface and those that are diffusely injected from the interior of the body. A coefficient, δ, is defined to handle the two types of diffuse reflection and is made proportional to the ratio of the injection area to the total area of the surface. Therefore, the number of molecules that reflect diffusely

from the solid surface with a Maxwellian distribution and zero macroscopic velocity is proportional to $(1 - \delta)$. The number of molecules that are injected with a Maxwellian distribution relative to the macroscopic injection velocity is proportional to δ.

The molecular velocity of the fluid near the outside surface is assumed to vary slightly from a Maxwellian distribution and is given by

$$F_G = F_o(1 + G) \ , \tag{3.1}$$

where F_o is the Maxwellian distribution function and G is a function of the molecular velocities that is given in the literature (see Patterson (1956), for example).

Now an expression for the total mass transport across a unit area of surface per unit time can be written as follows:

$$\int_{-\infty}^{\infty}\int_{-\infty}^{\infty}\int_{-\infty}^{\infty}(V + v^*)F_G \, dU^* \, dV^* \, dW^* =$$

$$\int_{-\infty}^{\infty}\int_{-\infty}^{-v^*}\int_{-\infty}^{\infty}(V^* + v^*)F_G \, dU^* \, dV^* \, dW^*$$

$$+ (1 - \theta)\int_{-\infty}^{\infty}\int_{-v^*}^{\infty}\int_{-\infty}^{\infty}(V^* + v^*)F_G' \, dU^* \, dV^* \, dW^*$$

$$+ \delta\theta\int_{-\infty}^{\infty}\int_{-v_w^*}^{\infty}\int_{-\infty}^{\infty}(V^* + v_w^*)F_o \, dU^* \, dV^* \, dW^*$$

$$+ (1 - \delta)\theta\int_{-\infty}^{\infty}\int_{0}^{\infty}\int_{-\infty}^{\infty}V^*F_o \, dU^* \, dV^* \, dW^* \ . \tag{3.2}$$

The left side of equation (3.2) represents the total transport of mass across a unit area of surface per unit of time. The first term on the right side corresponds to the flow of incident molecules onto the surface. The second term represents the mass flow of molecules that undergo specular reflection. The next term, having δ as a coefficient, corresponds to the mass of molecules that are diffusely injected with a Maxwellian distribution relative to the injection velocity, v_w^*; the last term represents the mass of molecules that reflects diffusely from the solid surface with zero macroscopic velocity and with a Maxwellian distribution. The integration in each case is over the necessary molecular velocities to insure that each molecule crossing the surface is taken into account. In the specular reflection term, the distribution function, F_G', is defined as follows:

$$F_G'(U^*,V^*,W^*) = F_G(U^*,-V^*,W^*) \ . \tag{3.3}$$

The molecular velocities can be transformed as in Shidlovskiy (1967) as follows:

$$Q_1 = \frac{U^*}{\sqrt{\bar{R}T^*}} \ , \tag{3.4a}$$

$$Q_2 = \frac{V^*}{\sqrt{\bar{R}T^*}} \ , \tag{3.4b}$$

and

$$Q_3 = \frac{W^*}{\sqrt{\bar{R}T^*}} \ , \tag{3.4c}$$

Also, for convenience, define

$$v' = \frac{v^*}{\sqrt{\bar{R}T^*}}, \tag{3.5a}$$

$$u' = \frac{u^*}{\sqrt{\bar{R}T^*}}, \tag{3.5b}$$

$$v_w' = \frac{v_w^*}{\sqrt{\bar{R}T_w^*}}. \tag{3.5c}$$

The Maxwellian distribution function as given by Shidlovskiy (1967) is,

$$F_o = N(2\pi\bar{R}T^*)^{-3/2}\, e^{-\frac{1}{2}Q_iQ_i}. \tag{3.6}$$

If equations (3.4), (3.5), and (3.6) are substituted into equation (3.2) the mass-transport integral equation becomes,

$$\begin{aligned}
&N\sqrt{\bar{R}T^*}\int_{-\infty}^{\infty}\int_{-\infty}^{\infty}\int_{-\infty}^{\infty}(Q_2+v')(1+G)\,e^{-\frac{1}{2}Q_iQ_i}\,dQ_1\,dQ_2\,dQ_3\\
&= N\sqrt{\bar{R}T^*}\int_{-\infty}^{\infty}\int_{-\infty}^{-v'}\int_{-\infty}^{\infty}(Q_2+v')(1+G)\,e^{-\frac{1}{2}Q_iQ_i}\,dQ_1\,dQ_2\,dQ_3\\
&+ (1-\theta)N\sqrt{\bar{R}T^*}\int_{-\infty}^{\infty}\int_{-v'}^{\infty}\int_{-\infty}^{\infty}(Q_2+v')(1+G')\,e^{-\frac{1}{2}Q_iQ_i}\,dQ_1\,dQ_2\,dQ_3\\
&+ \delta\theta N_I\sqrt{\bar{R}T_w^*}\int_{-\infty}^{\infty}\int_{-v_w'}^{\infty}\int_{-\infty}^{\infty}(Q_2+v_w')\,e^{-\frac{1}{2}Q_iQ_i}\,dQ_1\,dQ_2\,dQ_3\\
&+ (1-\delta)\theta N_w\sqrt{\bar{R}T_w^*}\int_{-\infty}^{\infty}\int_{0}^{\infty}\int_{-\infty}^{\infty}Q_2\,e^{-\frac{1}{2}Q_iQ_i}\,dQ_1\,dQ_2\,dQ_3
\end{aligned} \tag{3.7}$$

where $i = 1, 2, 3$,

and

$$G'(Q_1, Q_2, Q_3) = G(Q_1, -Q_2, Q_3) \ , \tag{3.8a}$$

where

$$G = a_1 Q_1 + \ldots \frac{1}{2} a_{11} Q_1^2 + \frac{1}{2} a_{12} Q_1 Q_2 + \ldots \frac{1}{6} a_{111} Q_1^3 + \frac{1}{6} a_{112} Q_1^2 Q_2 + \ldots \tag{3.8b}$$

The integration, although lengthy, is straightforward and results in the following mass transport equation;

$$N\sqrt{\bar{R}T^*}\left[\sqrt{2\pi}\, v' \left(1 + \operatorname{erf}\frac{v'}{\sqrt{2}}\right) + e^{-\frac{v'^2}{2}} \left\{2 + a_{22} - \frac{(2-\theta)}{\theta} v' \frac{a_{222}}{3}\right\}\right.$$
$$\left. - \delta \frac{N_I}{N} \sqrt{\frac{T^*}{T_w^*}} \left\{2e^{-\frac{v_w'^2}{2}} + \sqrt{2\pi}\, v_w' \left(1 + \operatorname{erf}\frac{v_w'}{\sqrt{2}}\right)\right\}\right] = 2(1-\delta) N_w \sqrt{\bar{R}T_w^*} \ . \tag{3.9}$$

In a similar manner, an equation for the normal momentum transport across the boundary can be written, resulting in the following integral equation:

$$M \int_{-\infty}^{\infty}\int_{-\infty}^{\infty}\int_{-\infty}^{\infty} (V^* + v^*)^2 F_G \, dU^* \, dV^* \, dW^* = M \int_{-\infty}^{\infty}\int_{-\infty}^{-v^*}\int_{-\infty}^{\infty} (V^* + v^*)^2 F_G \, dU^* dV^* dW^*$$
$$+ (1-\theta) M \int_{-\infty}^{\infty}\int_{-v^*}^{\infty}\int_{-\infty}^{\infty} (V^* + v^*)^2 F_G' \, dU^* \, dV^* \, dW^*$$
$$+ \delta\theta M \int_{-\infty}^{\infty}\int_{-v_w^*}^{\infty}\int_{-\infty}^{\infty} (V^* + v_w^*)^2 F_o \, dU^* \, dV^* \, dW^*$$
$$+ (1-\delta)\theta M \int_{-\infty}^{\infty}\int_{0}^{\infty}\int_{-\infty}^{\infty} V^{*2} F_o \, dU^* \, dV^* \, dW^* \ . \tag{3.10}$$

Transforming and integrating as before results after simplification in the following normal-momentum transport equation;

$$P^*\left[1 + v'^2 + a_{22}\right)\left(1 + \operatorname{erf}\frac{v'}{\sqrt{2}}\right) + \sqrt{\frac{2}{\pi}}\, e^{-\frac{v'^2}{2}}\left(v' + \frac{2-\theta}{\theta}\,\frac{a_{222}}{3}\right)\Big]$$

$$= \delta P_I^*\left[\left(1 + \operatorname{erf}\frac{v'_w}{\sqrt{2}}\right)\left(1 + v_w'^2\right) + \sqrt{\frac{2}{\pi}}\, v'_w\, e^{-\frac{v_w'^2}{2}}\right] + (1-\delta)P_w^*\,, \qquad (3.11)$$

where use has been made of the fact that, for a perfect gas,

$$P^* = MN\bar{R}T^*\,. \qquad (3.12)$$

If the same procedure is followed, the tangential momentum transport can be written in the following integral form;

$$\int_{-\infty}^{\infty}\int_{-\infty}^{\infty}\int_{-\infty}^{\infty}(U^* + u^*)(V^* + v^*)F_G\, dU^*\, dV^*\, dW^*$$

$$= \int_{-\infty}^{\infty}\int_{-\infty}^{-v^*}\int_{-\infty}^{\infty}(U^* + u^*)(V^* + v^*)F_G\, dU^*\, dV^*\, dW^*$$

$$+ (1-\theta)\int_{-\infty}^{\infty}\int_{-v^*}^{\infty}\int_{-\infty}^{\infty}(U^* + u^*)(V^* + v^*)F_G'\, dU^*\, dV^*\, dW^*$$

$$+ \delta\theta\int_{-\infty}^{\infty}\int_{-v_w^*}^{\infty}\int_{-\infty}^{\infty}U^*(V^* + v_w^*)F_o\, dU^*\, dV^*\, dW^*$$

$$+ \theta(1-\delta)\int_{-\infty}^{\infty}\int_{0}^{\infty}\int_{-\infty}^{\infty}U^*\, V^*\, F_o\, dU^*\, dV^*\, dW^*\,. \qquad (3.13)$$

Since the last two terms on the right side of equation (3.13) are zero,

it is a simple matter to integrate and solve for the tangential velocity on the surface. The resulting equation for u' is

$$u' = \frac{\left[-\frac{(2-\theta)}{\theta}\, a_{12}\left(1 + \operatorname{erf}\frac{v'}{\sqrt{2}}\right) - \frac{1}{\sqrt{2\pi}}\, e^{-\frac{v'^2}{2}}\, a_{221}\right]}{\left[v'\left(1 + \operatorname{erf}\frac{v'}{\sqrt{2}}\right) + \sqrt{\frac{2}{\pi}}\, e^{\frac{-v'^2}{2}}\right]} . \qquad (3.14)$$

The only additional equation to be written is an equation for the energy transport across the boundary. Using Shidlovskiy's (1967) definition of the thermal accomodation coefficient, α_t, and assuming translational energy only, the energy transport across the surface may be written as follows:

$$\int_{-\infty}^{\infty}\int_{-\infty}^{\infty}\int_{-\infty}^{\infty} [(U^* + u^*)^2 + (V^* + v^*)^2 + W^{*2}][V^* + v^*] F_G \, dU^* \, dV^* \, dW^*$$

$$= \alpha_t \int_{-\infty}^{\infty}\int_{-\infty}^{-v^*}\int_{-\infty}^{\infty} [(U^* + u^*)^2 + (V^* + v^*)^2 + W^{*2}][V^* + v^*] F_G \, dU^* \, dV^* \, dW^*$$

$$+ \delta\alpha_t \int_{-\infty}^{\infty}\int_{-v_w^*}^{\infty}\int_{-\infty}^{\infty} [U^{*2} + (V^* + v_w^*)^2 + W^{*2}][V^* + v^*] F_o \, dU^* \, dV^* \, dW^*$$

$$+ (1 - \delta)\, \alpha_t \int_{-\infty}^{\infty}\int_{0}^{\infty}\int_{-\infty}^{\infty} [U^{*2} + V^{*2} + W^{*2}] V^* \, F_o \, dU^* \, dV^* \, dW^* . \qquad (3.15)$$

The integration is quite long but, as in the other cases, straightforward. Also, the coefficients a_i, a_{ij}, a_{ijk} are assumed small (see Patterson (1956)) and, from the tangential momentum transport equation, u is of the same order as the coefficients. Therefore, the squares and

products of these terms may be neglected. The energy transport equation that results from integrating and substituting for $N_w \bar{R} T_w^*$ from equation (3.9) is

$$T^* \left[\sqrt{2\pi}\, \frac{2 - \alpha_t\left(1 - \operatorname{erf} \frac{v'}{\sqrt{2}}\right)}{\alpha_t} \left(v'^3 + 5v'\right) + e^{-\frac{v'^2}{2}} \left(8 + 2v'^2\right)\right.$$

$$-\delta \frac{N_I}{N} \left(\frac{T_w^*}{T^*}\right)^{3/2} \left\{e^{-\frac{v_w'^2}{2}} \left(8 + 2v_w'^2\right) + \sqrt{2\pi}\, \left(1 + \operatorname{erf} \frac{v_w'}{\sqrt{2}}\right)\left(5v_w' + v_w'^3\right)\right\}$$

$$+ a_{22} \left\{\left(\frac{2 - \alpha_t\left(1 - \operatorname{erf} \frac{v'}{\sqrt{2}}\right)}{\alpha_t}\right) 2\sqrt{2\pi}\, v' + 6e^{-\frac{v'^2}{2}}\right\}$$

$$\left. - a_2 \left\{\left(\frac{2 - \alpha_t\left(1 - \operatorname{erf} \frac{v'}{\sqrt{2}}\right)}{\alpha_t}\right) 2\sqrt{2\pi} + \frac{2}{5}\left(5v' + 2v'^3\right) e^{-\frac{v'^2}{2}}\right\}\right]$$

$$= 4T_w^* \left[\sqrt{2\pi}\, v' \left(1 + \operatorname{erf} \frac{v'}{\sqrt{2}}\right) + e^{-\frac{v'^2}{2}} \left(2 + a_{22}\right) + \frac{2 - \theta}{\theta} v' e^{-\frac{v'^2}{2}} \left(\frac{2}{5} a_2\right)\right.$$

$$\left. - \delta \frac{N_I}{N} \left(\frac{T_w^*}{T^*}\right)^{1/2} \left\{2e^{-\frac{v_w'^2}{2}} + \sqrt{2\pi}\, \left(1 + \operatorname{erf} \frac{v_w'}{\sqrt{2}}\right) v_w'\right\}\right] . \qquad (3.16)$$

Equations (3.9), (3.11), (3.14) and (3.16) describe conditions at a porous surface through which mass is injected into a slightly rarefied flow field. To be of use as boundary conditions, the coefficients a_i, a_{ij}, a_{ijk} must be known. These coefficients depend on the type of molecular model chosen. Patterson (1956) determines the coefficients for the model of a perfectly elastic sphere. Written in terms of the boundary-layer coordinate system given in Figure 1, Patterson's coefficients are:

$$a_2 = \frac{75}{32}\sqrt{\frac{\pi}{2}}\frac{\ell}{T^*}T^*_{n^*} , \tag{3.17a}$$

$$a_{12} = -\frac{5}{4}\frac{\ell}{\bar{c}}(u^*_{n^*} - \kappa^* u^* - v^*_{s^*}) , \tag{3.17b}$$

$$a_{22} = \frac{5}{6}\frac{\ell}{\bar{c}}(u^*_{s^*} - 2v^*_{n^*}) , \tag{3.17c}$$

$$a_{122} = -\frac{15}{16}\sqrt{\frac{\pi}{2}}\frac{\ell}{T^*}T^*_{s^*} , \tag{3.17d}$$

and

$$a_{222} = -\frac{45}{16}\sqrt{\frac{\pi}{2}}\frac{\ell}{T^*}T^*_{n^*} ; \tag{3.17e}$$

where ℓ is the mean free path defined by

$$\ell = \frac{\mu^*}{P^*}\sqrt{\frac{\pi \bar{R} T^*}{2}} , \tag{3.17f}$$

and

$$\frac{\ell}{\bar{c}} = \frac{\pi}{4}\frac{\mu^*}{P^*} , \tag{3.17g}$$

where $\bar{c}$ is the mean value of the random molecular speeds in a given volume.

When these coefficients are substituted into equations (3.9), (3.11), (3.14), and (3.16), the equations can be non-dimensionalized by the variables defined in the nomenclature. All the variables are taken to be of order (1) except n which is assumed to be of order (ε). These orders of magnitude are those that prevail near the surface of the body. When the above substitutions are made and terms to order (ε)

are kept, the following equations result;

Mass Transport

$$N\sqrt{\frac{\bar{R}}{c_p^*}T}\left[\sqrt{2\pi}\,v'\left(1+\operatorname{erf}\frac{v'}{\sqrt{2}}\right)+e^{-\frac{v'^2}{2}}\left\{2-\varepsilon^2\left(\frac{5\pi}{12}\frac{\mu}{P}v_n\right.\right.\right.$$

$$\left.\left.\left.-\frac{2-\theta}{\theta}\frac{15\pi}{32}v'\sqrt{\frac{\bar{R}}{c_{p\infty}^*}\frac{1}{T}\frac{\mu}{P}T_n}\right)\right\}-\delta\frac{N_I}{N}\sqrt{\frac{T_w}{T}}\left\{2e^{-\frac{v_w'^2}{2}}\right.\right.$$

$$\left.\left.+\sqrt{2\pi}\,v_w'\left(1+\operatorname{erf}\frac{v_w'}{\sqrt{2}}\right)\right\}\right]=2(1-\delta)N_w\sqrt{\frac{\bar{R}}{c_{p\infty}^*}T_w}\,, \tag{3.18}$$

Normal Momentum Transport

$$P\left[(1+v'^2)\left(1+\operatorname{erf}\frac{v'}{\sqrt{2}}\right)+\sqrt{\frac{2}{\pi}}\,v'\,e^{-\frac{v'^2}{2}}\right]$$

$$=\delta P_I\left[\left(1+\operatorname{erf}\frac{v_w'}{\sqrt{2}}\right)\left(1+v_w'^2\right)+\sqrt{\frac{2}{\pi}}\,v_w'\,e^{-\frac{v_w'^2}{2}}\right]+(1-\delta)P_w$$

$$+\varepsilon^2\left[\frac{5\pi}{12}\left(1+\operatorname{erf}\frac{v'}{\sqrt{2}}\right)\mu v_n+\sqrt{\frac{\pi}{2}}\frac{15}{16}\frac{2-\theta}{\theta}e^{-\frac{v'^2}{2}}\sqrt{\frac{\bar{R}}{c_{p\infty}^*}\frac{1}{T}}\;\mu T_n\right]\,, \tag{3.19}$$

Tangential Momentum Transport

$$u'=\frac{\varepsilon^2\,\frac{2-\theta}{\theta}\,\frac{5\pi}{16}\left(1+\operatorname{erf}\frac{v'}{\sqrt{2}}\right)\frac{\mu}{P}\left(u_n-\kappa u\right)}{v'\left(1+\operatorname{erf}\frac{v'}{\sqrt{2}}\right)+\sqrt{\frac{2}{\pi}}\;e^{\frac{-v'^2}{2}}}\,, \tag{3.20}$$

Energy Transport

$$T = 4T_w \{\frac{C}{A} - \varepsilon^2 (\frac{CB}{A^2} - \frac{D}{A})\} \quad , \tag{3.21a}$$

where

$$A = \sqrt{2\pi}\ (\frac{2 - \alpha_t(1 - \text{erf}\ \frac{v'}{\sqrt{2}})}{\alpha_t})(5v' + v'^3) + e^{-\frac{v'^2}{2}}\ (8 + 2v'^2)$$

$$-\delta\ \frac{N_I}{N}(\frac{T_w}{T})^{3/2}\ \{e^{-\frac{v_w'^2}{2}}\ (8 + 2v_w'^2) + \sqrt{2\pi}\ (1 + \text{erf}\ \frac{v_w'}{\sqrt{2}})(5v_w' + v_w'^3)\} \quad , \tag{3.21b}$$

$$B = -\ (\frac{2 - \alpha_t(1 - \text{erf}\ \frac{v'}{\sqrt{2}})}{\alpha_t}\sqrt{2\pi}\ v' + 3e^{-\frac{v'^2}{2}})\ \frac{5\pi}{6}\frac{\mu}{P}\ v_n$$

$$- \{\frac{1}{5}(5v' + 2v'^3)e^{\frac{-v'^2}{2}} + \sqrt{2\pi}\ (\frac{2 - \alpha_t(1 - \text{erf}\ \frac{v'}{\sqrt{2}})}{\alpha_t})\}\ \frac{75\pi}{32}\frac{\mu}{P}\sqrt{\frac{\bar{R}}{c^*_{p\infty}}\frac{1}{T}}\ T_n \quad , \tag{3.21c}$$

$$C = \sqrt{2\pi}\ v'(1 + \text{erf}\ \frac{v'}{\sqrt{2}}) + 2e^{-\frac{v'^2}{2}} - \delta\ \frac{N_I}{N}\sqrt{\frac{T_w}{T}}\{2e^{-\frac{v_w'^2}{2}} + \sqrt{2\pi}\ v_w'(1 + \text{erf}\ \frac{v_w'}{\sqrt{2}})\}, \tag{3.21d}$$

$$D = 5\pi\ \frac{\mu}{P}\ e^{-\frac{v'^2}{2}}(-\frac{1}{12}\ v_n + \frac{2 - \theta}{\theta}\ \frac{3\pi}{32}\ v'\sqrt{\frac{\bar{R}}{c^*_{p\infty}}\frac{1}{T}}\ T_n), \tag{3.21e}$$

where in terms of dimensionless variables

$$v' = \frac{1}{\sqrt{\frac{\bar{R}}{c^*_{p\infty}}\ T}}\ v \quad , \tag{3.22a}$$

$$v_w' = \frac{1}{\sqrt{\frac{\bar{R}}{c_{p\infty}^*} T_w}} v_w, \tag{3.22b}$$

and

$$u' = \frac{1}{\sqrt{\frac{\bar{R}}{c_{p\infty}^*} T}} u . \tag{3.22c}$$

Equations (3.18) through (3.21) give expressions for the slip velocity, temperature jump and pressure jump at the surface of a porous body with mass injection in two-dimensional or axisymmetric slightly rarefied flow. For the case of no injection and a solid boundary ($v_w = 0$ and $\delta = 0$), these equations reduce to those given by Shidlovskiy (1967).

For the case of small injection velocity, where $v_I = 0(\varepsilon)$, equations (3.18) through (3.21) can be expanded and simplified to give the following equations if terms to order (ε) are retained:

Mass Transport

$$N \sqrt{\frac{\bar{R}}{c_{p\infty}^*} T} \left[\sqrt{2\pi}\, v' + 2 - \delta \frac{N_I}{N} \sqrt{\frac{T_w}{T}} \left(2 + \sqrt{2\pi}\, v_w'\right)\right]$$

$$= 2(1 - \delta)\, N_w \sqrt{\frac{\bar{R}}{c_{p\infty}^*} T_w} , \tag{3.23}$$

Normal Momentum Transport

$$P = \delta P_I[1 + 2\sqrt{\frac{2}{\pi}}(v'_w - v')] + (1-\delta)P_w[1 - 2\sqrt{\frac{2}{\pi}}v']$$

$$+ \varepsilon^2 \sqrt{\frac{\pi}{2}} \frac{15}{16} \frac{2-\theta}{\theta} \sqrt{\frac{\bar{R}}{c^*_{p\infty}}} \frac{1}{T} \mu T_n \,, \tag{3.24}$$

Tangential Momentum Transport

$$u = \varepsilon^2 \frac{5\pi}{16} \sqrt{\frac{\pi}{2}} \frac{2-\theta}{\theta} \sqrt{\frac{\bar{R}}{c^*_{p\infty}}} T \frac{\mu}{P} (u_n - \kappa u) \tag{3.25}$$

Energy Transport

$$T = T_w[(1 - \delta \frac{N_I}{N} \sqrt{\frac{T_w}{T}}) \{1 + (-\frac{5\sqrt{2\pi}}{8} \frac{2-\alpha_t}{\alpha_t} v' + \delta \frac{N_I}{N} (\frac{T_w}{T})^{3/2} \frac{5\sqrt{2\pi}}{8} v'_w$$

$$+ \varepsilon^2 \frac{2-\alpha_t}{\alpha_t} \frac{75\pi\sqrt{2\pi}}{256} \sqrt{\frac{\bar{R}}{c^*_{p\infty}}} \frac{1}{T} \frac{\mu}{P} T_n)/(1 - \delta \frac{N_I}{N} (\frac{T_w}{T})^{3/2})\}$$

$$+\sqrt{\frac{\pi}{2}} v' - \delta \frac{N_I}{N} \sqrt{\frac{T_w}{T}} \sqrt{\frac{\pi}{2}} v'_w] \left[\frac{1}{1 - \delta \frac{N_I}{N} (\frac{T_w}{T})^{3/2}} \right] . \tag{3.26}$$

Notice that for $v = 0(\varepsilon)$ the slip velocity is not affected by injection to order (ε). Also, the expression for the macroscopic mass transport across the surface,

$$\rho v = \rho_w v_w \,, \tag{3.27}$$

must be used to relate v and v_w.

The boundary condition at the body surface for the species equation is found by considering species mass conservation at the body surface and is found to be:

$$(c_i)_n - \frac{\rho_w v_w}{\rho D_{IA}} c_i + \frac{\rho_w v_w}{\rho D_{IA}} = 0 \ . \tag{3.28}$$

Finally, transforming the small-injection surface conditions in terms of the shock-normalized variables results in the following boundary conditions at the body:

Surface Conditions

$$\bar{\rho}\bar{v} = \bar{\rho}_w \bar{v}_w \ , \tag{3.29}$$

$$(c_i)_\eta - n_{sh} v_{sh} \frac{\bar{\rho}_w \bar{v}_w}{\bar{\rho} D_{IA}} c_i + n_{sh} v_{sh} \frac{\bar{\rho}_w \bar{v}_w}{\bar{\rho} D_{IA}} = 0 \tag{3.30}$$

$$\bar{u} = \epsilon^2 \frac{2-\theta}{\theta} \sqrt{\frac{\pi}{2}} \frac{5\pi}{16} \sqrt{\frac{\bar{R}}{c^*_{p\infty}} T_{sh} \bar{t}} \ \frac{\mu_{sh}}{p_{sh} n_{sh}} \frac{\bar{\mu}}{\bar{p}} (\bar{u}_\eta - \kappa n_{sh} \bar{u}) \ , \tag{3.31}$$

$$\bar{t} = \bar{t}_w \left[\left(1 - \delta \frac{N_I}{N} \sqrt{\frac{\bar{t}_w}{\bar{t}}}\right) \left\{ 1 + \left(\frac{5\sqrt{2\pi}}{8} \frac{2-\alpha}{\alpha} \frac{v_{sh}\,\bar{v}}{\sqrt{\frac{\bar{R}}{c^*_{p\infty}} T_{sh}\,\bar{t}}} \right.\right.\right.$$

$$\left. + \delta \frac{N_I}{N} \left(\frac{\bar{t}_w}{\bar{t}}\right)^{3/2} \frac{5\sqrt{2\pi}}{8} \frac{v_{sh}\,\bar{v}_w}{\sqrt{\frac{\bar{R}}{c^*_{p\infty}} T_{sh}\,\bar{t}_w}} + \varepsilon^2 \frac{2-\alpha}{\alpha} \frac{75\pi\sqrt{2\pi}}{256} \sqrt{\frac{\bar{R}}{c^*_p} \frac{1}{T_{sh}\,\bar{t}}} \frac{\mu_{sh} T_{sh}}{p_{sh} n_{sh}} \frac{\bar{\mu}}{\bar{p}}\,\bar{t}_\eta \right)$$

$$\left. \left. \sqrt{\left(1 - \delta \frac{N_I}{N} \left(\frac{\bar{t}_w}{\bar{t}}\right)^{3/2}\right)} \right\} + \sqrt{\frac{\pi}{2}} \frac{v_{sh}\,\bar{v}}{\sqrt{\frac{\bar{R}}{c^*_{p\infty}} T_{sh}\,\bar{t}}} \right.$$

$$\left. - \delta \frac{N_I}{N} \sqrt{\frac{\bar{t}_w}{\bar{t}}} \sqrt{\frac{\pi}{2}} \frac{v_{sh}\,\bar{v}_w}{\sqrt{\frac{\bar{R}}{c^*_{p\infty}} T_{sh}\,\bar{t}_w}} \right] \left[\frac{}{1 - \delta \frac{N_I}{N} \left(\frac{t_w}{\bar{t}}\right)^{3/2}} \right], \qquad (3.32)$$

$$\bar{P} = \delta \bar{P}_I \left[1 + 2\sqrt{\frac{2}{\pi}}\, v_{sh} \left(\frac{\bar{v}_w}{\sqrt{\frac{\bar{R}}{c^*_{p\infty}} T_{sh}\,\bar{t}_w}} - \frac{\bar{v}}{\sqrt{\frac{\bar{R}}{c^*_{p\infty}} T_{sh}\,\bar{t}}} \right) \right]$$

$$+ (1 - \delta) \bar{P}_w \left[1 - 2\sqrt{\frac{2}{\pi}} \frac{v_{sh}\,\bar{v}}{\sqrt{\frac{\bar{R}}{c^*_{p\infty}} T_{sh}\,t^*}} \right]$$

$$+ \varepsilon^2 \sqrt{\frac{\pi}{2}} \frac{15}{16} \frac{2-\theta}{\theta} \sqrt{\frac{\bar{R}}{c^*_{p\infty}} \frac{1}{T_{sh}\,\bar{t}}} \frac{\mu_{sh}\, T_{sh}}{p_{sh}\, n_{sh}} \bar{\mu}\, \bar{t}_\eta \,. \qquad (3.33)$$

The pressure condition (3.33) is not needed as a boundary condition, but can be used to determine the surface pressure after the solution to the problem has been obtained. The complete slip-flow surface conditions (3.18) through (3.21) can be written in the same form as the small-injection conditions above but are not shown here. The surface condition for enthalpy can be obtained directly from the temperature surface condition and the relationship between enthalpy and temperature.

As mentioned previously, the slip conditions are for a one-component gas. To modify the conditions for use in a binary-mixture problem, several approaches can be used. If the two gases are of approximately the same molecular weight, the mixture will act as a one-component gas as far as the slip-conditions are concerned. If the gases are of widely different molecular weights, then average properties and molecular weights can be used to approximate the mixture. Should the injection rate be high or low enough so that the gas at the body surface is predominantly free-stream species or injected species, then the molecular weight of the predominant gas can be used.

Therefore, with the appropriate modifications, equations (3.29), (3.30), (3.31) and (3.33) will provide the necessary surface boundary conditions for low to moderate Reynolds number flow of a non-reacting binary mixture including mass injection at the body surface.

Shock Conditions

The boundary conditions used at the shock are the modified

Rankine-Hugoniot or "shock-slip" conditions given by Cheng (1963) and modified by Davis (1970b). The necessary conditions at the shock are

$$\rho_{sh} v'_{sh} = -\sin\alpha \ , \tag{3.34}$$

$$\varepsilon^2 \mu_{sh} (u'_n)_{sh} + \sin\alpha \, u'_{sh} = \sin\alpha \cos\alpha \ , \tag{3.35}$$

$$\varepsilon^2 K_{sh} (T_n)_{sh} + \sin\alpha [c_{I1}(h_I - h_A) + h_A]$$

$$= \sin\alpha \left[\frac{(u'_{sh} - \cos\alpha)^2}{2} - \frac{v'^2_{sh} - \sin^2\alpha}{2} + c_{I1}(h_{I1} - h_{A1}) + h_{A1}\right] , \tag{3.36}$$

or in terms of enthalpy,

$$\frac{\varepsilon^2 K_{sh}}{(\bar{c}_p)_{sh}} (H_n)_{sh} + \sin\alpha \, H_{sh}$$

$$= \sin\alpha \left[\frac{1}{2} + c_{I1}(h_{I1} - h_{A1}) + h_{A1} + (h_I - h_A)(c_I - c_{I1}) + u'_{sh}(u'_{sh} - \cos\alpha)\right]$$

$$+ \frac{\varepsilon^2 K_{sh}}{(\bar{c}_p)_{sh}} [u'_{sh}(u'_n)_{sh} - v'_{sh}(v'_n)_{sh} + (h_I - h_A)(c_I)_n] \ , \tag{3.37}$$

$$P_{sh} = P_1 + \sin\alpha(v'_{sh} + \sin\alpha) \ , \tag{3.38}$$

$$(c_{in})_{sh} + \frac{\sin\alpha}{\rho D_{IA}} (c_i)_{sh} = \sin\alpha (c_i)_1 \ , \tag{3.39}$$

and

$$\rho_{sh} = \frac{(c^*)_{p^\infty} \bar{M}_{sh}}{R} \frac{P_{sh}}{T_{sh}} \quad ; \tag{3.40}$$

where u'_{sh} and v'_{sh} are the components of velocity tangent and normal to the shock interface respectively. The velocity components at the shock tangent and normal to the body surface are given by the following equations:

$$u_{sh} = u'_{sh} \sin(\alpha + \beta) + v'_{sh} \cos(\alpha + \beta) \ , \tag{3.41}$$

and

$$v_{sh} = -u'_{sh} \cos(\alpha + \beta) + v'_{sh} \cos(\alpha + \beta) \ . \tag{3.42}$$

The angles used in the shock conditions are shown in Figure 1. The subscripts 1 refers to conditions outside the shock.

If the shock conditions are transformed using the shock-normalized variables, the shock conditions become:

$$\bar{H} = \bar{u} = \bar{v} = \bar{t} = \bar{p} = \bar{\rho} = 1 \text{ at } \eta = 1 \ .$$

The shock conditions therefore are actually included in the governing equations (2.12) through (2.18) and are evaluated using equations (3.34) through (3.42).

IV. THERMODYNAMIC AND TRANSPORT PROPERTIES

The necessary thermodynamic and transport properties for each species are h^*, c_p^*, μ^*, K^*, and D_{IA}^*. Since cases are to be considered for two species of air, the properties for both equilibrium and undissociated air are needed as well as properties for the inert injectants, argon and helium. The thermodynamic and transport properties in every case are given in dimensional form.

Equilibrium Air

The molecular weight for equilibrium air is taken to be 28.966. The values for specific heat and enthalpy are taken from two sources for two temperature ranges. For the temperature range, $0 \leq T^* \leq 3600°R$, a curve fit for c_p^* presented by Lewis, Adams, and Gilley (1968) is used. The curve fit consists of two fifth-degree polynomials fit to data given by Dommett (1956). The curve fits have the form

$$c_p^* = A + BT^* + CT^{*2} + DT^{*3} + ET^{*4} + FT^{*5} \quad , (ft^2/sec^2\text{-}°R) \qquad (4.1)$$

where the coefficients are given in Table I-a. The enthalpy for the same temperature range is given by

$$h^* = \int c_p^* \, dT^* \quad (ft^2/sec^2) \qquad (4.2)$$

For the temperature range, $3600°R \leq T^* \leq 20{,}000°R$, the data for enthalpy

tabulated by Brahinsky and Neel (1969) is used. They present data for enthalpy at constant pressure for incremental temperatures. The data used here is for 0.1 atmosphere. This data is fitted by the use of a ratio of two Chebyshev polynomials of the form

$$\Psi = A_o \psi_o + A_1 \psi_1 + A_2 \psi_2 + \ldots + A_9 \psi_9 \tag{4.3a}$$

where

$$\psi_o = 1 , \tag{4.3b}$$

$$\psi_1 = \lambda , \tag{4.3c}$$

$$\psi_2 = 2\lambda^2 - 1 , \tag{4.3d}$$

$$\vdots$$

$$\psi_n = 2\lambda\psi_{n-1} - \psi_{n-2} , \tag{4.3e}$$

and

$$-1 \leq \lambda \leq 1 .$$

The coefficients for the Chebyshev polynomials are given in Table I-b. The specific heat in this temperature range is found by differentiating the curve fit for enthalpy. The curve fits for enthalpy and specific heat for the entire temperature range agree quite well with Brahinsky and Neel's (1969) data.

The viscosity for equilibrium air is approximated from the data given by Hansen (1958) for a pressure of 0.1 atmosphere. This data

is approximated using the following linear relation;

$$\mu^* = (8.68 + 0.0038(T^*(°K) - 1{,}000)) \times 10^{-7} \ (lb\text{-}sec/ft^2), \qquad (4.4)$$

for the temperature range, $1800°R \leq T^* \leq 18{,}000°R$.

The thermal conductivity, K*, is found using the semi-empirical Eucken (1913) relation,

$$K^* = (c_p^* + \frac{5}{4}\frac{R}{M})\mu^* \ldots (lbf/sec\text{-}°R) \qquad (4.5)$$

Equation (4.5) was formulated for a one-component gas. However, a comparison of Prandtl numbers for equilibrium air based on thermal conductivities calculated using this formula with Prandtl numbers for equilibrium air given by Hansen (1953) from a more sophisticated approach show good agreement. It is felt that this approach is at least as good as assuming a constant Prandtl number for equilibrium air as is done by several authors.

Frozen Air

For the case where the reaction rates in the shock-layer are considered to be so slow that the air remains in the undissociated free-stream composition, the air is assumed to be a mixture of nitrogen and oxygen molecules. The mass ratios for the air mixture are assumed to be 0.8 for nitrogen and 0.2 for oxygen. The molecular weight of nitrogen is taken to be 28.016 and that of oxygen to be 32.0. After the

properties are determined for the nitrogen and oxygen molecules, the air species properties are determined as follows:

For specific heat and enthalpy,

$$c_p^* = 0.8[(c_p^*)_{N_2} - (c_p^*)_{O_2}] + (c_p^*)_{O_2} , \quad (ft^2/sec^2\text{-}°R) \tag{4.6}$$

and

$$h^* = 0.8[h^*_{N_2} - h^*_{O_2}] + h^*_{O_2} ; \quad (ft^2/sec^2) \tag{4.7}$$

for viscosity and thermal conductivity, Wilke's (1950) semi-empirical formulas are used.

The specific heats for nitrogen and oxygen are obtained using equations given by Owczarek (1964) for example. The form of these equations is

$$c_p^* = \frac{7}{2}\bar{R} + \frac{\bar{R}\left(\frac{\theta_t}{T^*}\right)^2 e^{\frac{\theta_t}{T^*}}}{\left(e^{\frac{\theta_t}{T^*}} - 1\right)^2} , \quad (ft^2/sec^2\text{-}°R) \tag{4.8}$$

where

θ_t = 6012°R for nitrogen

and

θ_t = 4014°R for oxygen,

The specific heats predicted by this equation are based on translational, rotational, and vibrational energy of a diatomic molecule. The enthalpy is found using equation (4.2) .

For the viscosities of nitrogen and oxygen, an exponential curve-

fit function given by Blottner (1964) is used. The function is of the form

$$\mu^* = 2.0886 \times 10^{-3} \, e^{C} \, T^*(^\circ K)^{(A\ell nT^*(^\circ K) + B)}, \quad (lb\text{-}sec/ft^2) \qquad (4.9)$$

for the temperature range $1800^\circ R \leq T^* \leq 18{,}000^\circ R$, where the coefficients are given in Table II.

The thermal conductivity, K^*, for the oxygen and nitrogen molecules is found using the Eucken (1913) formula.

Inert Gases

The inert gases used as injectants, argon and helium, have molecular weights of 39.948 and 4.008 respectively. For the monatomic inert gases only translational energy is considered, which results in constant specific heats of the following form:

$$c_p^* = \frac{5}{2} \bar{R} \, . \quad (ft^2/sec^2\text{-}^\circ R) \qquad (4.10)$$

The enthalpy then has the form

$$h^* = c_p^* \, T^* \, . \quad (ft^2/sec^2) \qquad (4.11)$$

An exponential curve-fit function for the viscosity was obtained from Lewis (1970). The curve-fit function has the same form as equation (4.9) and the coefficients are found in Table II. As in the other cases,

the thermal conductivities for the argon and helium are found from equation (4.5).

The binary diffusion coefficients for argon-N_2 and helium-N_2 were obtained from Lewis (1970). Some authors (see Jaffe, Lind, and Smith (1967), for example) find the binary diffusion coefficients for argon-air and helium-air by using a reduced mass correction factor on the binary diffusion coefficients for nitrogen. This correction is small and appears to be somewhat arbitrary. Therefore, the correction factor is not used here and the binary diffusion coefficients for argon-N_2 and helium-N_2 are used for both air species. The binary diffusion coefficients are in the form

$$D^*_{IA} = \frac{1.0764 \times 10^{-3}}{P^*(ATM)} \left(e^{C\ T^*(°K)^{(A\ell nT^*(°K) + B)}}\right), \ (ft^2/sec^2) \qquad (4.12)$$

where the coefficients are given in Table III.

These thermodynamic and transport properties along with the boundary conditions and governing equations constitute all the information necessary to find a solution to the specified problem. The following chapter discusses the method of solution.

V. METHOD OF SOLUTION

The numerical technique used to solve the governing equations with the given boundary conditions and thermodynamic and transport properties is similar to a method developed by Blottner and Flügge-Lotz (1963) for solving the compressible boundary-layer equations and modified by Davis (1970a,b) to solve the viscous shock-layer equations for a one-component gas and a binary mixture. This method consists basically of solving the set of parabolic partial differential equations with an implicit finite-difference method. The procedure for writing equations in the form of (2.12) in the proper finite-difference form is given by Davis (1970b). This results in equations of the form:

$$A_n W_{n-1} + B_n W_n + C_n W_{n+1} = D \ . \tag{5.1}$$

The subscripts refer to grid points along a line normal to the body surface. A method of solution of finite-difference equations of this form is given by Richtmyer (1957).

Cases are considered here for two air models, and the method of solution depends upon which model is used. For one model, equilibrium air is assumed; that is, it is assumed that the air at each point in the flow field is at its equilibrium composition for the temperature and pressure at that point. The total enthalpy form of the energy equation (2.6) must be used in the solution for this model. This is necessary because the energy equation in terms of temperature contains a term of the form $\sum h_i w_i$ (see Fay and Riddell (1958)) where w_i is

the i^{th} species reaction rate. Now, while the reaction rates between the inert gas and air species are zero, the reaction rates between the gas components in the equilibrium air are not zero. Since the equilibrium air is considered here as one species (the inert gas being the other species), the reaction rates between the gas components in the equilibrium air model are unknown.

Putting the energy equation in terms of the total enthalpy eliminates this term and permits the equilibrium air to be considered as one species. Also, it is assumed in the equilibrium case that the Lewis number is unity between any two of the air components. This assumption is inherent in the assumption that the equilibrium air is one species, (see Hayes and Probstein (1959), equation 8.2.7, page 289).

The frozen air model is considered to be an undissociated mixture of oxygen and nitrogen molecules and the reaction rates are therefore zero and the temperature form of the energy equation (2.4) may be used for this case.

Consider first the equilibrium air case. Put the governing equations into the proper finite-difference form. The boundary conditions at the wall are given by writing the slip conditions (3.30) through (3.32) in three-point forward-difference form. Manipulation of these equations, equation (5.1), and the equation for the solution to the problem allows one to determine a condition to satisfy wall conditions. The modified Rankine-Hugoniot shock-slip conditions are of the same form as the body-slip conditions and when written in three-point backward difference form can be used to satisfy the boundary conditions at

the shock.

The solution to the problem then proceeds in the following manner. Start at the stagnation point where $\frac{\partial w}{\partial \xi} = 0$. Equation (2.12) then reduces to an ordinary differential equation. Make initial guesses for all of the flow profiles. Determine the reference quantities such as temperature, viscosity, specific heat, etc. from curve fits for thermodynamic properties using the given data for the problem. Also determine the thermodynamic properties in the stagnation region using the initial guesses for temperature, species concentration, etc. Integrate, using the finite-difference method, the species equation (2.12) and (2.16) determining the concentration profile. Now solve in the same manner the energy equation (2.12) and (2.15) finding the total enthalpy profile. The temperature profile is found based on the enthalpy profile found above. Proceed in the same way to solve the s-momentum equation (2.12) and (2.13) to determine the $\bar{u}$ profile. Next integrate the continuity equation (2.17) and (2.20) to determine first the shock standoff distance from equation (2.20) and then the $\bar{v}$ component of velocity from equation (2.17). Finally integrate equation (2.18) to determine the pressure. Evaluate the coefficients in the governing equations using the latest profiles, the shock values and the new thermodynamic properties calculated using the latest temperature and concentration profiles. Solve the governing equations again and repeat this process until the solution converges. Now proceed step-by-step down the body using the profiles of the previous step as a first guess at the next step.

In the first approximation it is assumed that n'_{sh} is equal to zero at each step on the body surface. The thin shock-layer form of the n-momentum equation (2.18b) is also used. These approximations are necessary to have the equations in parabolic form. One must also be careful to insure that the total enthalpy form of the energy equation is in a form consistent with the thin shock-layer form of the n-momentum equation. This can be achieved by recognizing that the total enthalpy form of the energy equation can be obtained by taking the dot product of the vector form of the momentum equation with the velocity vector and adding this to the energy equation in terms of temperature. By keeping track of the terms in the normal momentum equation that are omitted in the thin shock-layer approximation, the same terms can be omitted from the energy equation in the first approximation.

After the solution has been found back along the body in the first approximation, the thin shock-layer approximation can be eliminated. In the second iteration n'_{sh} is calculated from the stand-off distance found in the first approximation. The $\bar{v}$ terms calculated in the first approximation are used to eliminate the thin shock-layer approximation in the second iteration. These iterations are continued until the solution converges. Once the solution converges, the heat transfer and shear stress at the body surface can be found using equations (2.21) and (2.22).

The case in which the air species is considered to be an undissociated mixture of nitrogen and oxygen molecules is solved exactly as the equilibrium air case with the exception that the temperature form

of the energy equation (2.12) and (2.14) is used. Therefore, the solution to this equation gives the temperature directly.

Using the technique above, one need only specify the body geometry, the free stream conditions, the mass injection rates, and the injected mass properties to study a variety of problems. Some specific examples are presented in the following chapter.

VI. RESULTS AND CONCLUSIONS

The body chosen for finding example solutions is a hyperboloid asymptotic to a cone of total interior angle of 45°. This is an analytic blunt body that is a good approximation to blunt bodies used in re-entry conditions. The hyperboloid is taken to have a nose radius of one inch. Free-stream conditions of a re-entry nature are used. Solutions were found for altitudes from 100,000 ft. to 300,000 ft. Free-stream conditions for various altitudes are given in Table V and were taken from the U.S. Standard Atmosphere Tables (1962). The free-stream velocity in each case was taken to be 20,000 feet per second. The body temperature in every case was taken to be 1,800°R.

To consider solutions with mass injection at the body surface, some distribution must be assumed for the injected mass. The following dimensionless mass injection distribution has been assumed for the solutions found here:

$$\dot{m} = (\rho_w v_w)_{s.p.} e^{-cr^2} , \qquad (6.1)$$

where $\dot{m}$ is the mass flow rate per unit area. This function results in distributions of the form shown in Figure 2 for a 45° hyperboloid. Distributions of this form are logical for simulating ablation and practical for reduction of heat transfer in the stagnation region by inert gas injection.

The total mass flow rate can be found on an infinite axisymmetric

body as follows:

$$\dot{M} = 2\pi(\rho_w v_w)_{s.p.} \int_0^\infty re^{-cr^2} ds \ . \qquad (6.2)$$

If the integral $2\pi \int_0^\infty re^{-cr^2} ds$ for a particular body is made equal to unity by the proper choice of c, then $\dot{M} = (\rho_w v_w)_{s.p.}$, or the total dimensionless mass flow rate is equal to the ratio of the dimensionless stagnation-point injection rate to the external mass flow rate. For a 45° hyperboloid, c = 3.47, gives a value of unity for the integral. Therefore, by varying $(\rho_w v_w)_{s.p.}$, one can vary the total flux injected but keep the same injection distribution. Table IV gives values of $(\rho_w v_w)_{s.p.}$ used at different altitudes along with the corresponding dimensional total injected mass flow rates. It was found that the solutions were insensitive, especially at lower altitudes, to changes in the value of the injection area parameter, δ, if it was not chosen too large. For instance, $\delta = 0.1$, and $\delta = 0.3$ gave only minor changes in the results even at higher altitudes. Therefore, $\delta = 0.3$ was used for the results given here. The porosity of the body used in the experiments by Pappas and Lee (1969) was 0.34; therefore, 0.3 appears to be a reasonable choice here.

As noted previously, two models were used for the air species. For the frozen air model, solutions were found for various injection rates for altitudes ranging from 300,000 ft. to 100,000 ft. Both argon and helium are used as injectants. In addition, cases of air into air injection are studied where the frozen air model was used as the injected

gas as well as the free-stream gas. Solutions were found for the equilibrium air model for different injection rates at altitudes ranging from 200,000 ft. to 100,000 ft. for argon, helium, and air. For the air injection case here, the equilibrium air model was used for both the injected gas and the free-stream gas.

In the frozen case, solutions were found for approximately five nose radii back along the body. The equilibrium solutions, for which convergence was slower than in the frozen case, were made to approximately three nose radii back along the body due to the excessive computer times required to go further downstream. In all cases, two iterations were made in the ξ-direction. In the finite-difference grid, step sizes of $\Delta\xi = 0.2$ were taken in the ξ-direction. In order to obtain reasonable accuracy, the step size in the η-direction was varied with the shock Reynolds number: higher Reynolds numbers required smaller steps. In cases where the shock Reynolds numbers were quite high, say of the order of 10^3 or higher, variable step sizes were used in the η-direction with smaller steps taken near the body to insure sufficient accuracy in the viscous boundary-layer region near the body.

The slip-flow boundary conditions and shock-slip conditions given in Chapter III were used in every case. A comparison of the effect of the temperature slip on the temperature profile for one case using the present slip conditions and those found in Shidlovskiy (1967) is made in Figure 3. Notice that the present conditions predict less temperature slip at the body. The present velocity slip conditions are identical to Shidlovskiy's (1967) to the order used here, see equation

(3.31), therefore producing the same slip velocity.

The dimensionless heat transfer is plotted as a function of shock Reynolds number for different injection rates of argon for the frozen air model at various altitudes in Figure 4. The dimensionless heat transfer and wall shear stress for different injection rates of helium, argon, and air for altitudes ranging from 275,000 ft. to 200,000 ft. for the frozen air model are shown in Figures 5 through 15 along with velocity, temperature, and concentration profiles and shock stand-off distance for an altitude of 250,000 ft. For altitudes from 200,000 ft. to 125,000 ft., comparisons are made between the dimensionless heat transfer, wall shear stress, shock stand-off distance, and injectant concentration profiles for different injection rates of argon for the frozen and equilibrium air models (see Figures 20, 21, 24, and 26 for example). Also, for altitudes from 175,000 ft. to 100,000 ft., heat transfer, wall shear stress, injectant concentration profiles, and shock stand-off distance for injection of argon, helium, and air for the equilibrium air case are presented (see Figures 22, 23, 25, and 27 for example). Temperature and velocity profiles for the equilibrium air model with argon, helium, and air injection for altitudes of 175,000 ft. and 100,000 ft. are given in Figures 28, 29, 50, and 51.

Figures 4 and 5 indicate that at altitudes above 250,000 ft. even injection rates that are a sizable percentage of the free-stream flow rates are ineffective in reducing heat transfer. This was found to be the case by Chen, Aroesty, and Mobley (1967). Helium is the most effective injectant in reducing the heat transfer and wall shear stress

because of its higher heat capacity, but its effect is fairly small, as in Figures 5 and 6. At lower altitudes as the air density increases, the effect of the injectants on heat transfer and shear stress is more pronounced as shown in Figures 4, 7, and 8 for example. Helium in every case is the most effective injectant. This result is in agreement with the findings of Moore and Lee (1967) and Lewis, Adams, and Gilley (1968). Notice that when using the frozen air model as an injectant, it is only slightly more effective in reducing heat transfer than argon. This is because the frozen air model does not permit dissociation of the air and it therefore acts similar to an inert gas with only a slightly smaller molecular weight than argon.

In these high altitude cases, the heat transfer and wall shear stress return essentially to the no injection values a short distance down the body after the injection rate goes to zero. This is in agreement with the results given by Moore and Lee (1967) for injection cases for a sharp cone using boundary-layer theory. However, they did not allow for the effect of the injected gas on the inviscid conditions. Notice in Figure 9 that the shock stand-off distance and shock shape downstream of the injection returns quickly to its no injection values at an altitude of 250,000 ft. This indicates that the flow in the shock-layer is not altered significantly downstream by the injection and thus the agreement with Moore and Lee's (1967) results. This will not be true at altitudes below the 200,000 ft. level as will be seen later. Notice in Figure 12 that the injectants at higher altitudes diffuse through the entire shock-layer. This is reasonable since the

air density at these altitudes is low. The helium diffusion coefficient is larger than that for argon; therefore, helium diffuses into the shock-layer faster than argon. Davis' (1970a) results for a reacting binary mixture of oxygen atoms and molecules, show that above 225,000 ft. the oxygen dissociation is reasonably small. Therefore, the frozen air model should be a good approximation to the air species at these altitudes.

At altitudes below 200,000 ft. where comparisons are made between the heat transfer and wall shear stress for the equilibrium air model and frozen air model, the equilibrium air produces lower heat transfer and wall shear stress in every case (see Figures 20 and 21 for example). Since the equilibrium air model allows the air to dissociate, the temperatures and thus viscosities are considerably lower in the equilibrium case. The lower temperature produces greater densities as evidenced by the shock stand-off distance, see Figure 26, which for the equilibrium air model is approximately one-half of that found for the frozen air model case at the stagnation point at 175,000 ft. Thus, it is reasonable that the shear stress and heat transfer are lower in the equilibrium case.

Fairly small injection rates at the lower altitudes produce very large reductions in the heat transfer and wall shear stress as is evidenced by Figures 22 and 23 where helium injection produces a reduction of about 90 per cent in the stagnation-point heat transfer and about 25 per cent in the peak wall shear stress for $(\rho_w v_w)_{s.p.} = 0.119$ at 175,000 ft. It can be seen from Figure 22 that, for sufficiently high

injection rates for the injection distributions used here, the maximum heat transfer can occur at a point on the body other than the forward stagnation point. This is significant since stagnation-point injection studies would not show this result and could lead to erroneous conclusions as to the maximum heat transfer. Notice also that when the equilibrium air model is used as the injectant that air injection is about as effective as helium in reducing heat transfer and wall shear stress. This is because the equilibrium air model allows the air to dissociate, thus greatly increasing its heat capacity. This predicted reduction in heat transfer with air injection can be misleading since, in light of the high temperature gradients near the body, it would be impossible for the injected air to reach an equilibrium state in this region. The actual effectiveness for air injection would be somewhat less than predicted by the equilibrium air model. Another result not found in the high altitude cases is that the heat transfer does not regain its no injection value downstream of the injection, but shows a continued reduction in heat transfer, especially for helium injection (see Figure 22). Inger and Sayano (1969) found this to be the case for air into air injection in the stagnation region of a blunt body using a boundary-layer approach and allowing for the interaction of the injected gas on the inviscid flow. Observe in Figure 27 that for the 175,000 ft. case, the shock stand-off distance and shock shape are altered downstream by the injection, especially for helium. This indicates that the flow is sufficiently altered downstream of the injection to affect the heat transfer and wall shear stress even though

the injection rate downstream is zero. Thus, the results here are qualitatively in agreement with Inger and Sayano (1969).

Davis' (1970a) results indicate that for altitudes near 100,000 ft. the air should be near equilibrium in the shock-layer except just behind the shock. Therefore, the equilibrium air model should prove to be a good approximation to the air species at 100,000 ft. For the cases between 100,000 ft. and about 225,000 ft., above which the shock-layer is approximately frozen, the results shown provide the two limiting cases for the air species, since in reality the air would be neither frozen nor in equilibrium, but in a state of chemical non-equilibrium.

Some of the most interesting and unusual results are found for the lower altitudes with the equilibrium air model. Observe that for altitudes of 150,000 ft. and below, the wall shear stress for helium increases slightly over the no injection case after the peak shear stress is reached (see Figures 34, 42, and 48). Also the $\bar{u}$-velocity profiles, which are plotted for altitudes of 175,000 ft. and 100,000 ft. in Figures 28 and 50, respectively, show an unusual inflection point for the helium injection case. Argon and air injection do not show these effects. In searching for an explanation for these effects, one notices from the injectant concentration profiles (Figure 25 for 175,000 ft. and Figure 49 for 100,000 ft.) that the majority of the helium is confined to a region near the body and an interface is formed with a very light gas in a layer near the body and air in the outer portion of the shock-layer. To better observe this interface effect, a case was run for helium injection of $(\rho_w v_w)_{s.p.} = 0.119$ at 175,000 ft. with a

diffusion coefficient for helium of one-tenth the correct value. This makes the interface more pronounced and its effects are more clearly demonstrated. The concentration profile for this case is plotted along with the $\bar{u}$-velocity profile and the density profile in Figure 30. Notice from the no-injection velocity profile in Figure 28 that the interface occurs approximately at the outer edge of the boundary layer, that is, the interface occurs where the viscous effects are small. If the flow is assumed to be totally inviscid and recognizing that the pressure change across the shock-layer is small, the following relation can be found from the isentropic perfect gas relations:

$$\frac{u_I^2}{u_A^2} = \frac{(T_o)_I}{(T_o)_A} \frac{m_A}{m_I} , \tag{6.3}$$

where $(T_o)_I$ and $(T_o)_A$ are the total temperatures along the stagnation streamlines coming from the body and the shock, respectively. Using this relation, one can find the respective velocities of the air and helium at the interface, knowing the total temperatures and molecular weights. In our case, since the temperature profiles are smooth, the total temperatures should be approximately the same at the interface and the ratio of the velocities would tend to be inversely proportional to the square root of their molecular weights. This indicates that the injected gas velocity would tend to be greater than the air velocity because of the smaller molecular weight of the helium. Figure 30 clearly shows that this is what the velocities in the two gas regions are tending to do. However, viscous effects are, in fact, present and

these viscous effects turn the two velocity profiles together, creating the inflection region shown in the helium velocity profile. As would be expected, the stagnation point for the stagnation streamline is at this inflection point. A similar relation can be found to explain the sharp changes in the density profile.

The argon injection does not exhibit this inflection region, probably because, due to the similarity of the molecular weights of argon and air, the effect is small and is "smeared out" by the viscous effects. The effect of this interface on the $\bar{u}$-velocity profile downstream is probably the cause of the small increase in wall shear stress for helium over the no-injection case indicated in Figures 34, 42, and 48.

Summary

A summary of what has been accomplished by this study and what its contributions are seems appropriate as a conclusion to this chapter. Other studies of inert gas injection across surfaces of bodies in hypersonic flow have found solutions to the boundary-layer equations or have done stagnation region studies using viscous shock-layer equations. Boundary-layer solutions have two drawbacks that hinder their usefulness in a study of the type undertaken here. First, boundary-layer solutions are limited to high Reynolds numbers and therefore are not valid for the higher altitudes studied here where Reynolds numbers are low, see Figure 4. Second, boundary-layer theory does not take into account the effect of the blown boundary-layer on the inviscid flow conditions. For instance, Moore and Lee (1967) used boundary-layer theory to study

discontinuous injection of inert gases across the surface of a sharp cone and found that the heat transfer returned to its no injection value a short distance downstream of where the injection went to zero. Inger and Sayano (1969) did an approximate solution to the boundary-layer equations for discontinuous injection of air into air across a blunted cone but approximately allowed for the effect of the blown boundary layer on the inviscid stream. They found that the heat transfer did not return to its no injection value, but the decrease in heat transfer continued downstream. It is not clear from these investigations what the downstream effect of stagnation region injection is on heat transfer and wall shear stress. However, by solving the viscous shock-layer equations used in this study which are valid for the entire shock-layer, that is to say, for both the viscous and inviscid flow, the correct conclusions are obvious. The effect of the blown boundary layer on the inviscid flow is taken into account exactly as part of the solution and, as presented earlier, it was found that in cases where the shock shape and shock stand-off distance were not changed significantly downstream of the injection the heat transfer returned to its no injection value shortly after the injection rate went to zero. However, in cases where the shock shape and shock stand-off distance are altered downstream by the injection, the heat transfer remains below its no injection value well downstream of the injection for the injection distributions used in this study.

The results of this study are in agreement with the stagnation region results of inert gas injection using the viscous shock-layer

equations. For instance, they are in agreement with the conclusions of Chen, Aroesty, and Mobley (1967) that helium is the most effective injectant and that relatively small amounts of injection can result in large reductions in the stagnation region heat transfer. An additional result found in the present study, as presented earlier, was that for sufficiently high stagnation region injection rates the peak heat transfer can occur away from the stagnation region. Stagnation region studies obviously cannot show this and could lead to erroneous conclusions about the maximum heat transfer.

Therefore, the principal contributions of this study are that by solving a more complete and more exact set of equations, it has been possible to find solutions for lower Reynolds numbers than previously possible and to extend and clarify previous results at higher Reynolds numbers.

REFERENCES

Bird, R.B., Stewart, W.E. and Lightfoot, E.N., (1960) Transport Phenomena, John Wiley and Sons, Inc., New York, London, Sydney.

Blottner, F.G. and Flügge-Lotz, I., (1963) "Finite Difference Computation of the Boundary Layer with Displacement Thickness Interaction," Journal de Mecanique, Vol. II, No. 4.

Blottner, F.G., (1964) "Non-Equilibrium Laminar Boundary-Layer Flow of Ionized Air," G.E. Space Sciences Laboratory, Report No. R64SD56.

Brahinsky, H S. and Neel, C.A., (1969) "Tables of Equilibrium Thermodynamic Properties of Air, Vol. II, Constant Pressure," ARO, Inc., Report No. AEDC-TR-69-89.

Chen, S.Y., Aroesty, J. and Mobley, R., (1967) "The Hypersonic Viscous Shock Layer with Mass Transfer," Int. Journal of Heat Mass Transfer, Vol. 10, pp. 1143-1158.

Cheng, H.K., (1963) "The Blunt-Body Problem in Hypersonic Flow at Low Reynolds Number," CAL Report No. AF-1285-A10.

Davis, R.T., (1970a) "Hypersonic Flow of a Chemically Reacting Binary Mixture Past a Blunt Body," AIAA Paper No. 70-805, Los Angeles.

Davis, R.T., (1970b) "Numerical Solution of the Hypersonic Viscous Shock-Layer Equations," AIAA Journal, Vol. 8, No. 5, pp. 843-851.

Dommett, R.L., (1956) "Thermodynamic Properties of Air at High Temperatures," RAE-TN-GW429.

Eucken, A., (1913) Physik Z, 14, pp. 324-332.

Fay, J.A. and Riddell, F.R., (1958) "Theory of Stagnation Point Heat Transfer in Dissociated Air," Journal of the Aeronautical Sciences, Vol. 25, No. 2, pp. 73-85.

Hansen, C.F., (1953) "Note on the Prandtl Number for Dissociated Air," Journal of the Aeronautical Sciences, Vol. 20, No. 11, pp. 789-790.

Hansen, C.F., (1958) "Approximations for the Thermodynamic and Transport Properties of High Temperature Air," NACA TN 415.

Hayes, W.D. and Probstein, R.F., (1959) Hypersonic Flow Theory, Academic Press, New York and London.

Inger, G.R. and Sayano, S., (1969) "Effects of Gaseous Injection on the Hypersonic Flow Around Transpiration-Cooled Bodies," Journal of Spacecraft and Rockets, Vol. 6, No. 6, pp. 649-653.

Jaffe, N.A., Lind, R.C. and Smith, A.M.O., (1967) "Solution to the Binary Diffusion Laminar Boundary-Layer Equations with Second-Order Transverse Curvature," AIAA Journal, Vol. 5, No. 9, pp. 1563-1569.

Kogan, M.V., (1969) Rarefield Gas Dynamics, Plenum Press, New York.

Lewis, C.H., Adams, J.C. and Gilley, G.E., (1968) "Effects of Mass Transfer and Chemical Non-Equilibrium on Slender Blunted Cone Pressure and Heat-Transfer Distributions at M = 13.2," ARO Inc. Report No. AEDC-TR-68-214.

Lewis, C.H., (1970) Department of Aerospace Engineering, V.P.I.S.U., Private Communication, February 1970.

Moore, J.A. and Lee, J.T., (1967) "Discontinuous Injection of Inert Gases Into the Non-Equilibrium Laminar Boundary Layer," TRW Systems Inc., Report No. 063886018-R000.

Owczarek, J.A., (1964) Fundamentals of Gas Dynamics, International Textbook Co., Scranton, Pennsylvania.

Pappas, C.C. and Lee, G., (1969) "Effects of Mass Addition of Various Gases on the Heat Transfer and Surface Pressures on a Blunt Cone in Hypersonic Flow," AIAA Paper No. 69-716.

Patterson, G.N., (1965) Molecular Flow of Gases, John Wiley and Sons, Inc., New York.

Richtmyer, R.D., (1957) Difference Methods for Initial-Value Problems, Interscience Publishers, Inc., New York.

Shidlovskiy, V.P., (1967) Introduction to Dynamics of Rarefied Gases, American Elsevier Publishing Company Inc., New York, London, Amsterdam.

Street, R.E., (1960) "A Study of Boundary Conditions in Slip-Flow Aerodynamics," Rarefied Gas Dynamics (F.M. Devienne ed.), Pergamon Press, London.

U.S. Standard Atmosphere, (1962), Prepared under the sponsorship of NASA, USAF, and U.S. Weather Bureau.

Van Dyke, M., (1962) "Second-Order Compressible Boundary-Layer Theory with Application to Blunt Bodies in Hypersonic Flow," Hypersonic Flow Research (Riddell ed.), Academic Press, New York and London.

Whitehead, R.E. and Davis, R.T., (1969) "Surface Conditions in Slip-Flow with Mass Transfer," VPI School of Engineering Report No. VPI-E-69-11.

Wilke, C.R., (1950) "A Viscosity Equation for Gas Mixtures," J. Chem Phys., Vol. 18, pp. 517-519.

TABLE I-a Constant Pressure Specific Heat for Equilibrium Air Polynomial Coefficients

	TEMPERATURE RANGE - °R	
	0 - 2000	2000 - 3600
A	6.0371797×10^{3}	5.9028×10^{3}
B	$-9.4509125 \times 10^{-4}$	3.77072×10^{-1}
C	$-7.3022675 \times 10^{-4}$	9.64644×10^{-5}
D	$1.73022675 \times 10^{-6}$	-3.53769×10^{-8}
E	$-9.7657438 \times 10^{-10}$	3.48567×10^{-12}
F	$1.74657438 \times 10^{-13}$	-1.11502×10^{-16}

TABLE I-b Constant Pressure Specific Heat for Equilibrium Air Chebyshev Polynomial Coefficients

	TEMPERATURE RANGE °R 3600 - 20000	
	NUMERATOR	DENOMINATOR
A_o	0.49201343×10^3	1.00
A_1	0.78021201×10^3	0.97773808
A_2	0.46964398×10^3	0.43336467
A_3	0.37374505×10^3	0.55080246
A_4	0.42086184×10^3	0.56509599
A_5	0.42461222×10^3	0.6774741
A_6	0.31140219×10^3	0.39786704
A_7	0.15603035×10^3	0.25102755
A_8	0.44998477×10^2	$0.74115587 \times 10^{-2}$
A_9	0.43201901×10^1	$-0.53310891 \times 10^{-1}$

TABLE II Viscosity Curve Fit Coefficients

	A	B	C
N_2	0.048349	-0.022485	-9.9827
O_2	0.038271	0.021076	-9.5986
A_r	-0.014926	0.96839	-13.4721
H_e	0.0436198	0.131627	-10.7283

TABLE III Binary Diffusion Curve Fit Coefficients

	A	B	C
$N_2 - A_r$	0.0002744	1.7118	-11.3695
$N_2 - H_e$	0.0207088	1.4389	-9.1830

TABLE IV MASS INJECTION RATES

Total Mass Injection (lbm/sec)	Altitude (ft x 10^{-3})								
	300	275	250	225	200	175	150	125	100
	$(\rho_w v_w)_{s.p.}$								
.199 x 10^{-5}	.1								
.398	.2								
.597	.3								
.796	.4								
.800		.1							
.16[illegible] x 10^{-4}		.2							
.2[illegible]		.3							
.3[illegible]			.1						
.320		.4							
.604			.2						
.755			.25						
.966			.3	.103					
.128 x 10^{-3}			.4						
.176				.2					
.264				.3	.117	.0465			
.352				.4					
.452					.2				
.570						.1			
.678					.3	.119	.0458	.0155	.0048
.904					.4				
.114 x 10^{-2}						.2	.077	.026	.008
.148							.1		
.171						.3			

TABLE V. FREE STREAM CONDITIONS

Altitude (ft.)	T_∞ (°R)	ρ_∞ (slugs/ft^3)	P_∞ (lbf/ft^2)
300K	332.90	4.625×10^{-9}	2.641×10^{-3}
275K	325.17	1.918×10^{-8}	1.070×10^{-3}
250K	351.18	7.033×10^{-8}	3.842×10^{-2}
225K	405.47	2.051×10^{-7}	1.291×10^{-1}
200K	456.99	5.270×10^{-7}	3.470×10^{-1}
175K	483.94	1.324×10^{-6}	9.950×10^{-1}
150K	479.07	3.455×10^{-6}	2.571×10^{0}
125K	441.12	1.026×10^{-5}	7.027×10^{0}
100K	408.57	3.318×10^{-5}	2.105×10^{-1}

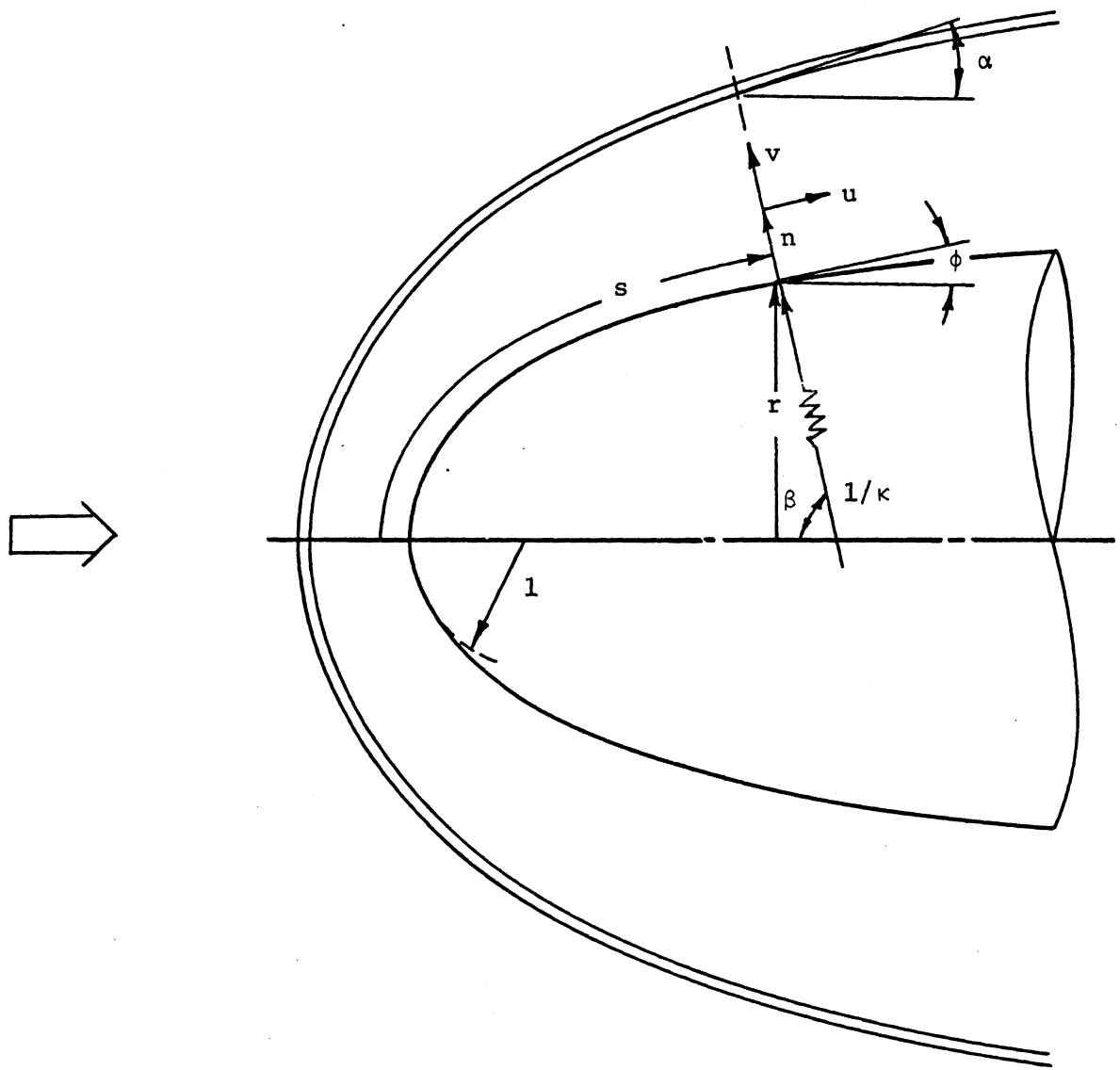

FIGURE 1 COORDINATE SYSTEM AND BODY GEOMETRY

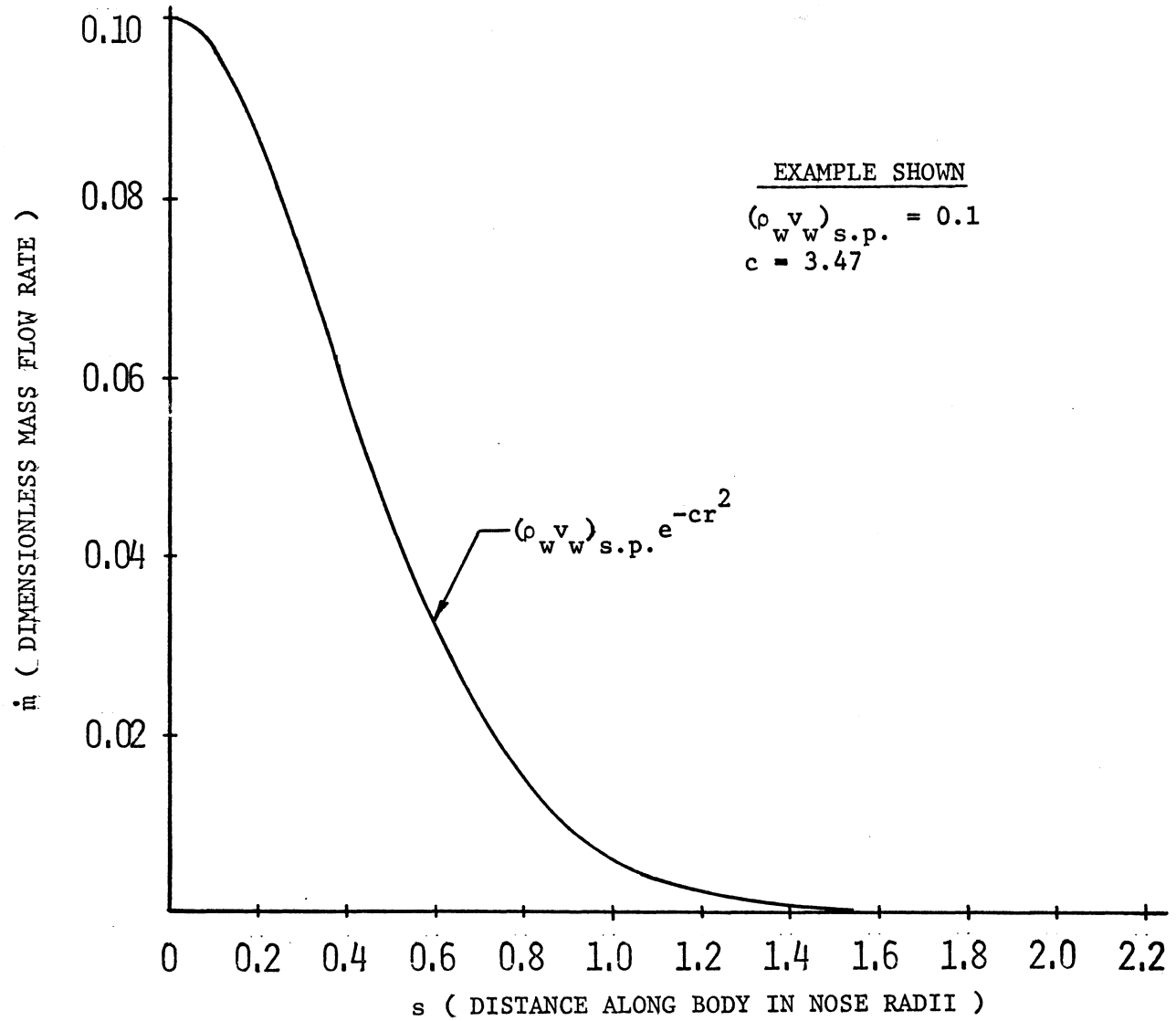

FIGURE 2 INJECTION MASS FLOW RATE DISTRIBUTION

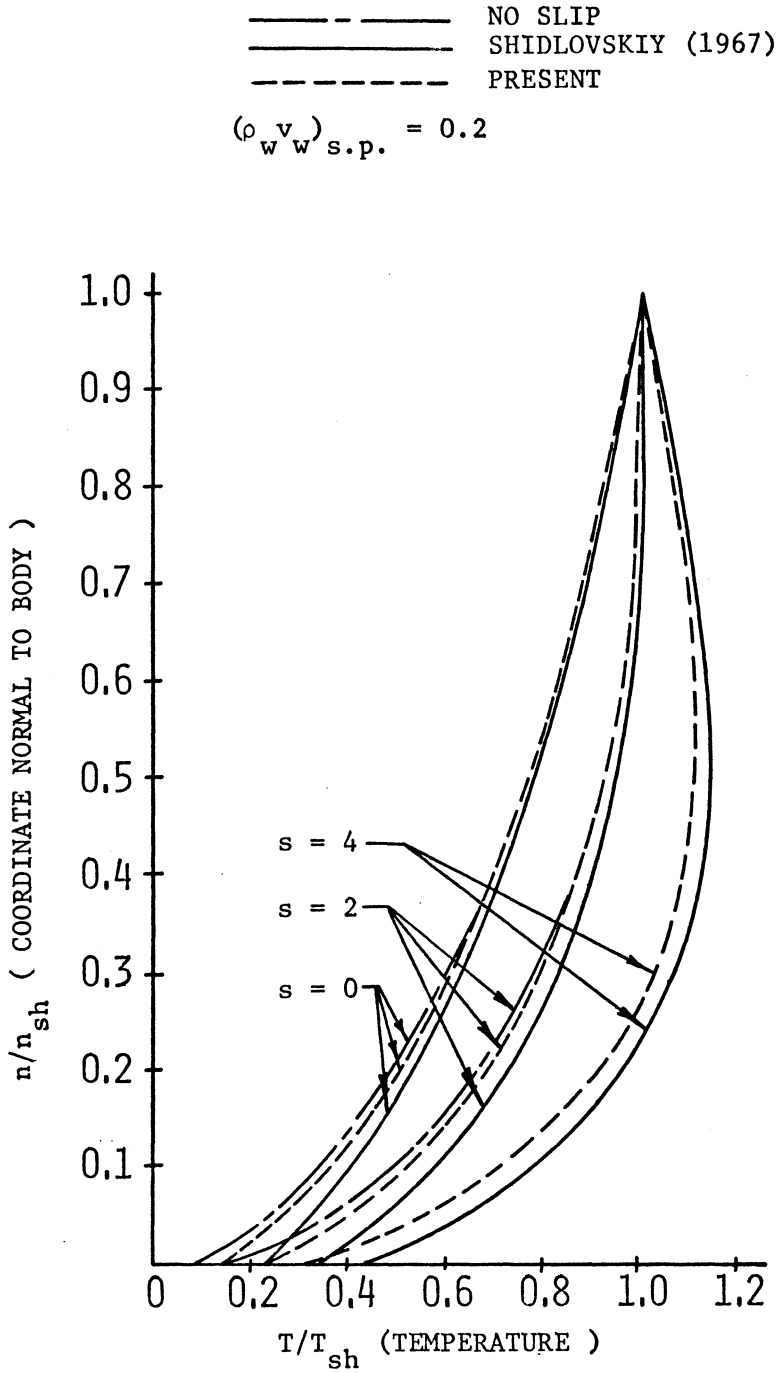

FIGURE 3 COMPARISON OF TEMPERATURE SLIP CONDITIONS FOR ARGON INJECTION FOR FROZEN AIR MODEL AT AN ALTITUDE OF 250,000 FT.

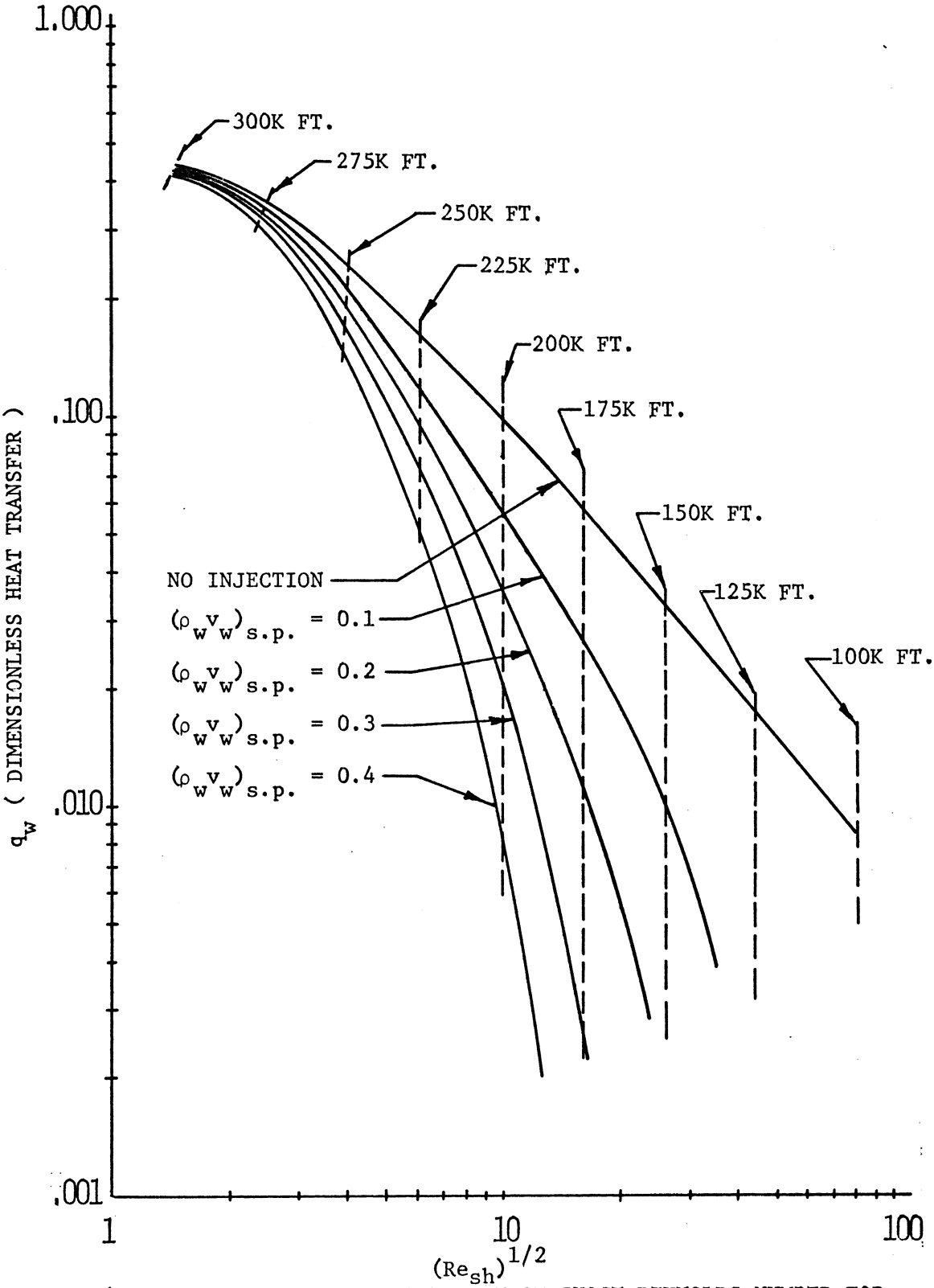

FIGURE 4 HEAT TRANSFER VS SQUARE ROOT OF SHOCK REYNOLDS NUMBER FOR ARGON INJECTION FOR FROZEN AIR MODEL

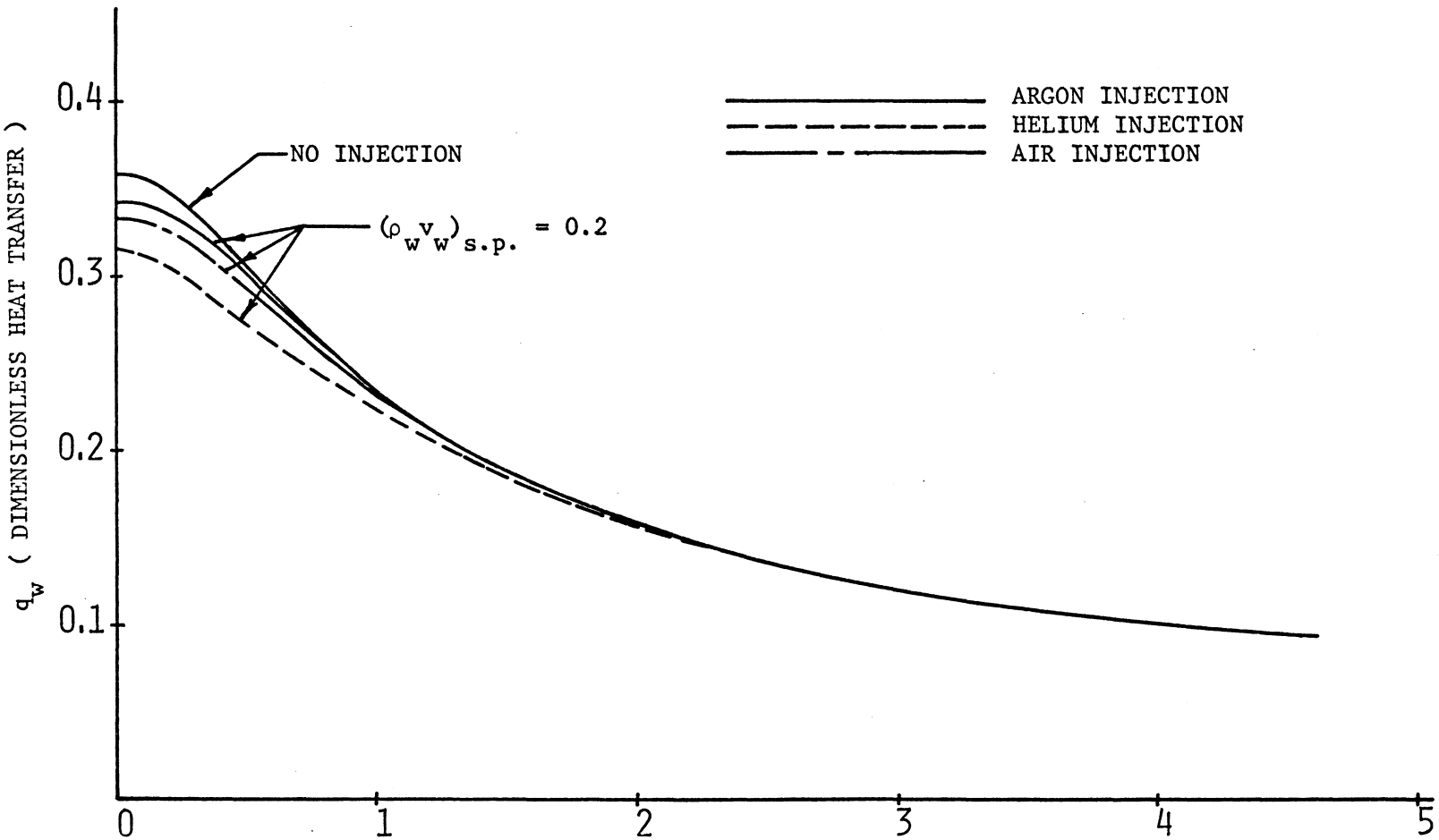

FIGURE 5 COMPARISON OF HEAT TRANSFER FOR DIFFERENT INJECTANTS FOR FROZEN AIR MODEL AT AN ALTITUDE OF 275,000 FT.

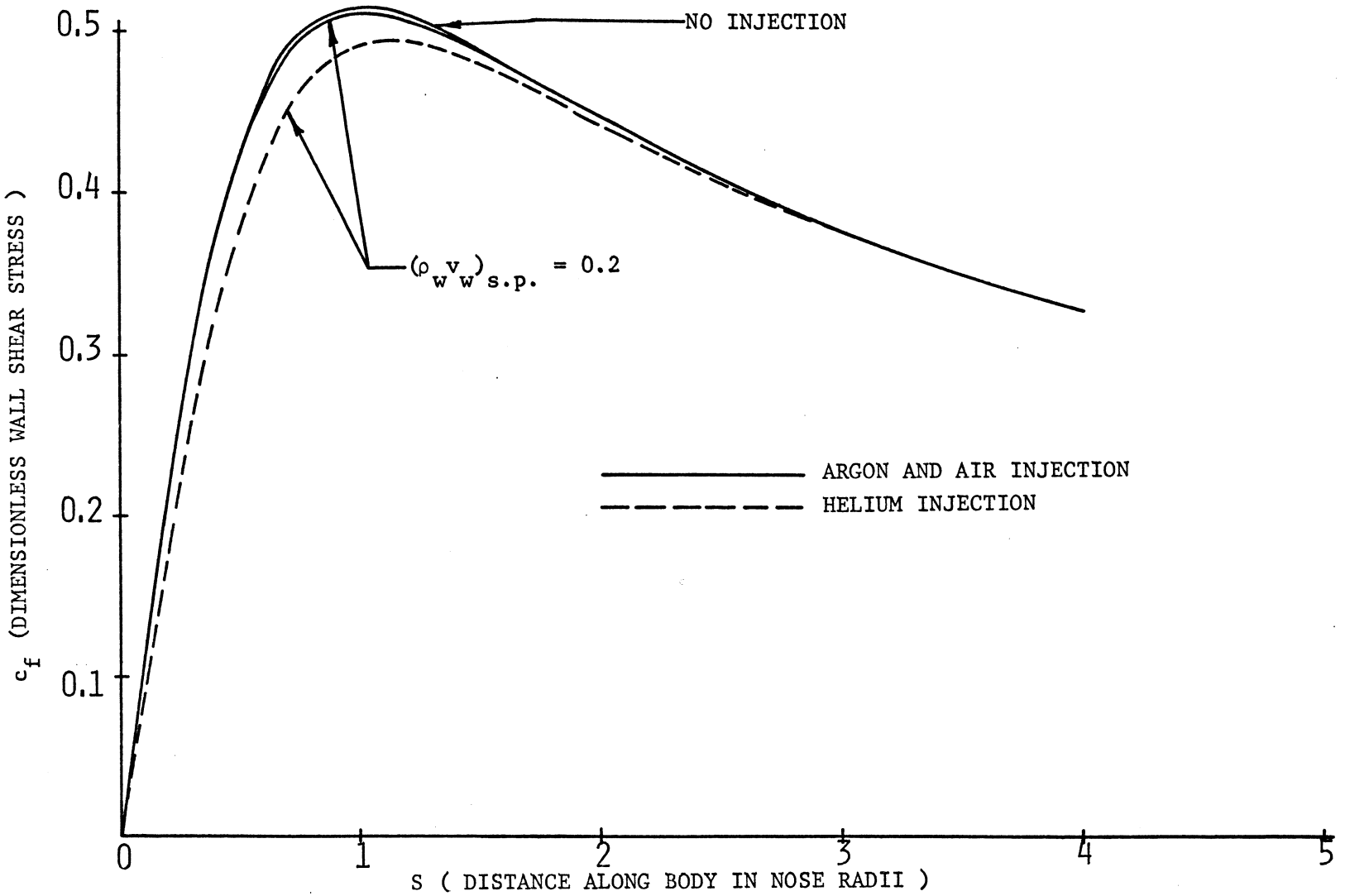

FIGURE 6 COMPARISON OF WALL SHEAR STRESS FOR DIFFERENT INJECTANTS FOR FROZEN AIR MODEL AT AN ALTITUDE OF 275,000 FT.

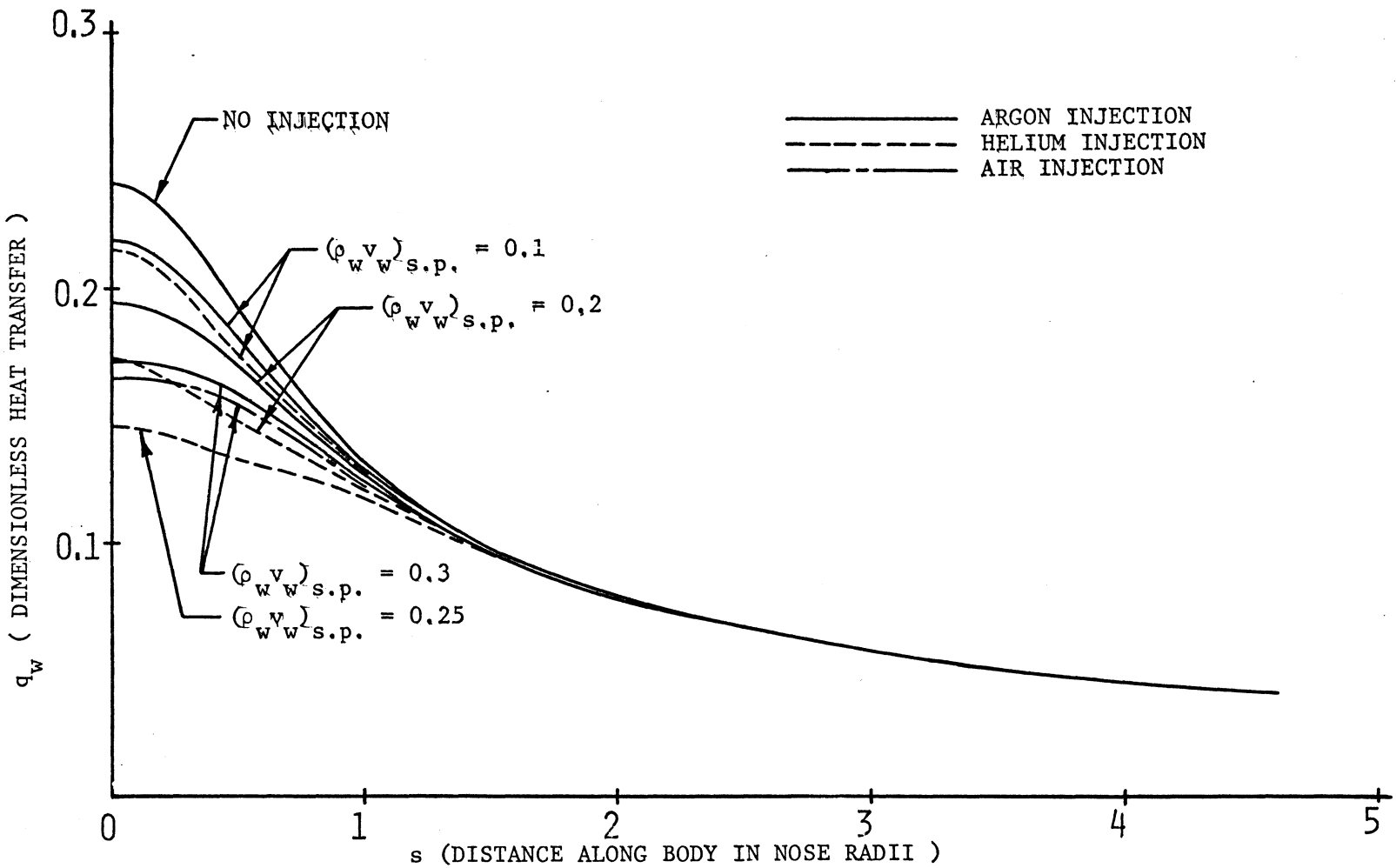

FIGURE 7 COMPARISON OF HEAT TRANSFER FOR DIFFERENT INJECTANTS FOR FROZEN AIR MODEL AT AN ALTITUDE OF 250,000 FT.

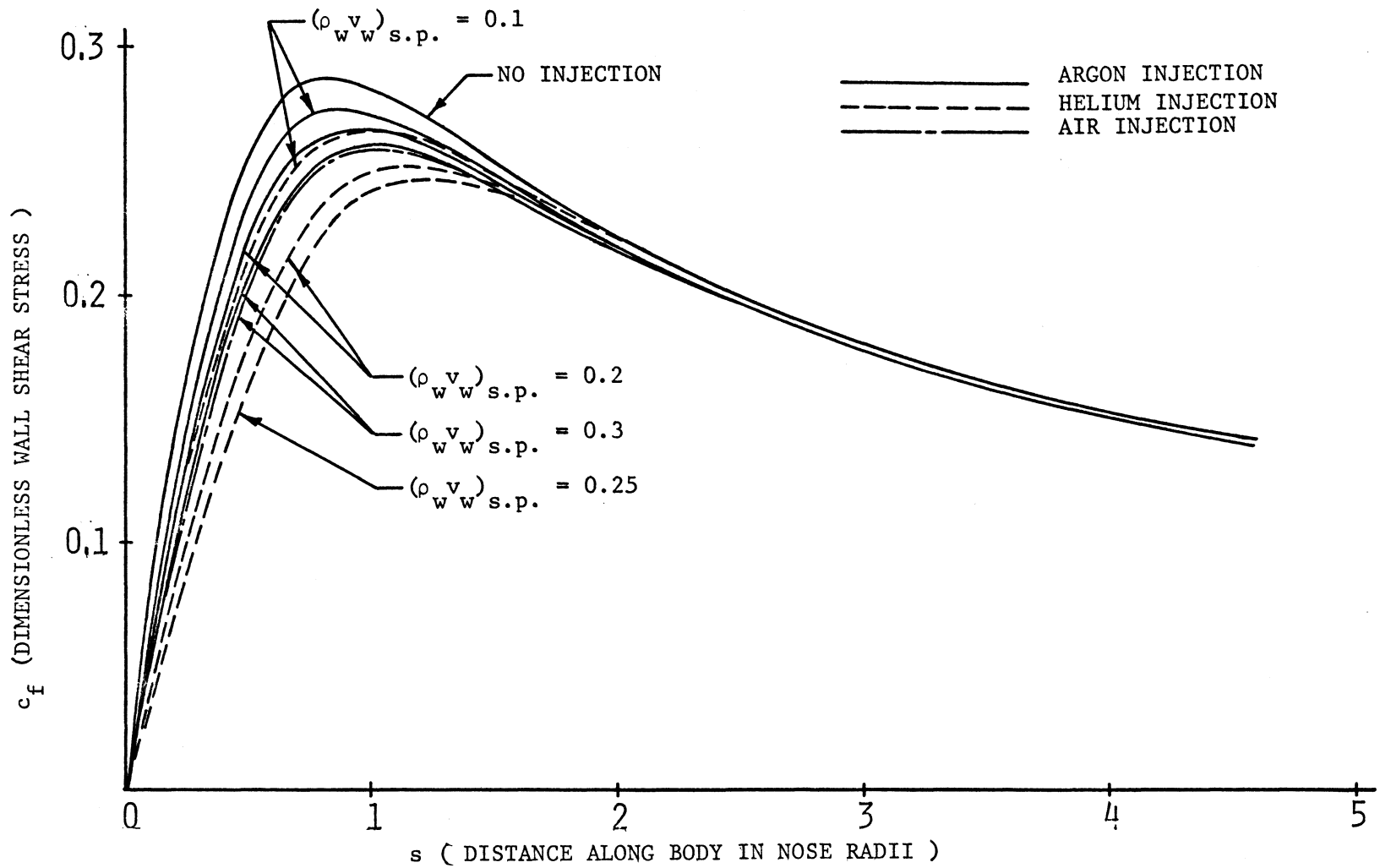

FIGURE 8 COMPARISON OF WALL SHEAR STRESS FOR DIFFERENT INJECTANTS FOR FROZEN AIR MODEL AT AN ALTITUDE OF 250,000 FT.

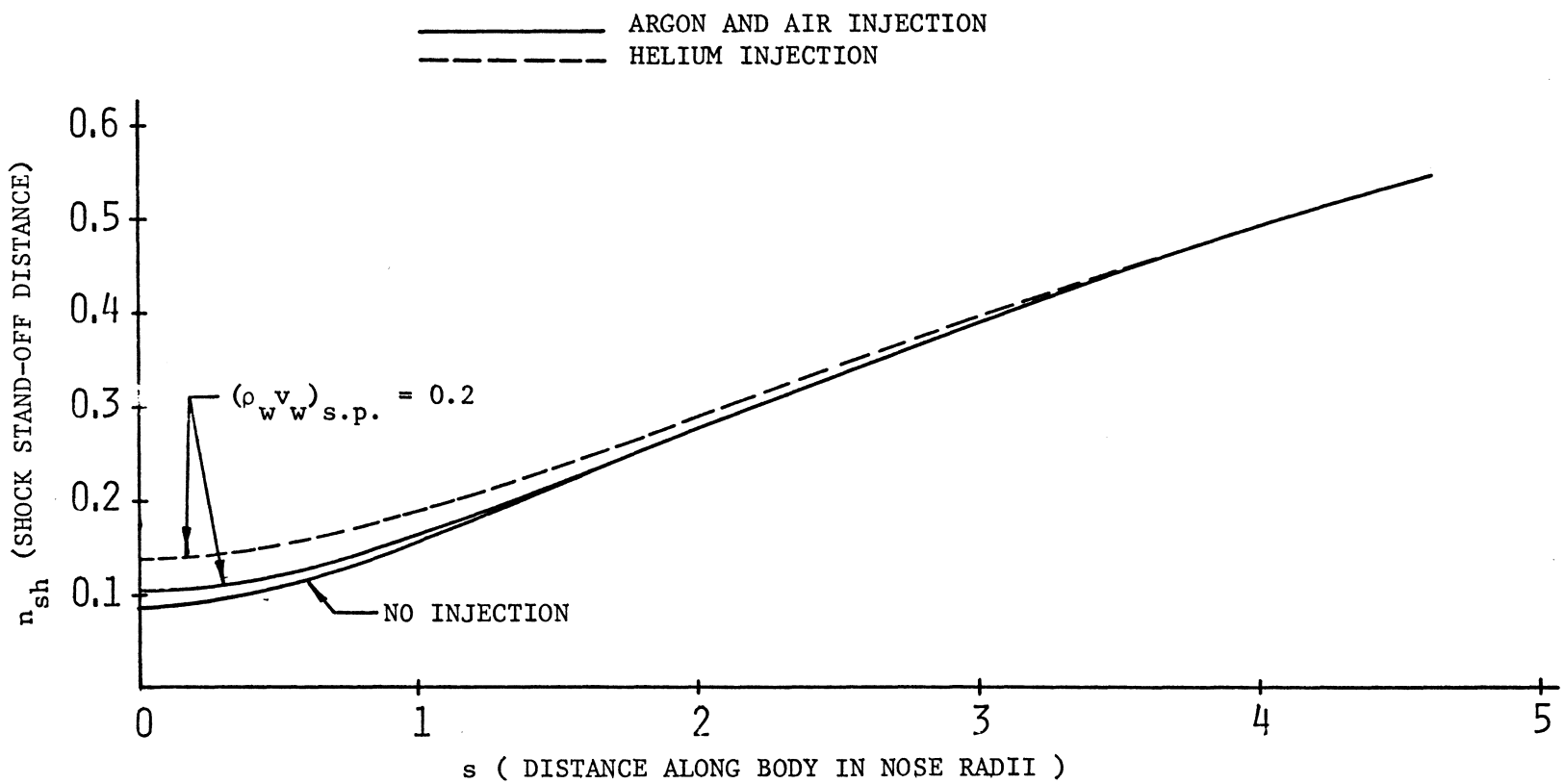

FIGURE 9 COMPARISON OF SHOCK STAND-OFF DISTANCE FOR DIFFERENT INJECTANTS FOR FROZEN AIR MODEL AT AN ALTITUDE OF 250,000 FT.

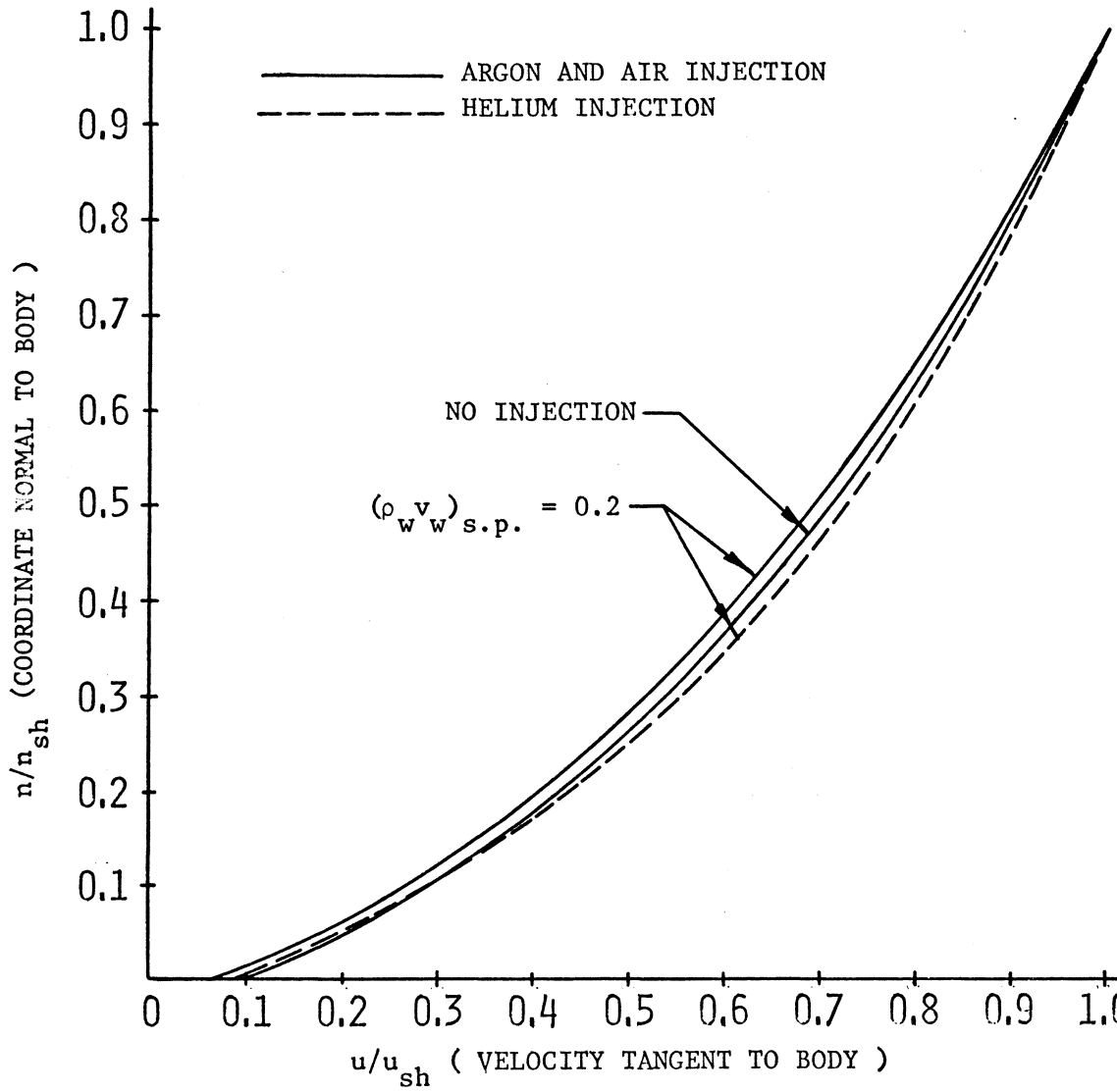

FIGURE 10 VELOCITY PROFILES AT STAGNATION POINT FOR DIFFERENT INJECTANTS FOR FROZEN AIR MODEL AT AN ALTITUDE OF 250,000 FT.

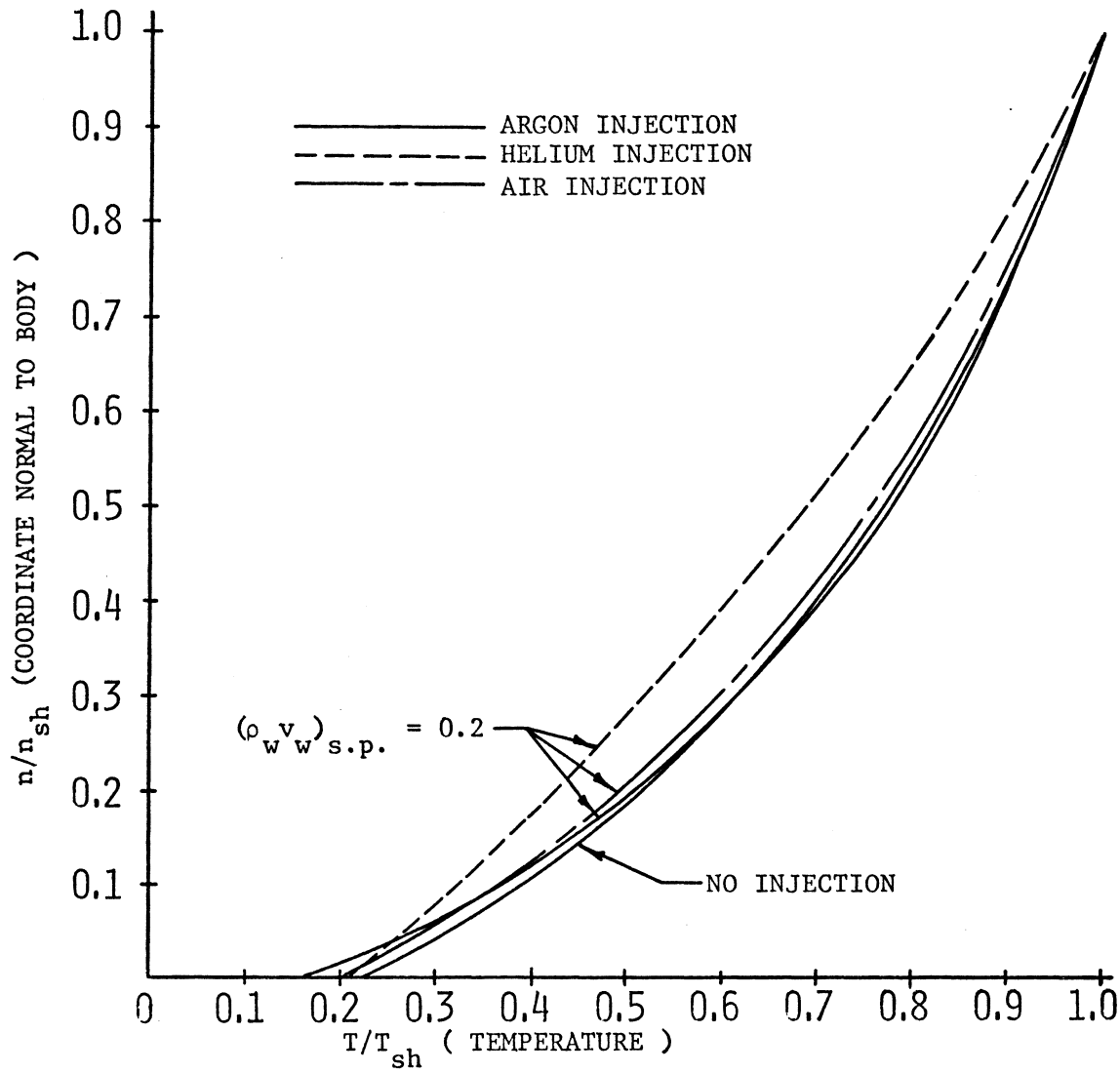

FIGURE 11 TEMPERATURE PROFILES AT STAGNATION POINT FOR DIFFERENT INJECTANTS FOR FROZEN AIR MODEL AT AN ALTITUDE OF 250,000 FT.

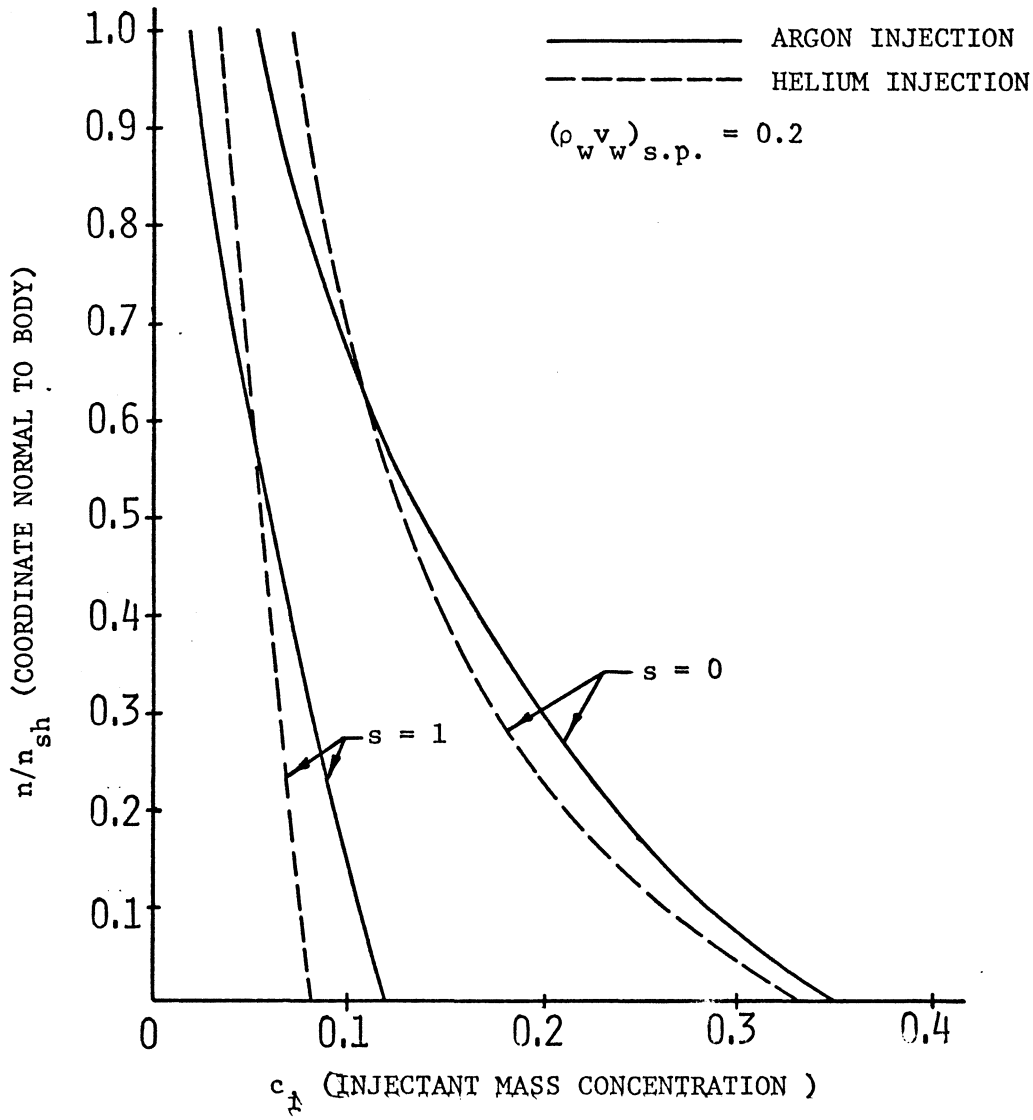

FIGURE 12 COMPARISON OF INJECTANT MASS CONCENTRATION FOR FROZEN AIR MODEL AT AN ALTITUDE OF 250,000 FT.

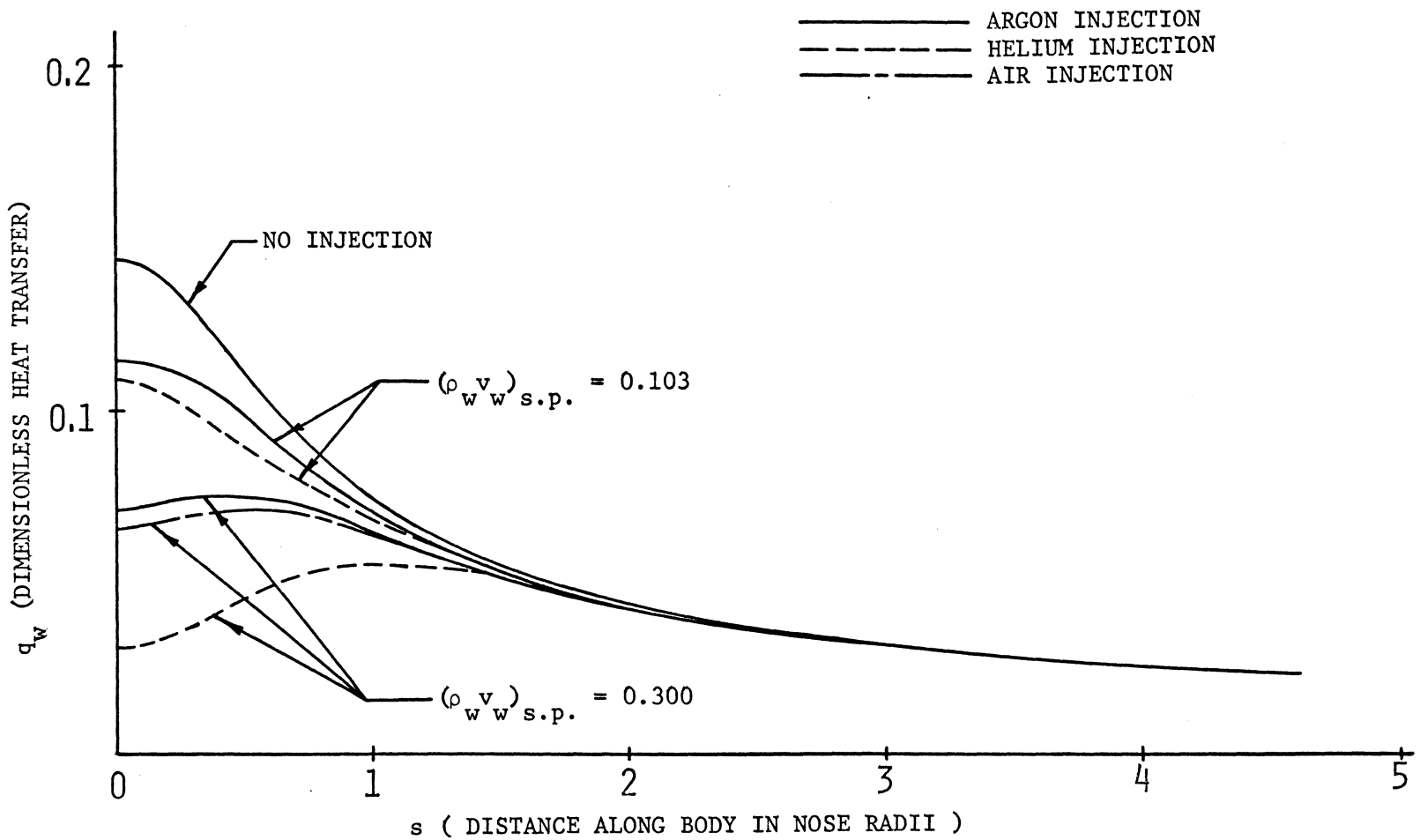

FIGURE 13 COMPARISON OF HEAT TRANSFER FOR DIFFERENT INJECTANTS FOR FROZEN AIR MODEL AT AN ALTITUDE OF 225,000 FT.

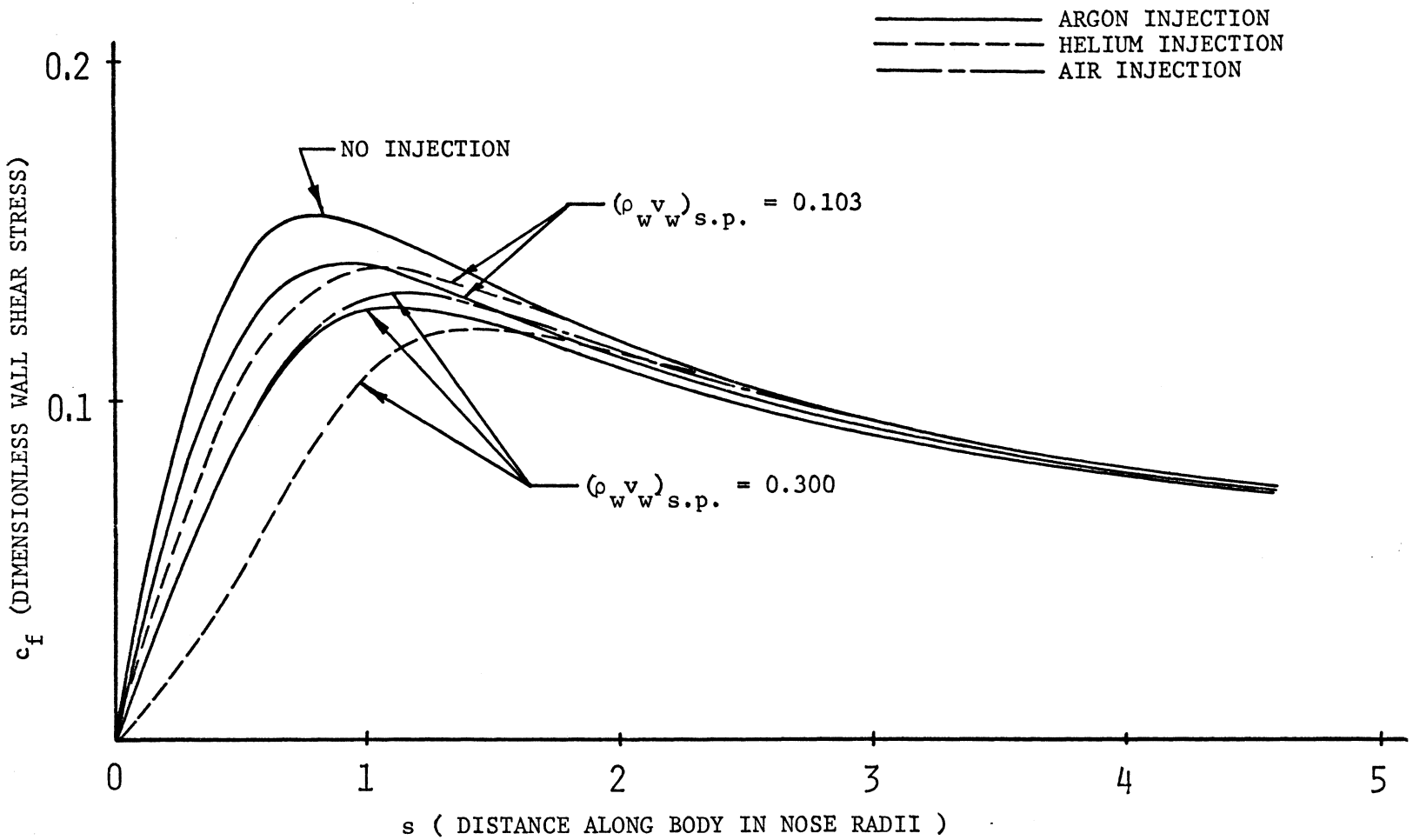

FIGURE 14 COMPARISON OF WALL SHEAR STRESS FOR DIFFERENT INJECTANTS FOR FROZEN AIR MODEL AT AN ALTITUDE OF 225,000 FT.

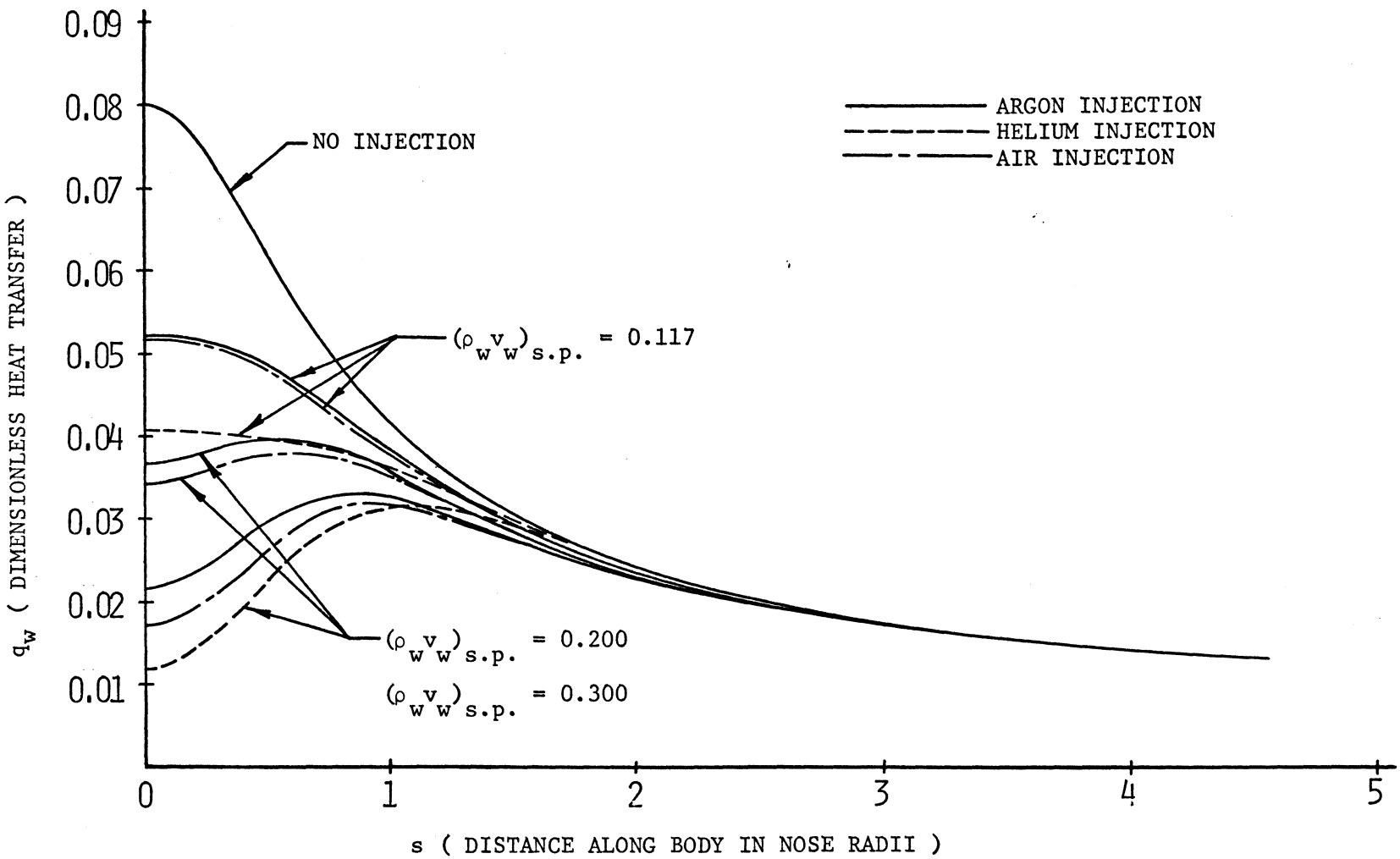

FIGURE 15 COMPARISON OF HEAT TRANSFER FOR DIFFERENT INJECTANTS FOR FROZEN AIR MODEL AT AN ALTITUDE OF 200,000 FT.

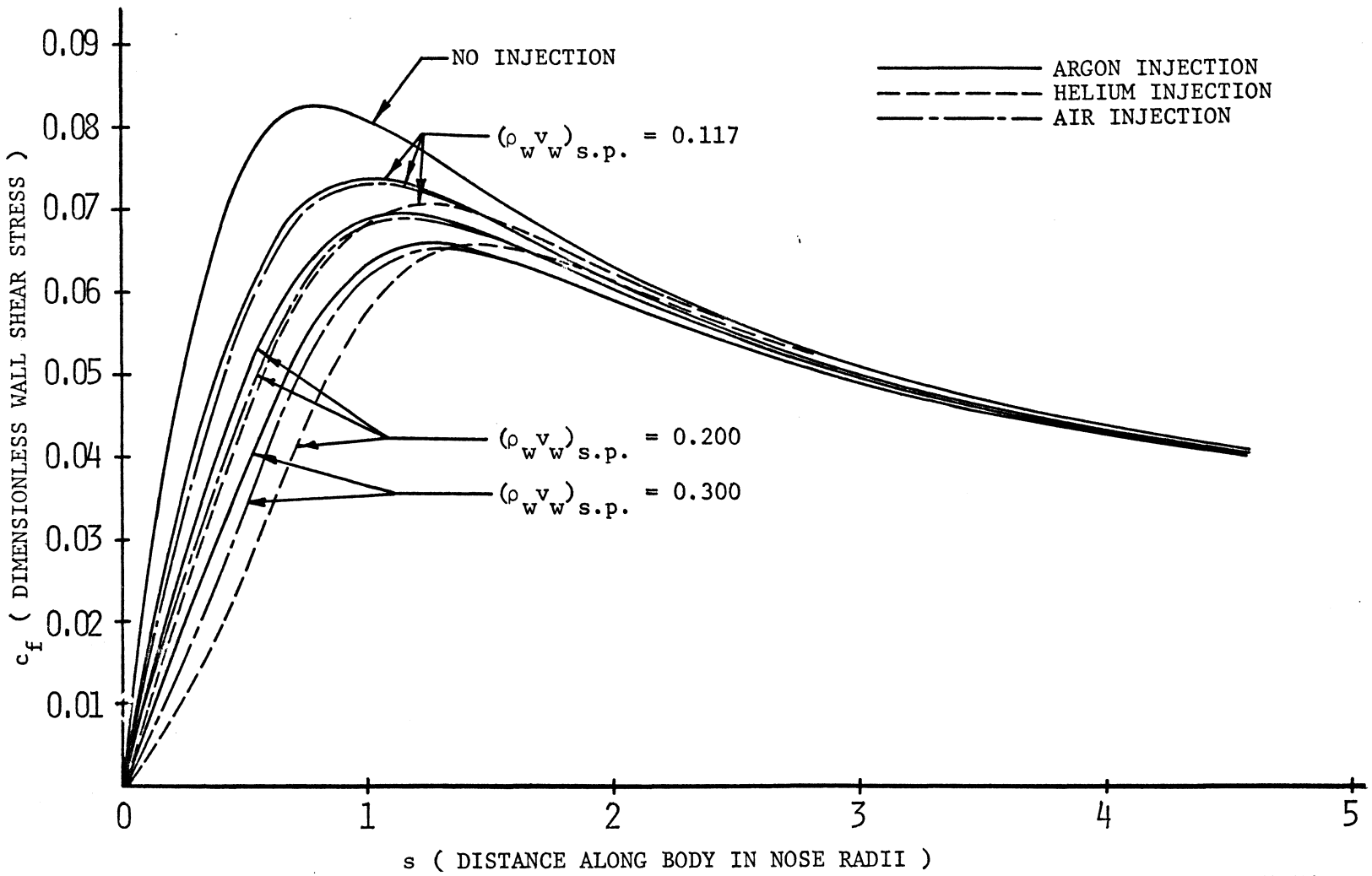

FIGURE 16 COMPARISON OF WALL SHEAR STRESS FOR DIFFERENT INJECTANTS FOR FROZEN AIR MODEL AT AN ALTITUDE OF 200,000 FT.

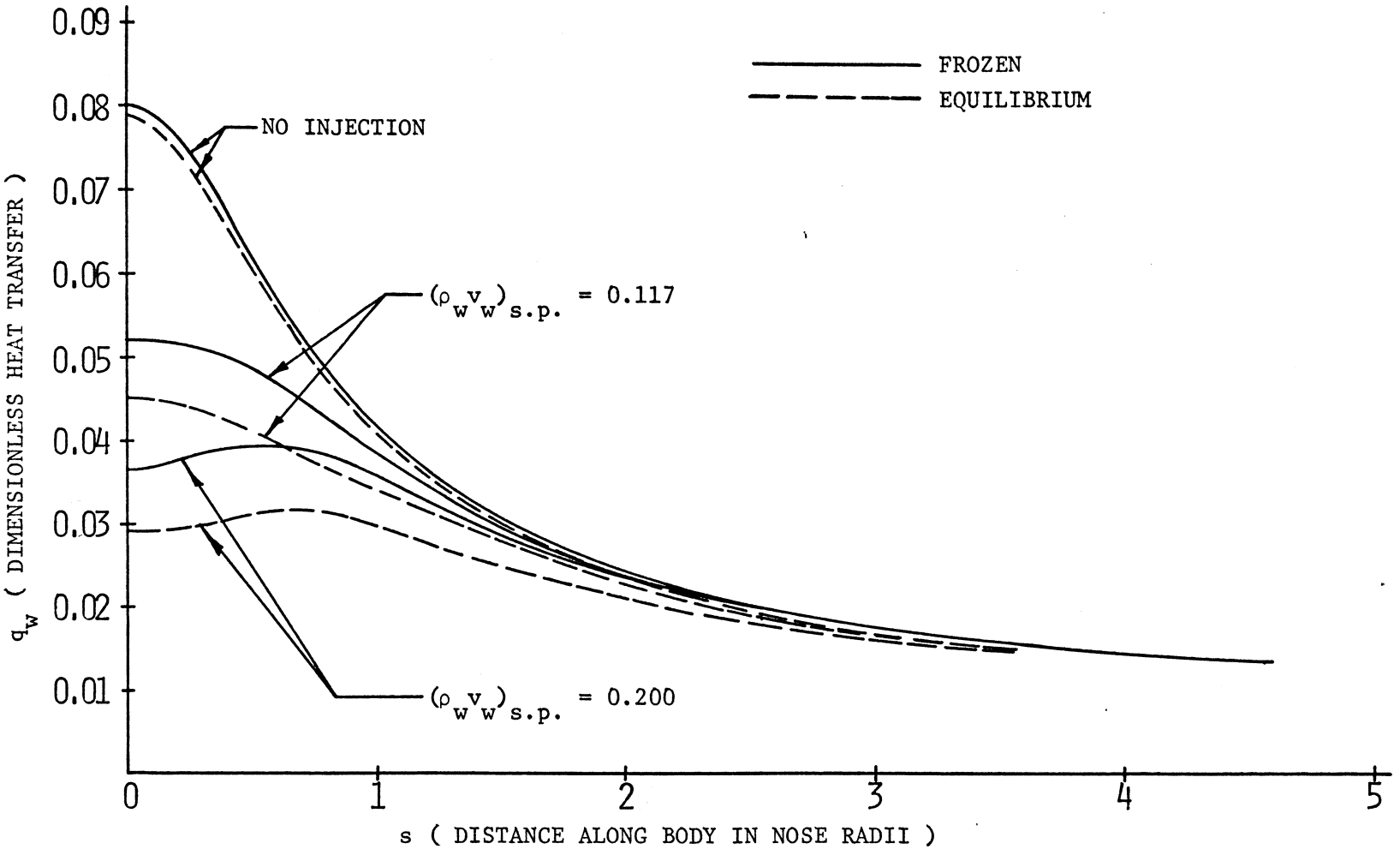

FIGURE 17 COMPARISON OF HEAT TRANSFER FOR EQUILIBRIUM AND FROZEN AIR MODELS WITH ARGON INJECTION AT AN ALTITUDE OF 200,000 FT.

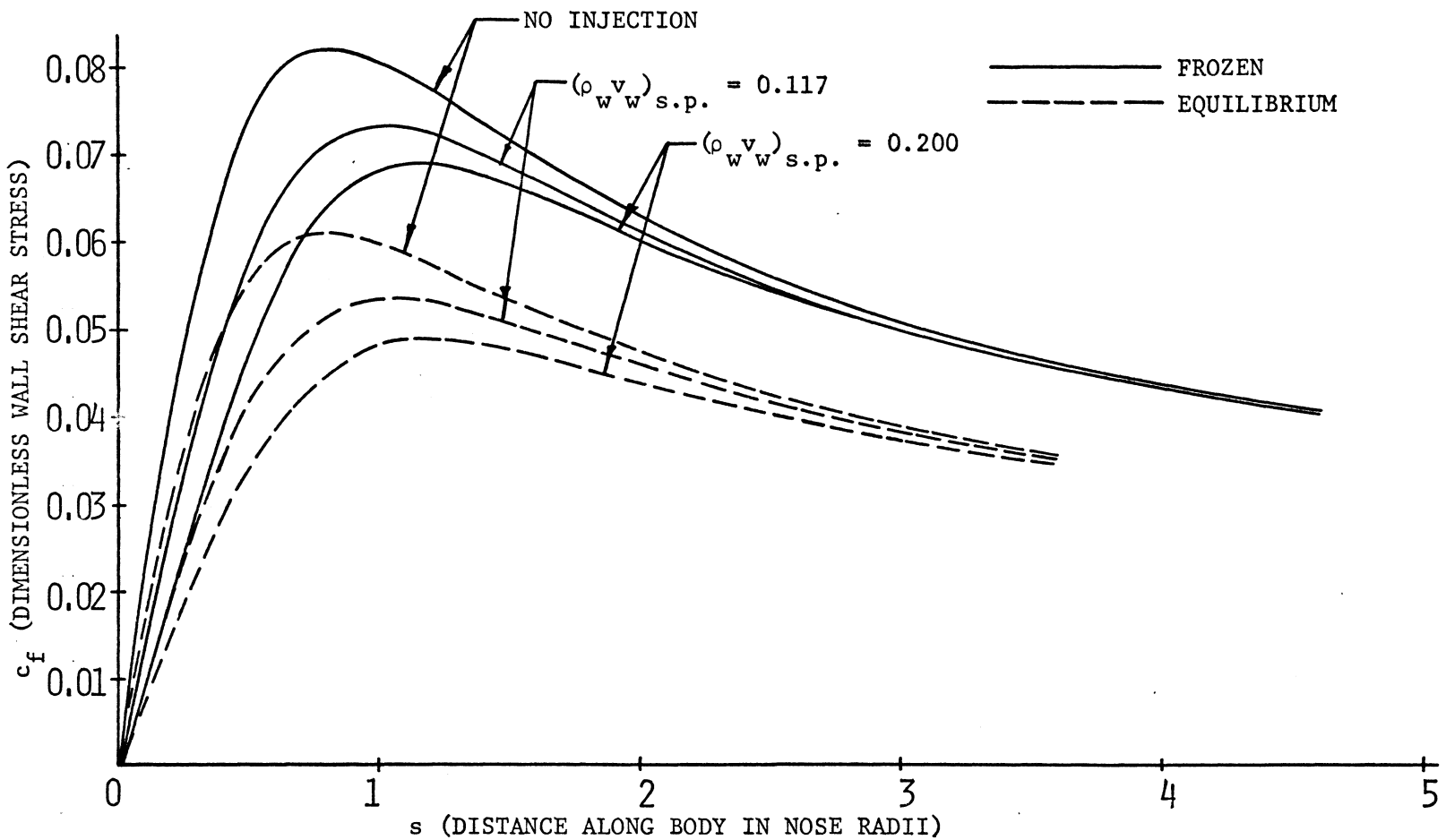

FIGURE 18 COMPARISON OF WALL SHEAR STRESS FOR EQUILIBRIUM AND FROZEN AIR MODELS WITH ARGON INJECTION AT AN ALTITUDE OF 200,000 FT.

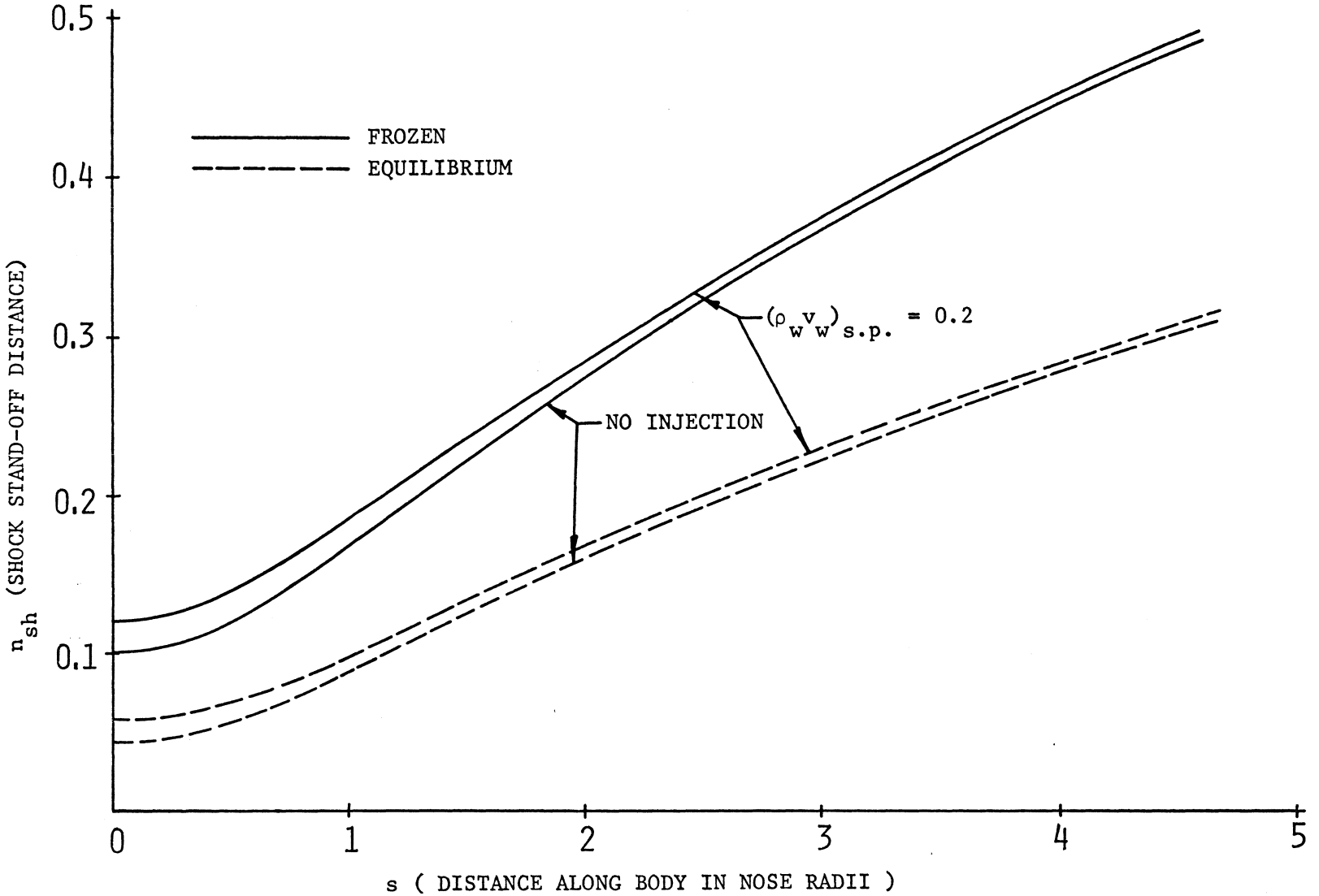

FIGURE 19 COMPARISON OF SHOCK STAND-OFF DISTANCE FOR EQUILIBRIUM AND FROZEN AIR MODELS WITH ARGON INJECTION AT AN ALTITUDE OF 200,000 FT.

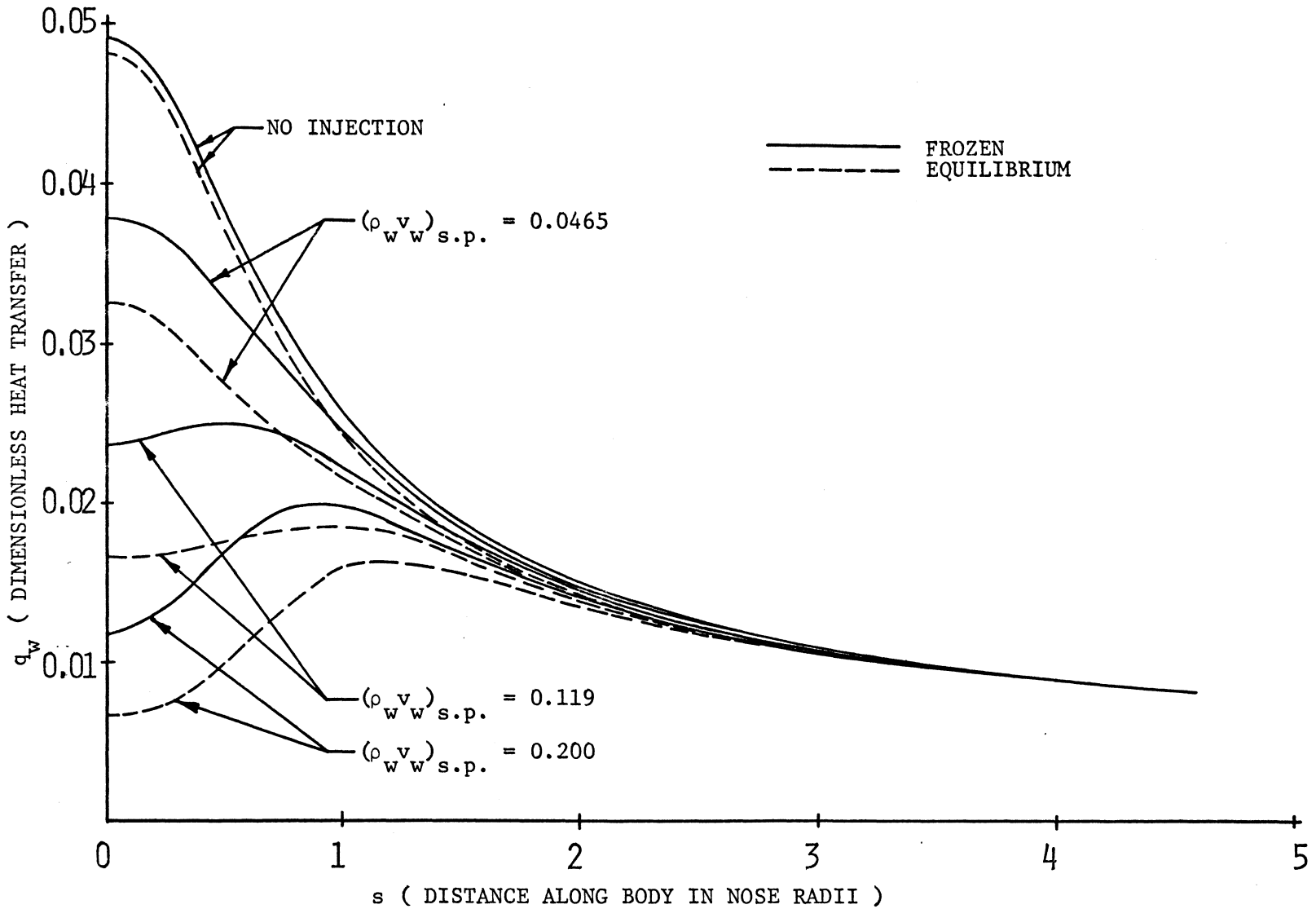

FIGURE 20 COMPARISON OF HEAT TRANSFER FOR FROZEN AND EQUILIBRIUM AIR MODELS WITH ARGON INJECTION AT AN ALTITUDE OF 175,000 FT.

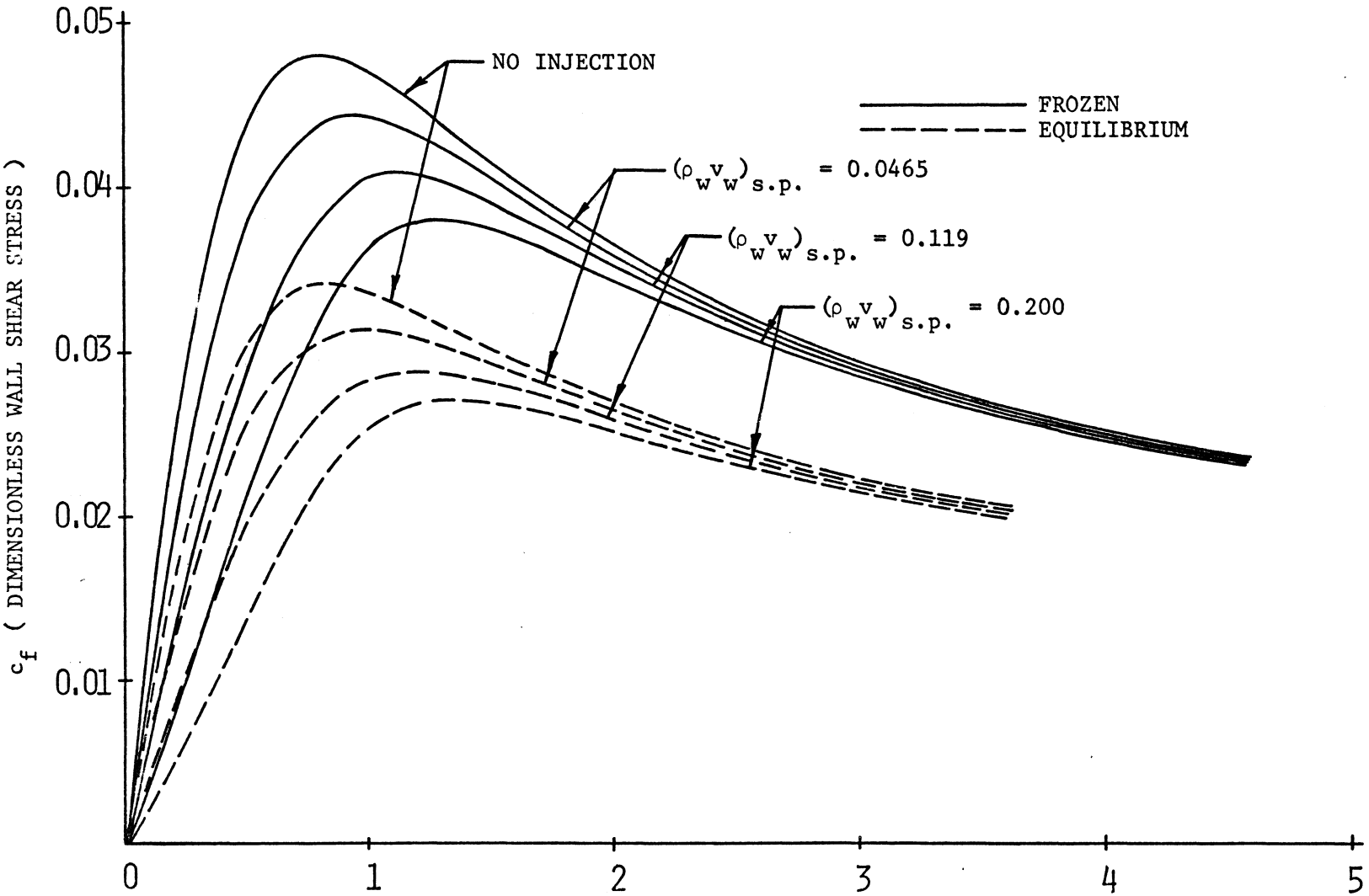

FIGURE 21 COMPARISON OF WALL SHEAR STRESS FOR EQUILIBRIUM AND FROZEN AIR MODELS WITH ARGON INJECTION AT AN ALTITUDE OF 175,000 FT.

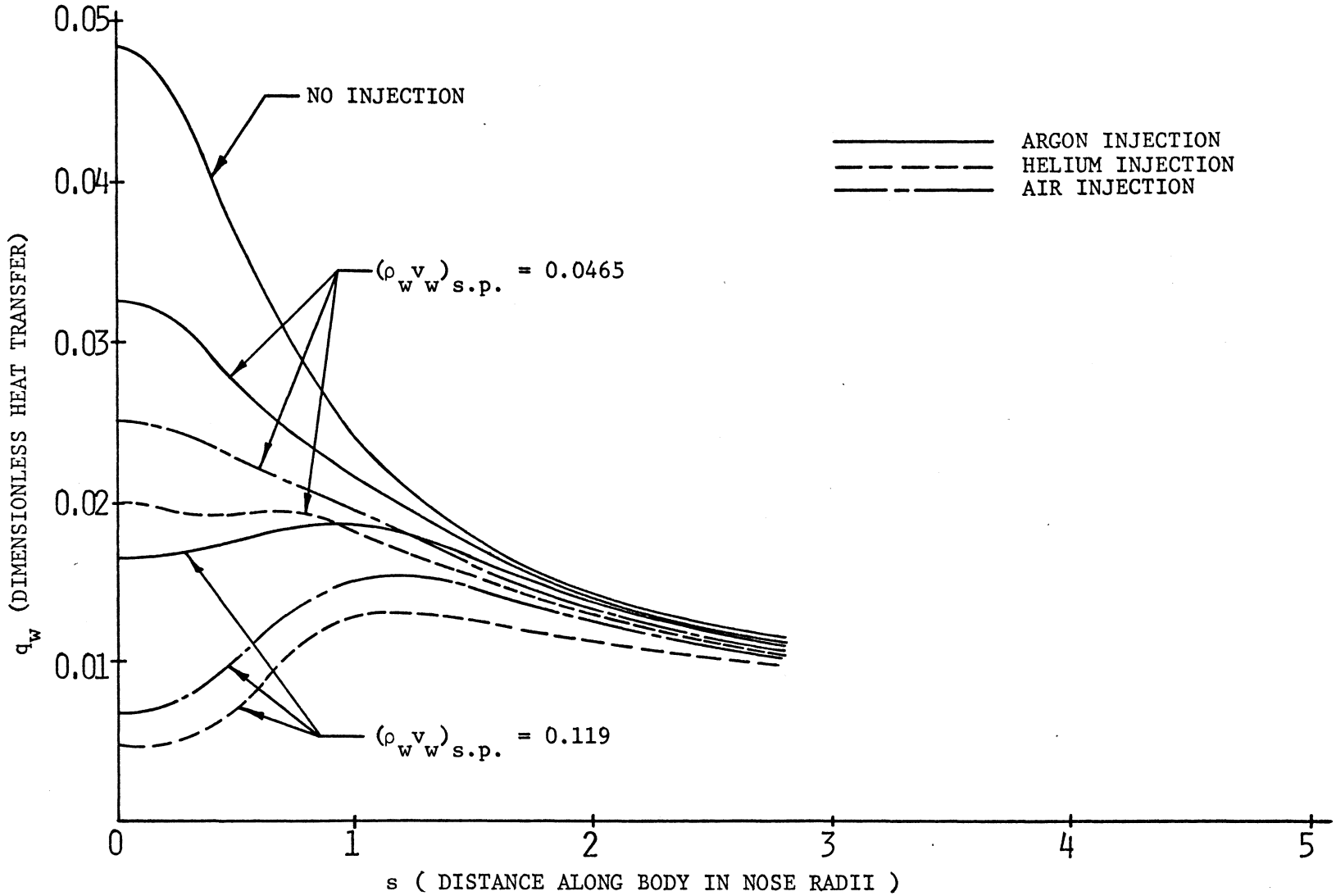

FIGURE 22 COMPARISON OF HEAT TRANSFER FOR DIFFERENT INJECTANTS FOR EQUILIBRIUM AIR MODEL AT AN ALTITUDE OF 175,000 FT.

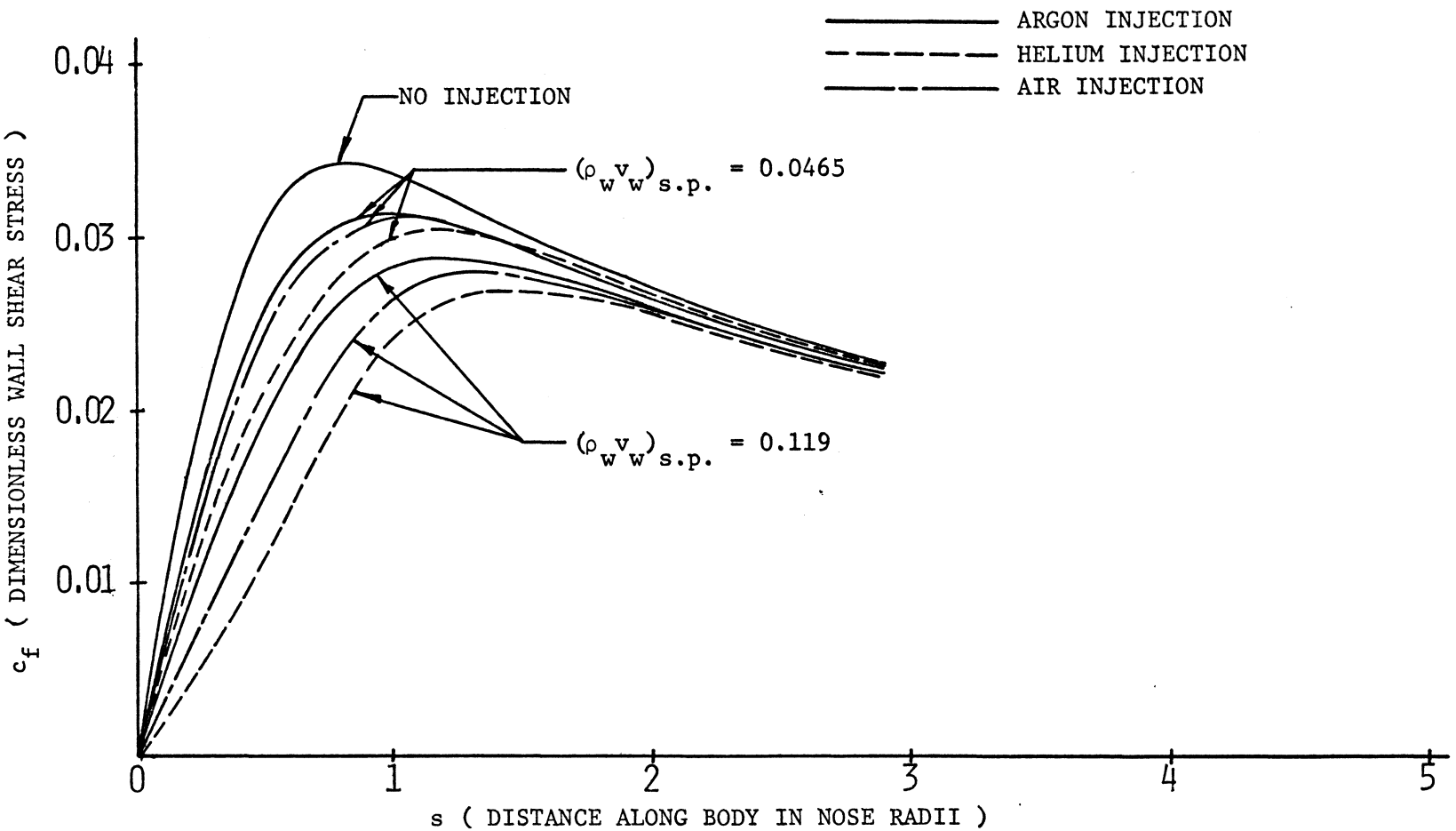

FIGURE 23 COMPARISON OF WALL SHEAR STRESS FOR DIFFERENT INJECTANTS FOR EQUILIBRIUM AIR MODEL AT AN ALTITUDE OF 175,000 FT.

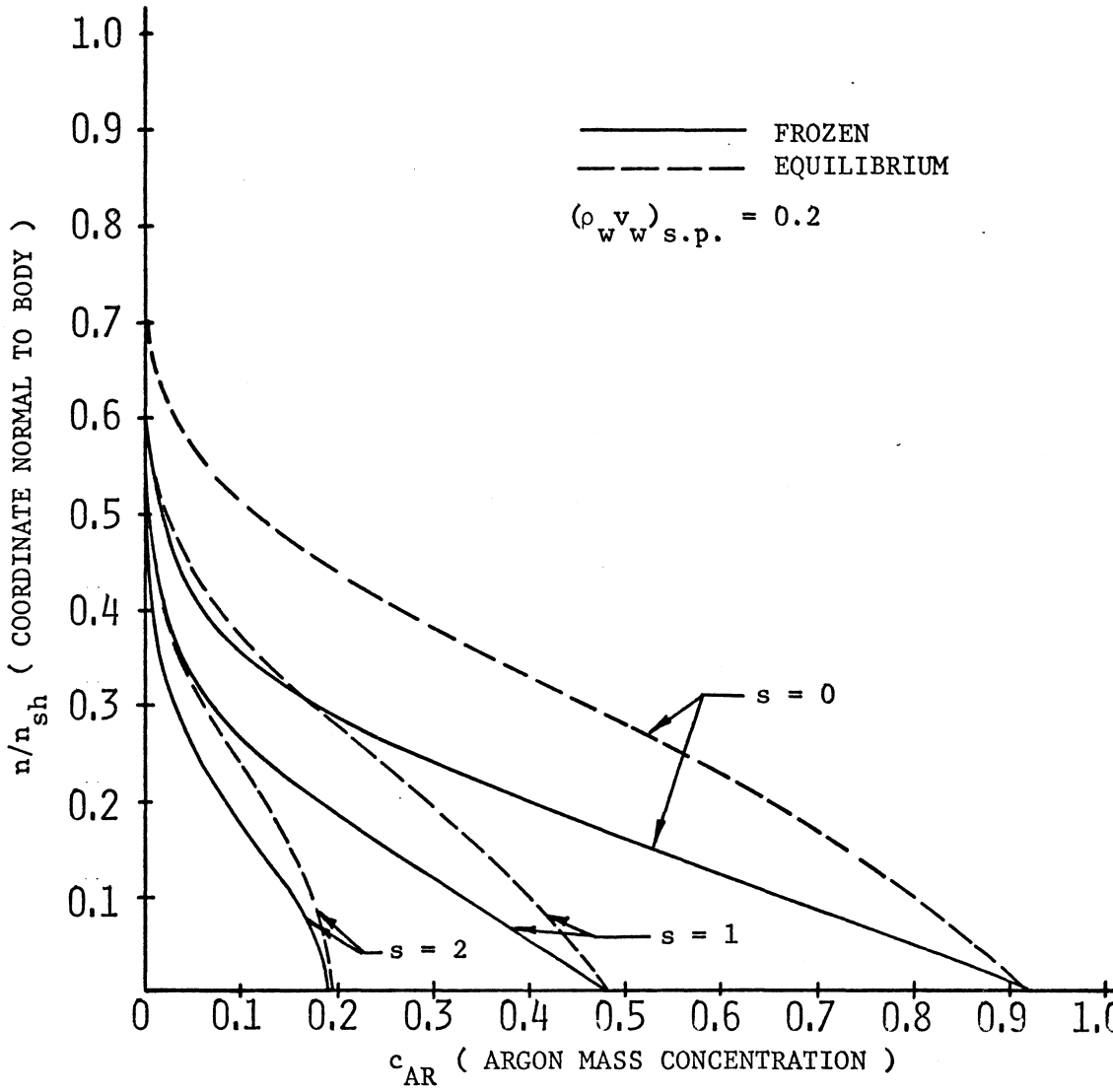

FIGURE 24 COMPARISON OF ARGON MASS CONCENTRATION FOR EQUILIBRIUM AND FROZEN AIR MODELS AT AN ALTITUDE OF 175,000 FT.

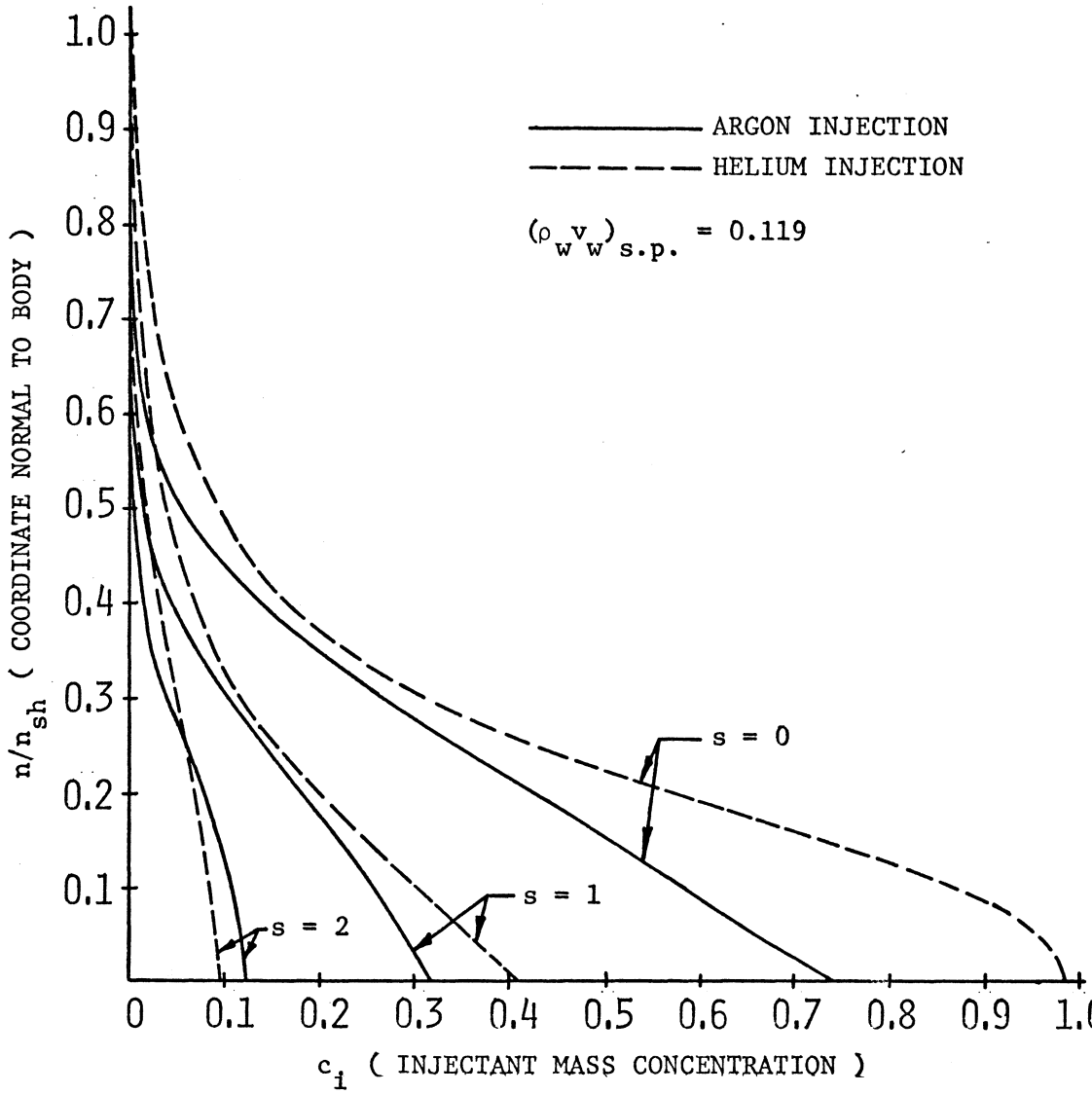

FIGURE 25 COMPARISON OF INJECTANT MASS CONCENTRATION FOR EQUILIBRIUM AIR MODEL AT AN ALTITUDE OF 175,000 FT.

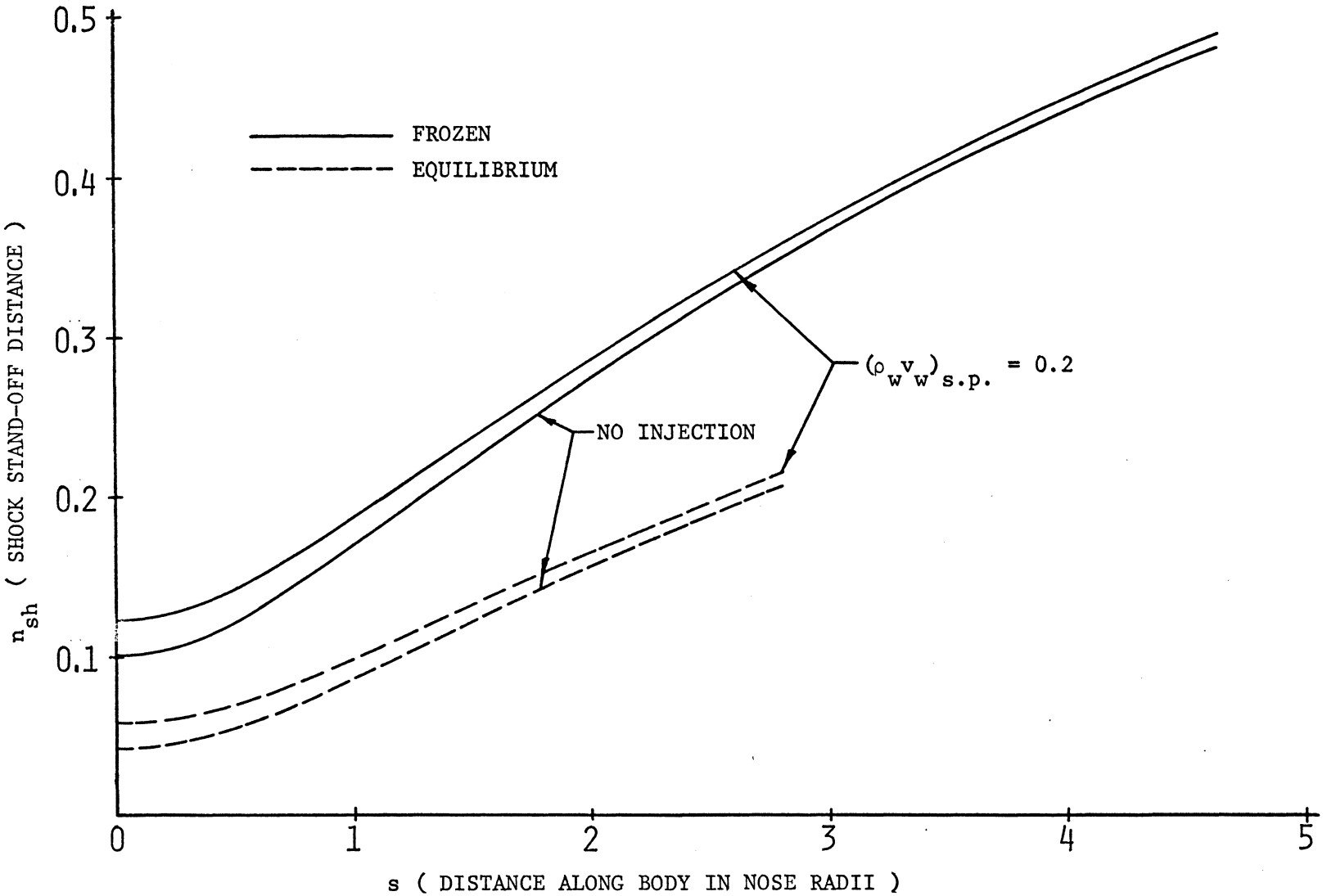

FIGURE 26 COMPARISON OF SHOCK STAND-OFF DISTANCE FOR EQUILIBRIUM AND FROZEN AIR MODELS WITH ARGON INJECTION AT AN ALTITUDE OF 175,000 FT.

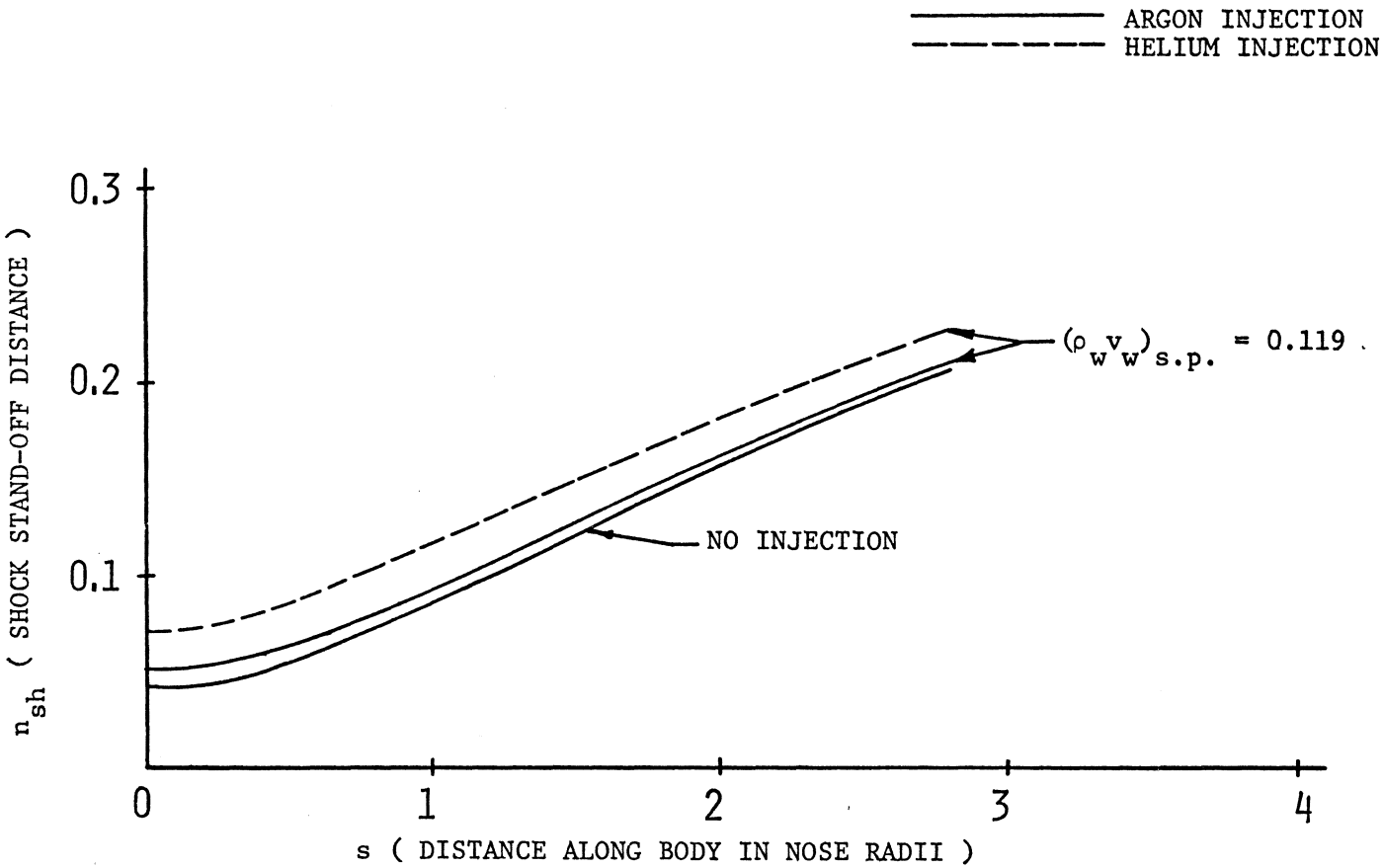

FIGURE 27 COMPARISON OF SHOCK STAND-OFF DISTANCE FOR DIFFERENT INJECTANTS FOR EQUILIBRIUM AIR MODEL AT AN ALTITUDE OF 175,000 FT.

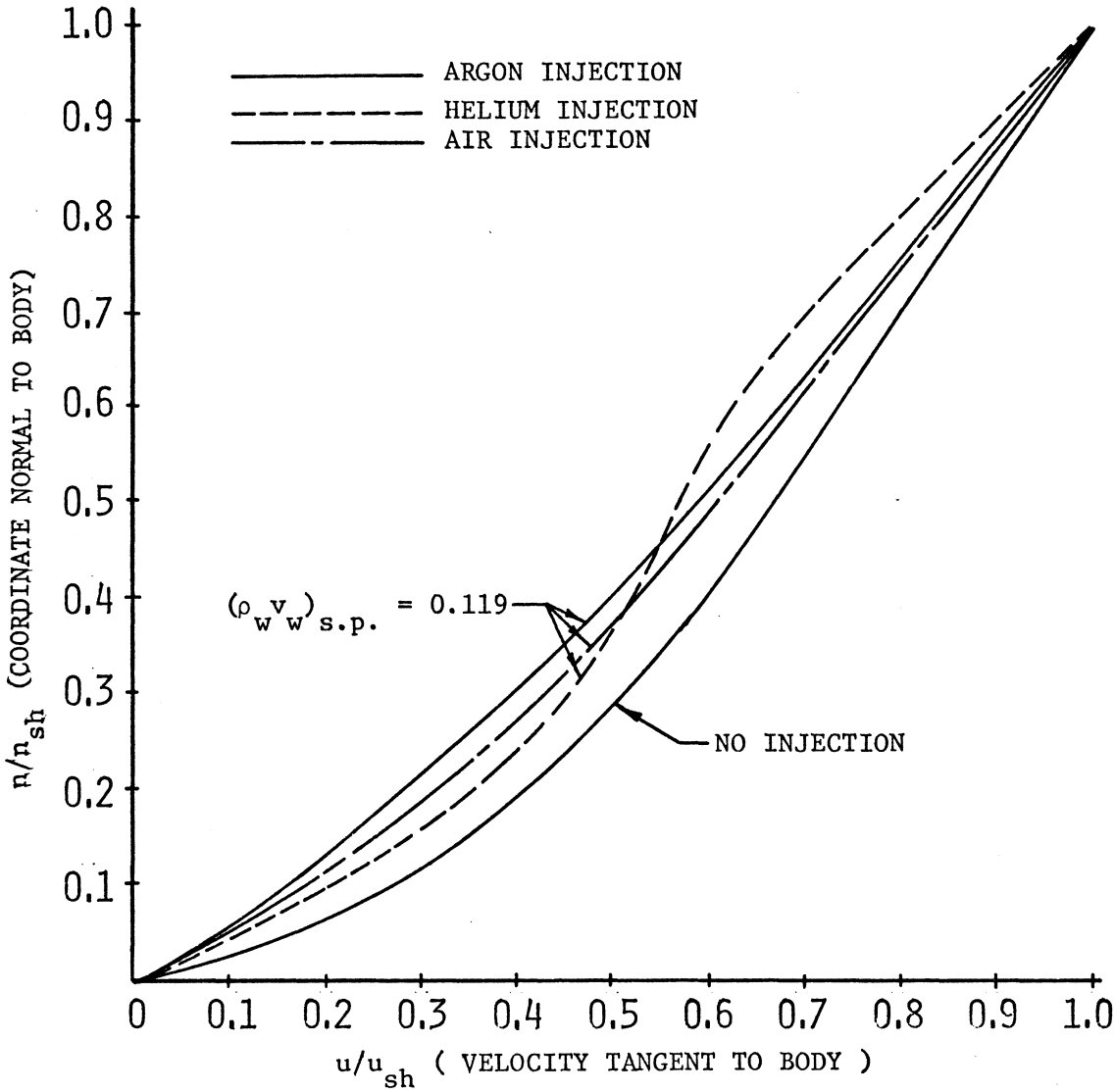

FIGURE 28 VELOCITY PROFILES AT STAGNATION POINT FOR DIFFERENT INJECTANTS FOR EQUILIBRIUM AIR AT AN ALTITUDE OF 175,000 FT.

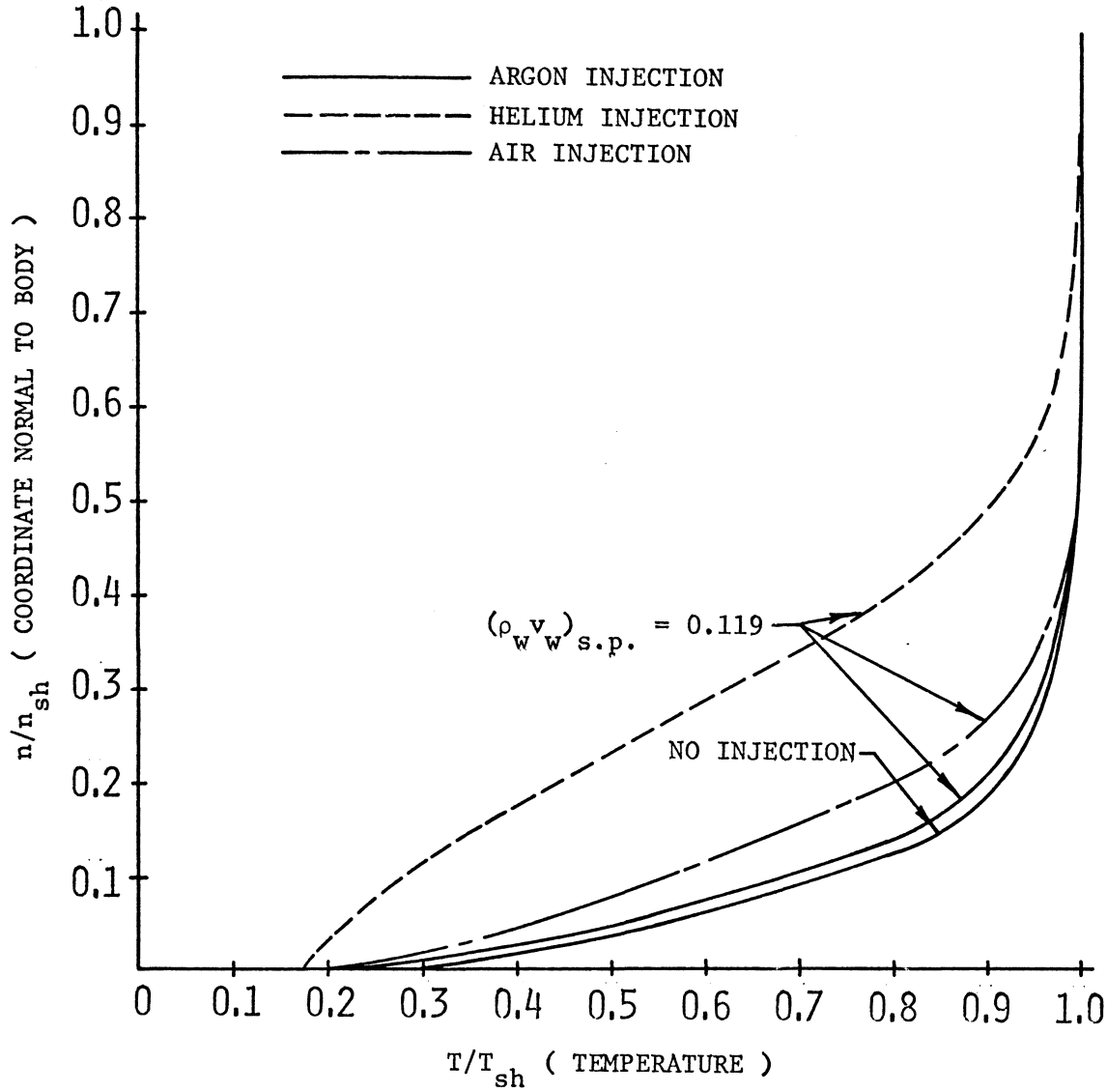

FIGURE 29 TEMPERATURE PROFILES AT STAGNATION POINT FOR DIFFERENT INJECTANTS FOR EQUILIBRIUM AIR MODEL AT AN ALTITUDE OF 175,000 FT.

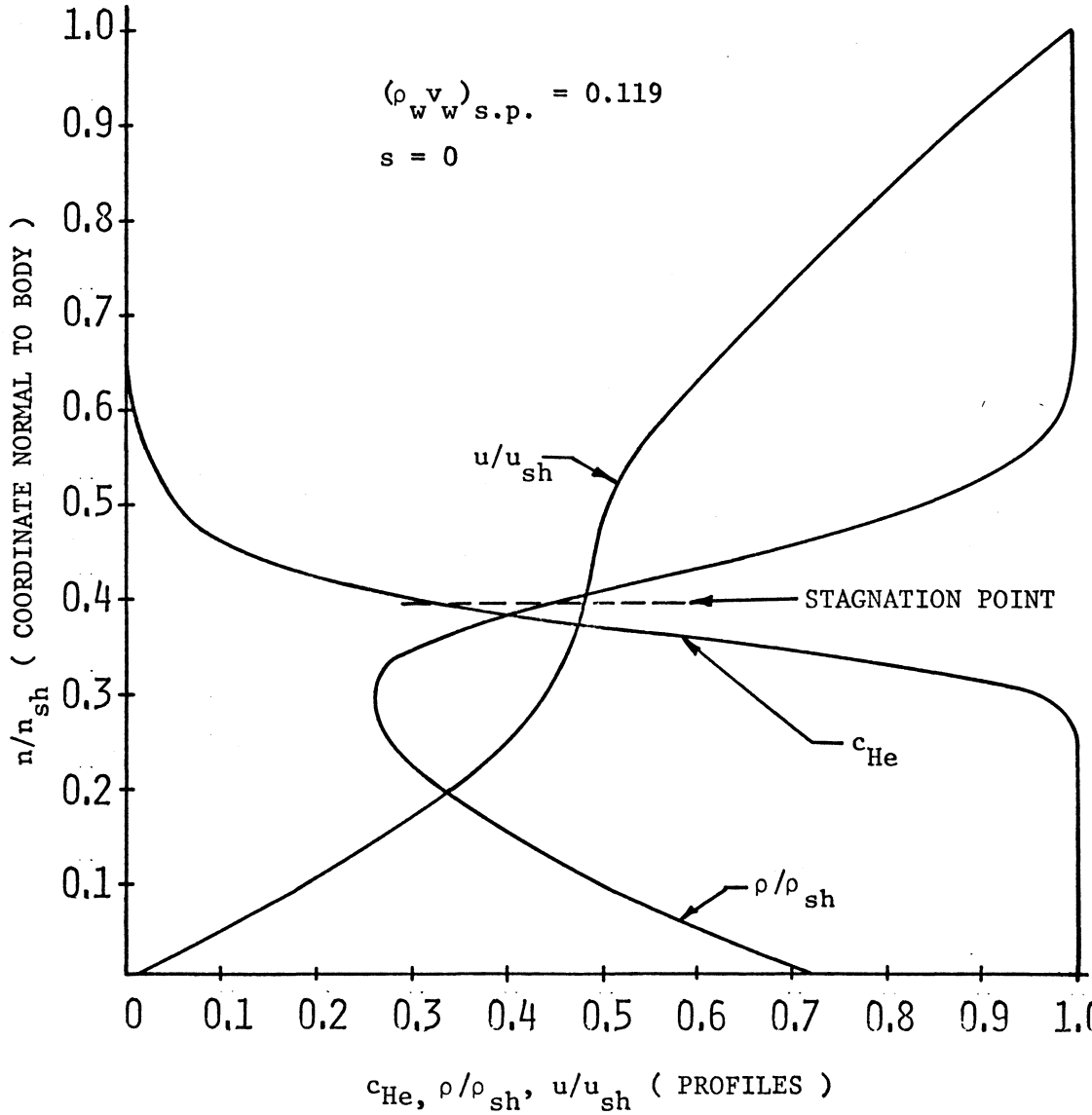

FIGURE 30 VARIOUS PROFILES FOR HELIUM INJECTION INTO EQUILIBRIUM AIR MODEL AT AN ALTITUDE OF 175,000 FT. WITH $D_{IA} = (D_{IA})_{He}/10$

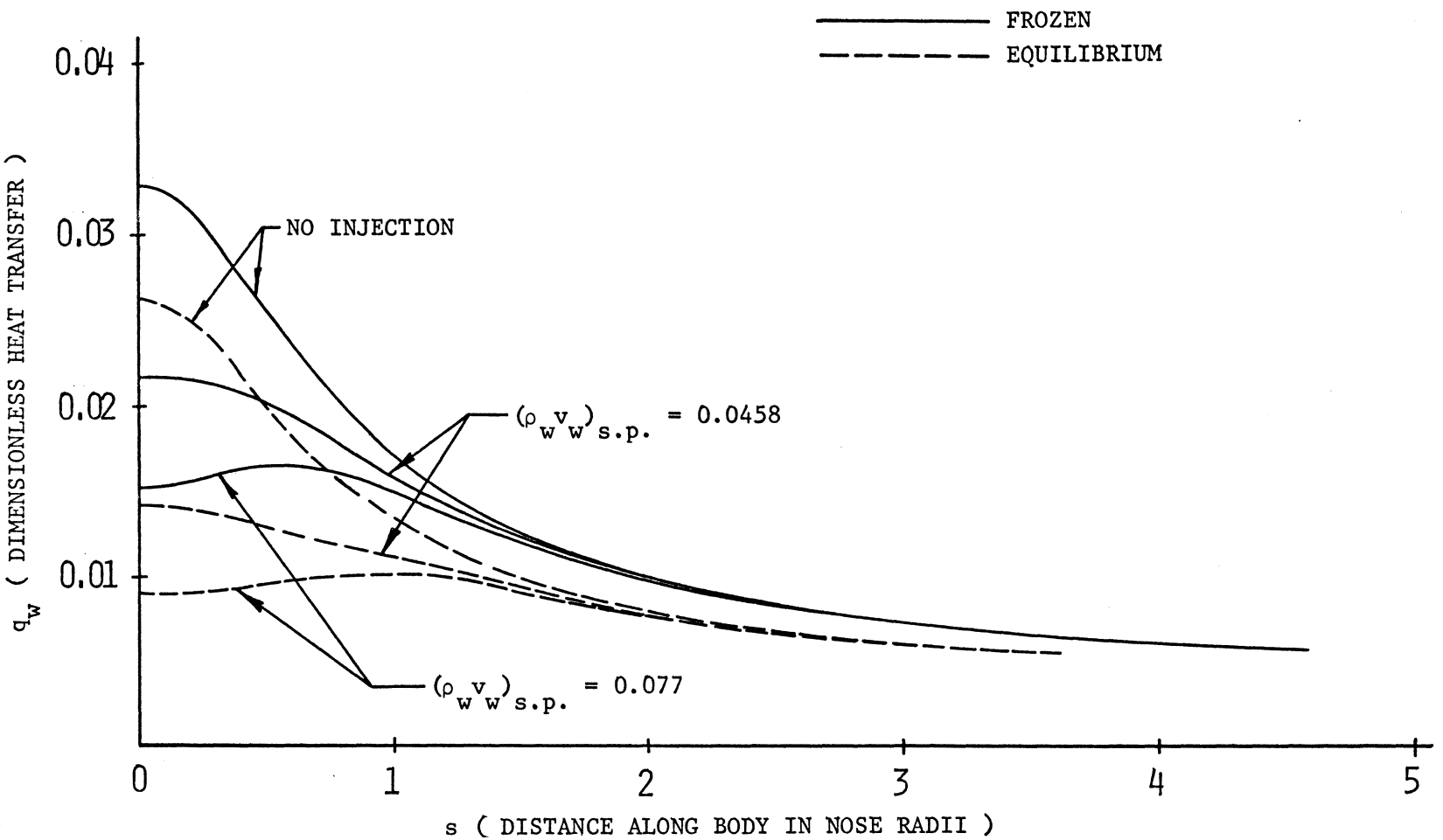

FIGURE 31 COMPARISON OF HEAT TRANSFER FOR EQUILIBRIUM AND FROZEN AIR MODELS WITH ARGON INJECTION AT AN ALTITUDE OF 150,000 FT.

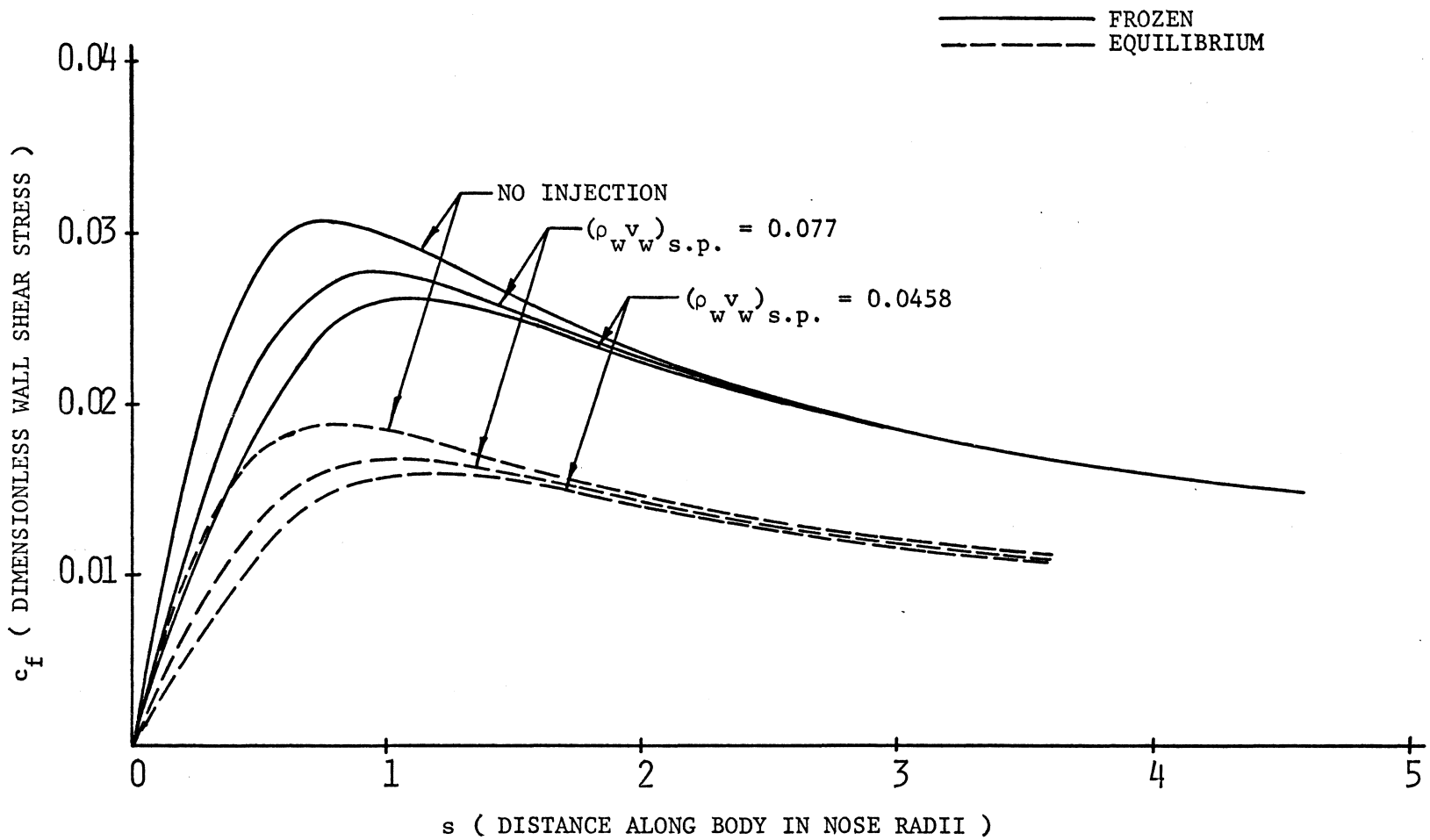

FIGURE 32 COMPARISON OF WALL SHEAR STRESS FOR EQUILIBRIUM AND FROZEN AIR MODELS WITH ARGON INJECTION AT AN ALTITUDE OF 150,000 FT.

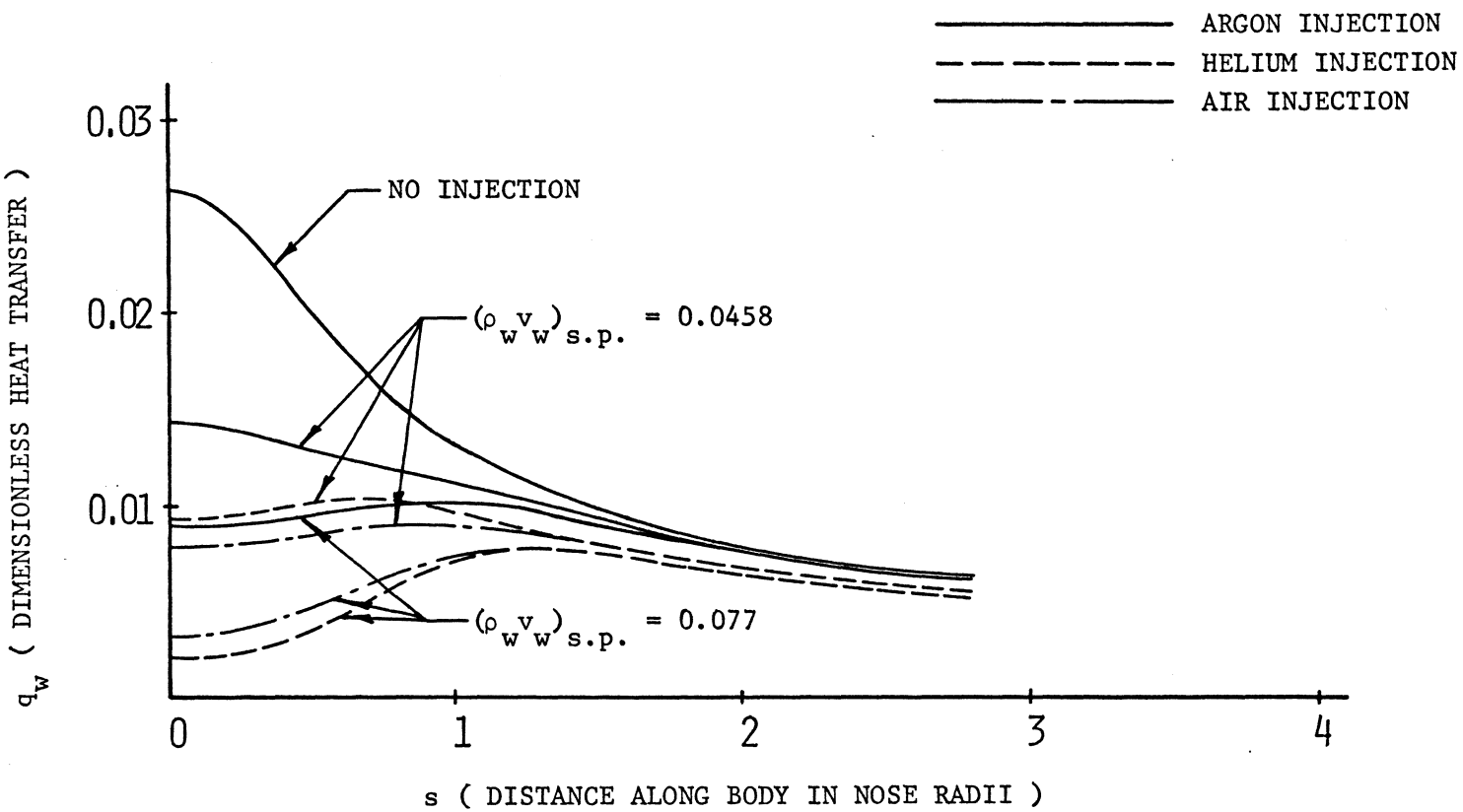

FIGURE 33 COMPARISON OF HEAT TRANSFER FOR DIFFERENT INJECTANTS FOR EQUILIBRIUM AIR MODEL AT AN ALTITUDE OF 150,000 FT.

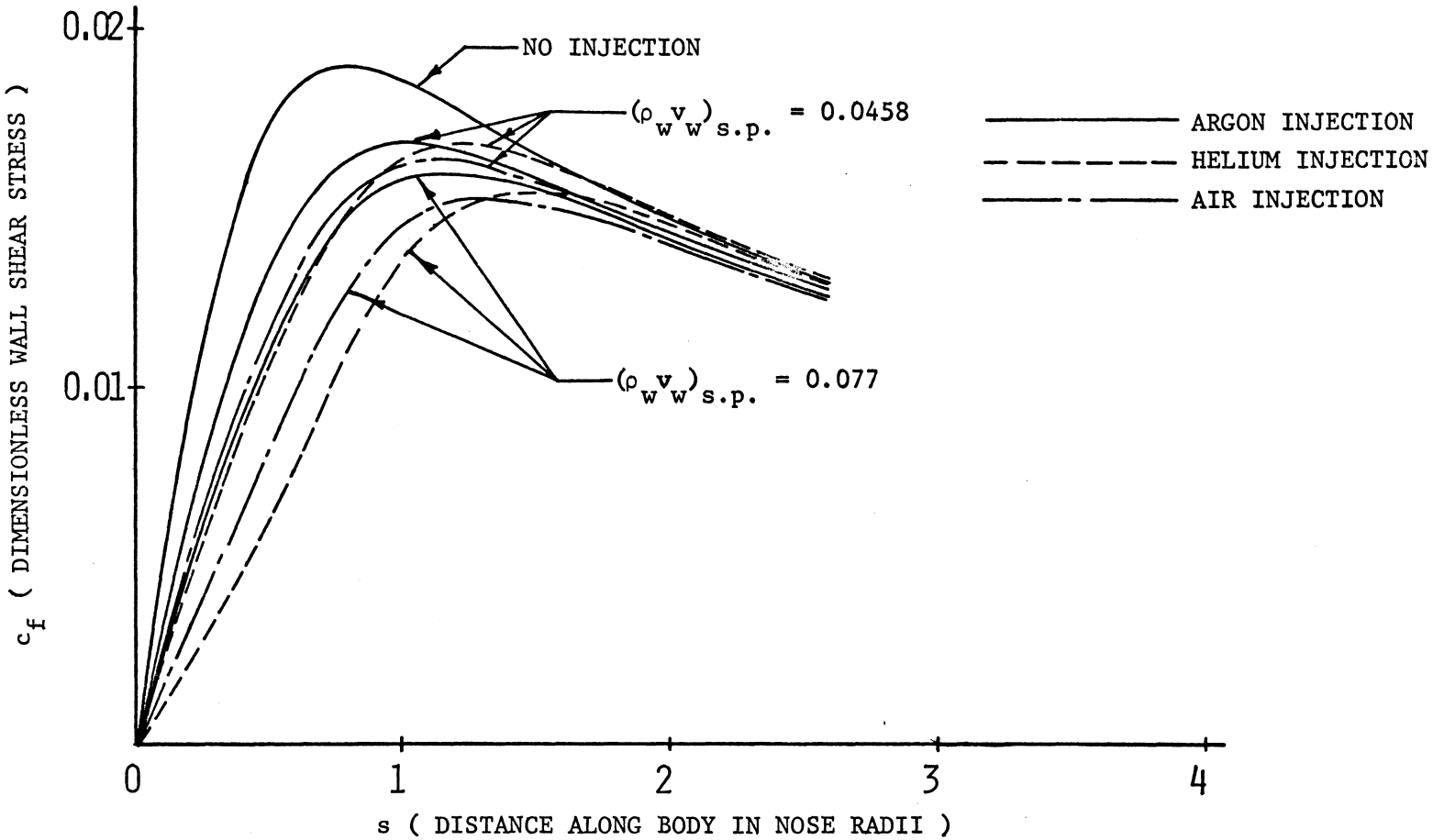

FIGURE 34 COMPARISON OF WALL SHEAR STRESS FOR DIFFERENT INJECTANTS FOR EQUILIBRIUM AIR MODEL AT AN ALTITUDE OF 150,000 FT.

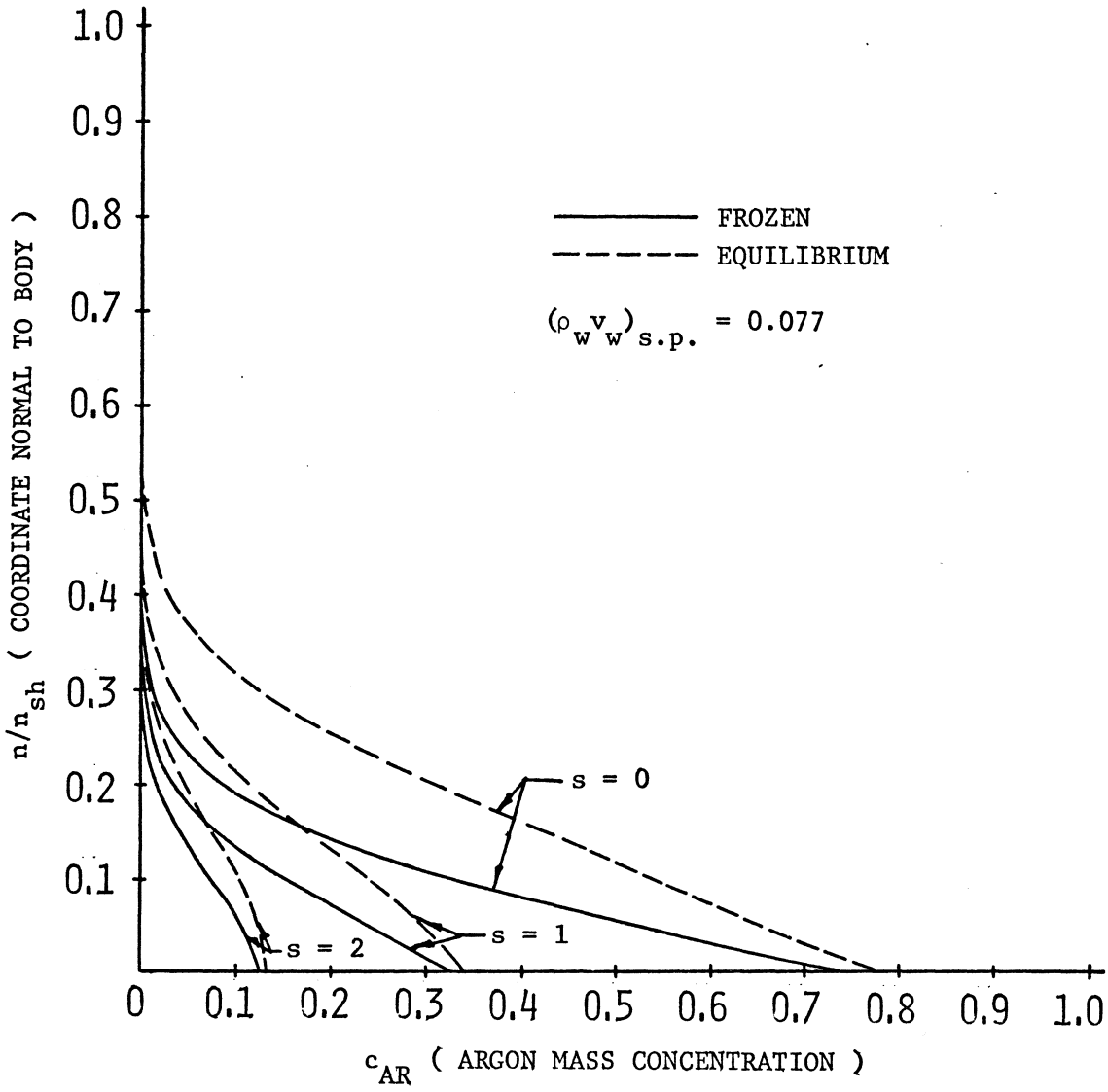

FIGURE 35 COMPARISON OF ARGON MASS CONCENTRATION FOR EQUILIBRIUM AND FROZEN AIR MODELS AT AN ALTITUDE OF 150,000 FT.

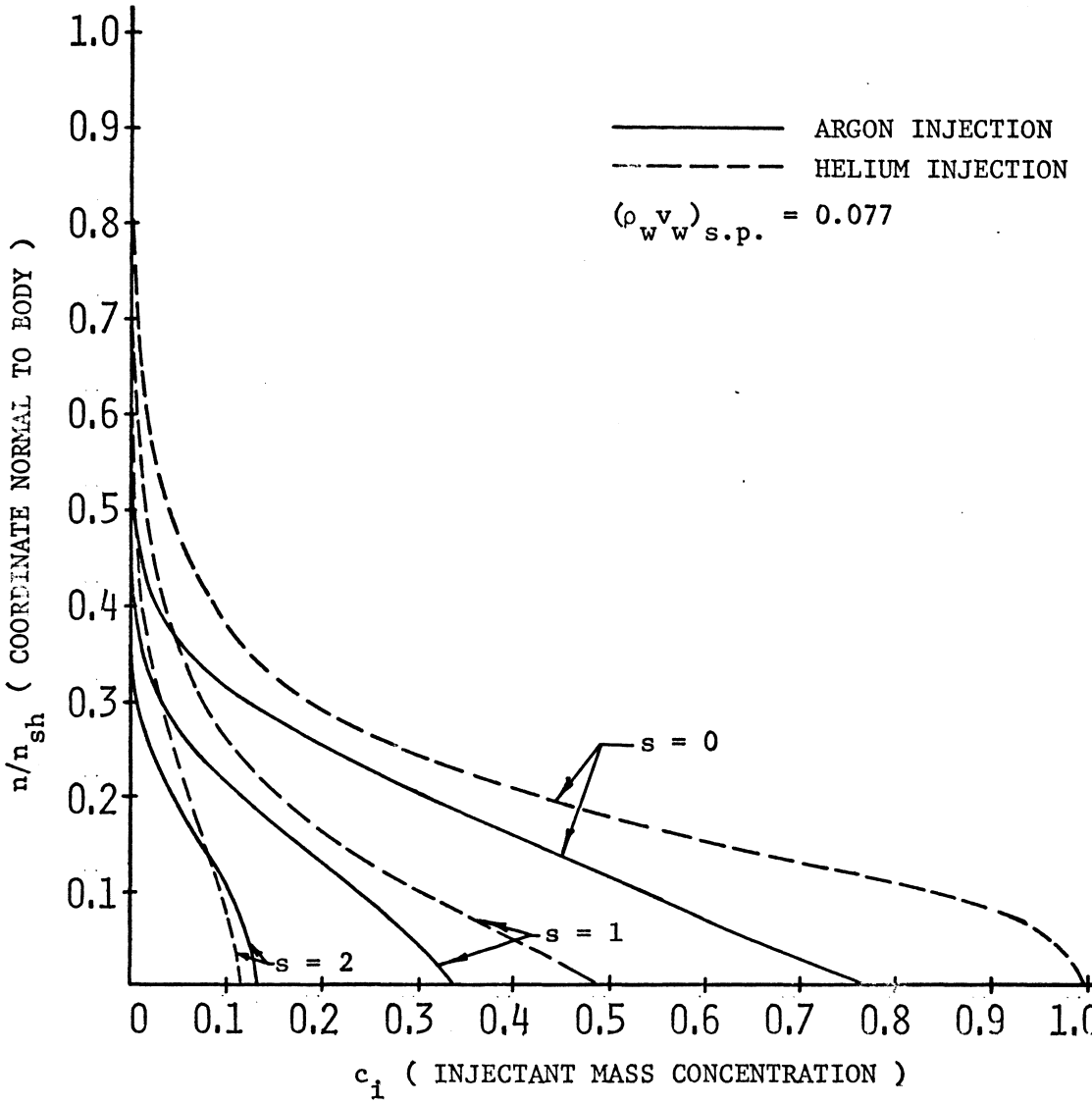

FIGURE 36 COMPARISON OF INJECTANT MASS CONCENTRATION FOR EQUILIBRIUM AIR MODEL AT AN ALTITUDE OF 150,000 FT.

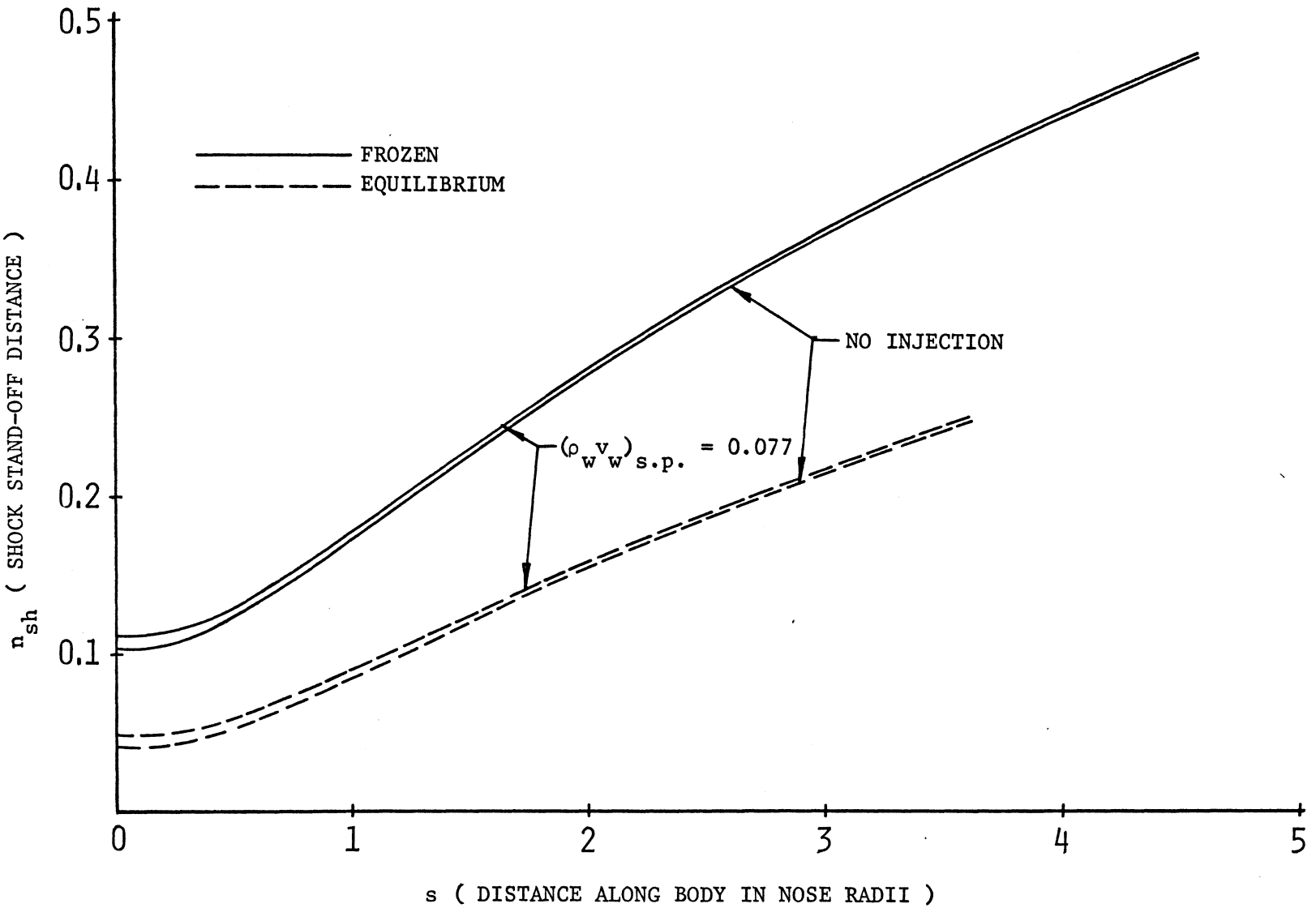

FIGURE 37 COMPARISON OF SHOCK STAND-OFF DISTANCE FOR EQUILIBRIUM AND FROZEN AIR MODELS WITH ARGON INJECTION AT AN ALTITUDE OF 150,000 FT.

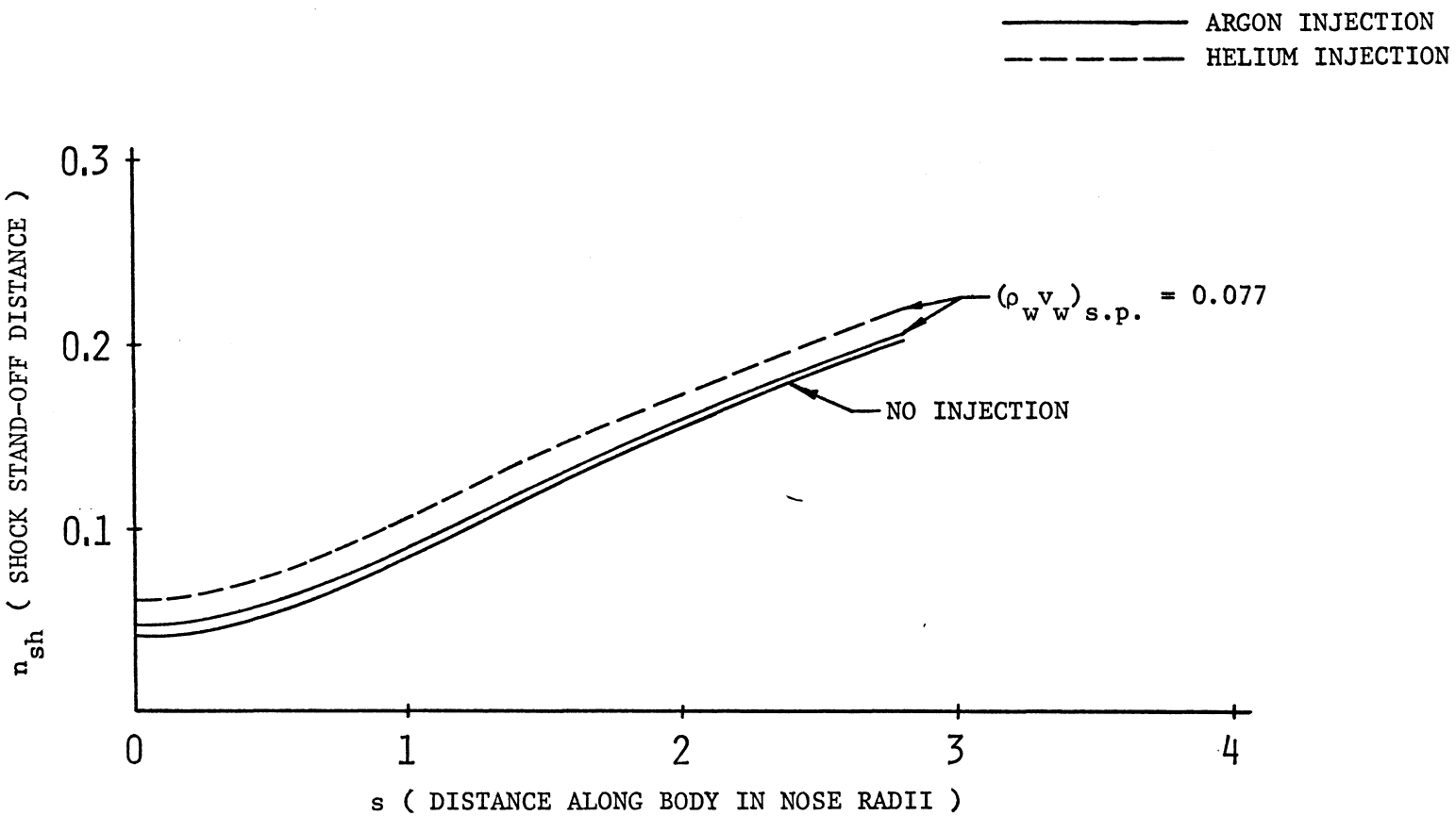

FIGURE 38 COMPARISON OF SHOCK STAND-OFF DISTANCE FOR DIFFERENT INJECTANTS FOR EQUILIBRIUM AIR MODEL AT AN ALTITUDE OF 150,000 FT.

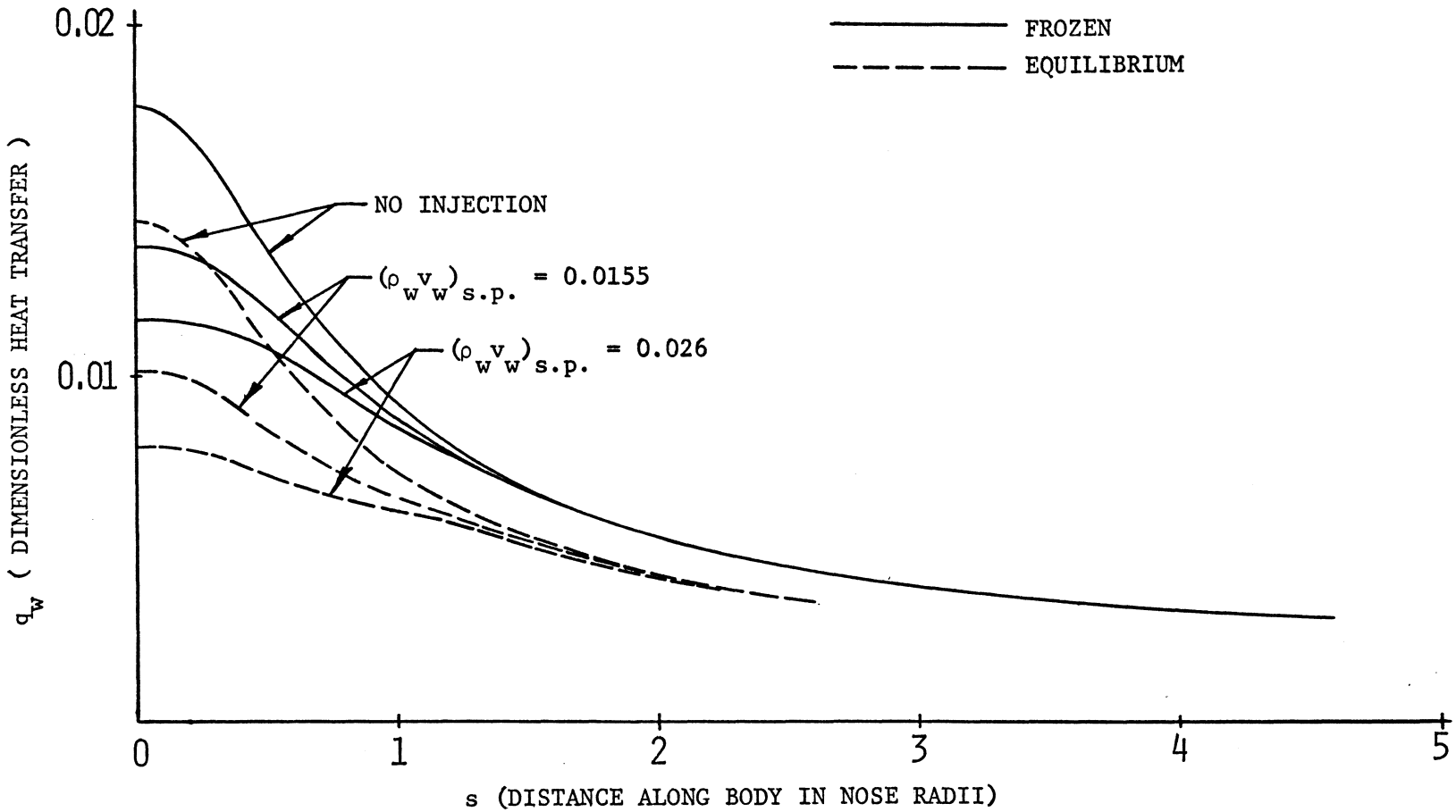

FIGURE 39 COMPARISON OF HEAT TRANSFER FOR EQUILIBRIUM AND FROZEN AIR MODELS WITH ARGON INJECTION AT AN ALTITUDE OF 125,000 FT.

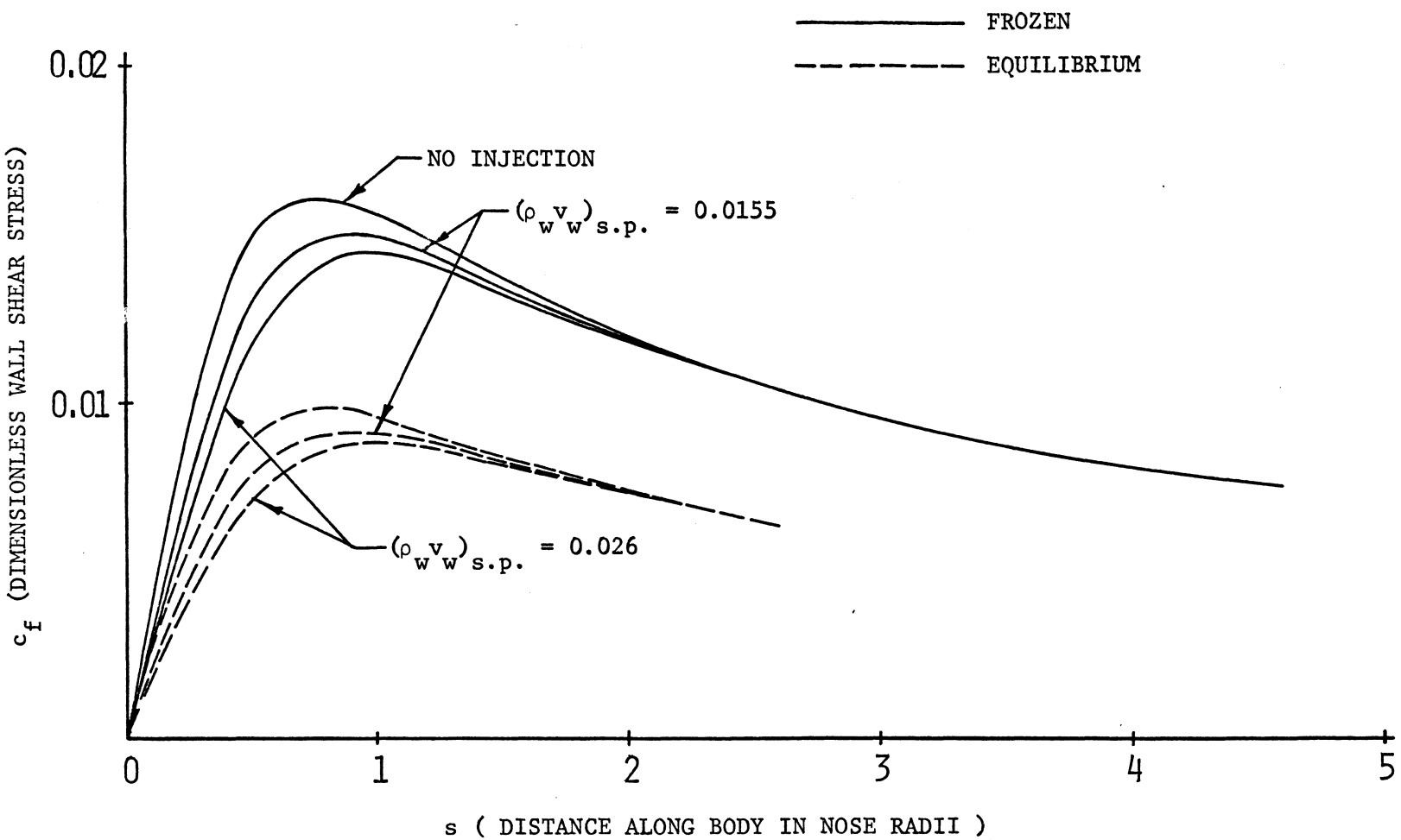

FIGURE 40 COMPARISON OF WALL SHEAR STRESS FOR EQUILIBRIUM AND FROZEN AIR MODELS WITH ARGON INJECTION AT AN ALTITUDE OF 125,000 FT.

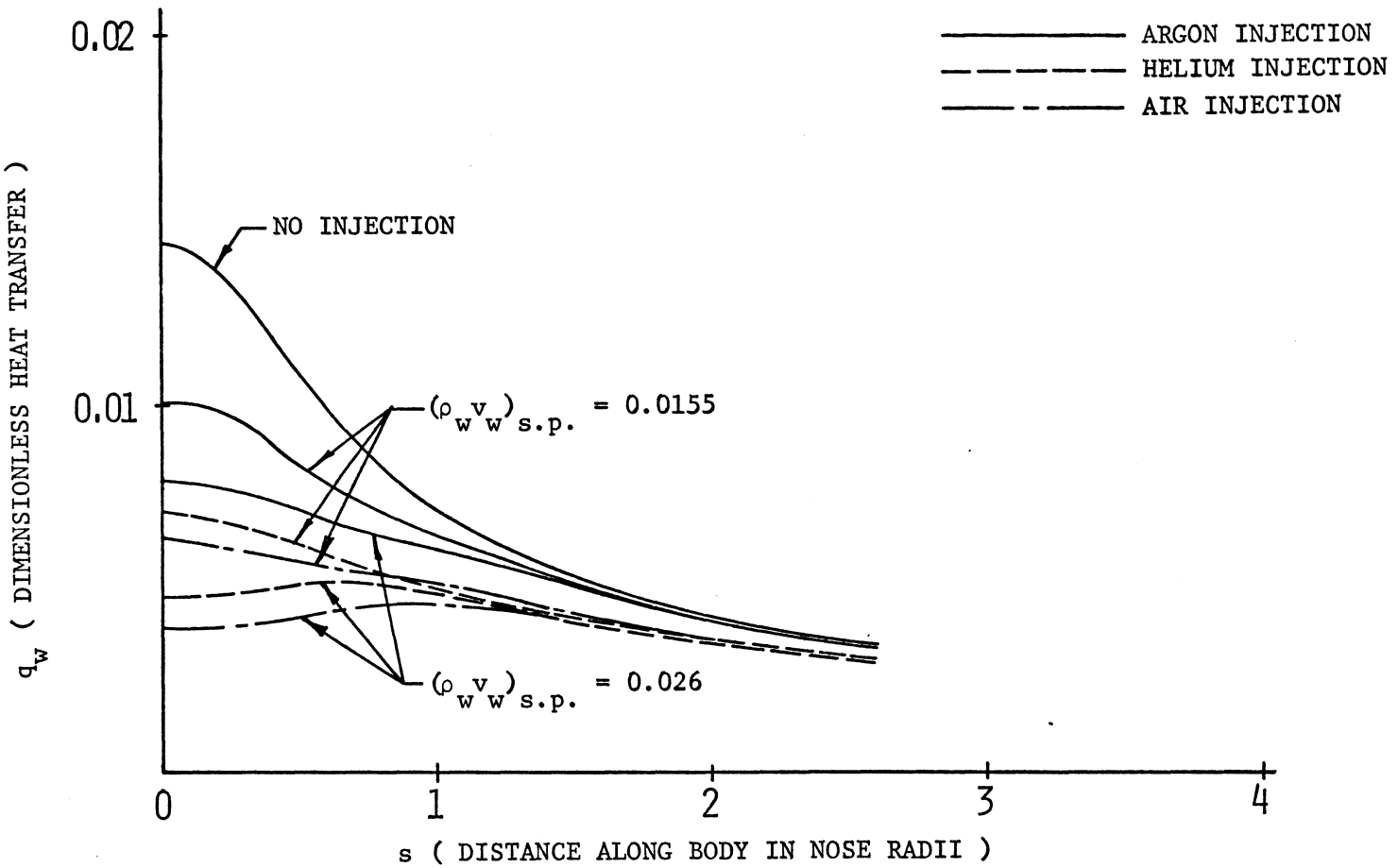

FIGURE 41 COMPARISON OF HEAT TRANSFER FOR DIFFERENT INJECTANTS FOR EQUILIBRIUM AIR MODEL AT AN ALTITUDE OF 125,000 FT.

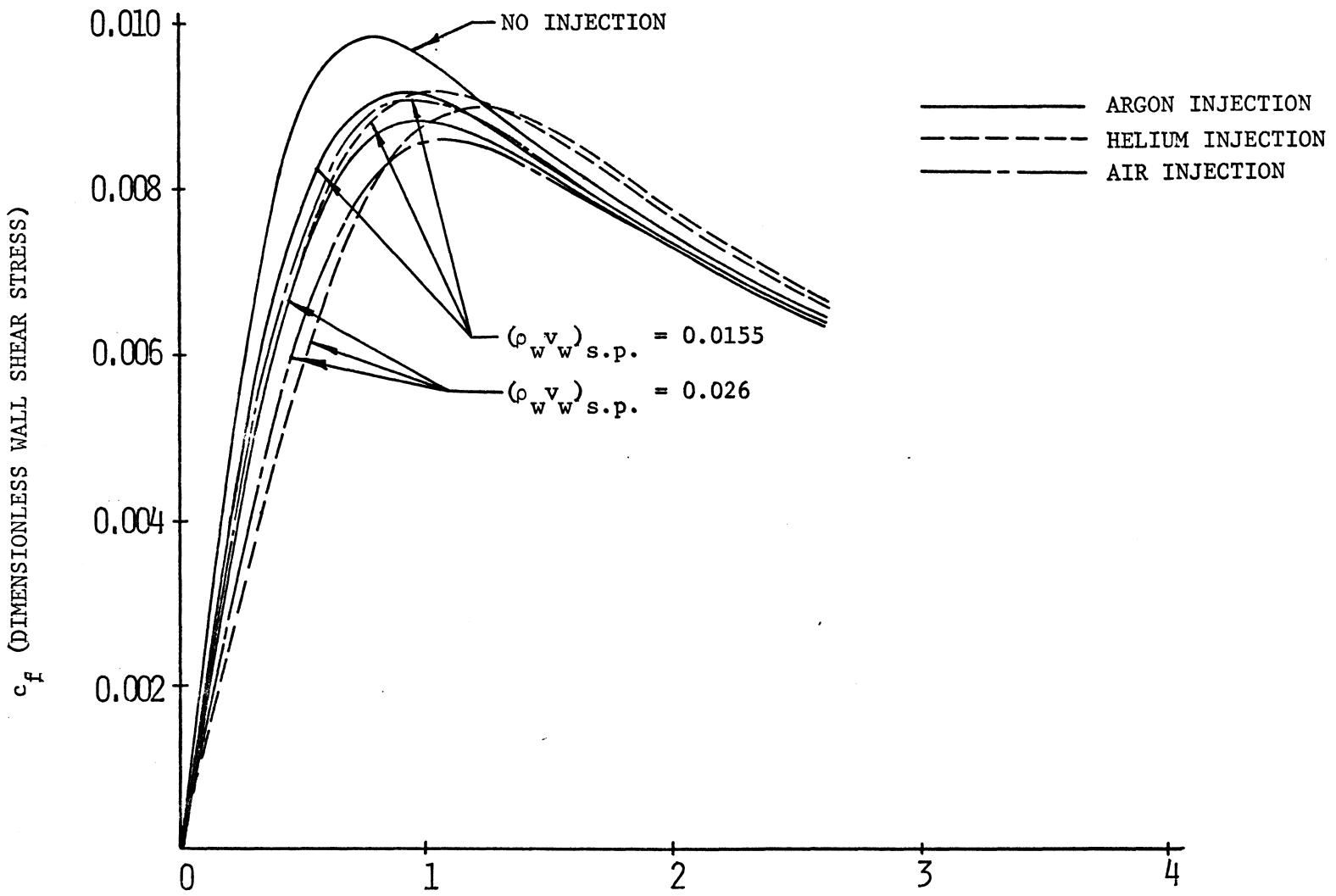

FIGURE 42 COMPARISON OF WALL SHEAR STRESS FOR DIFFERENT INJECTANTS FOR EQUILIBRIUM AIR MODEL AT AN ALTITUDE OF 125,000 FT.

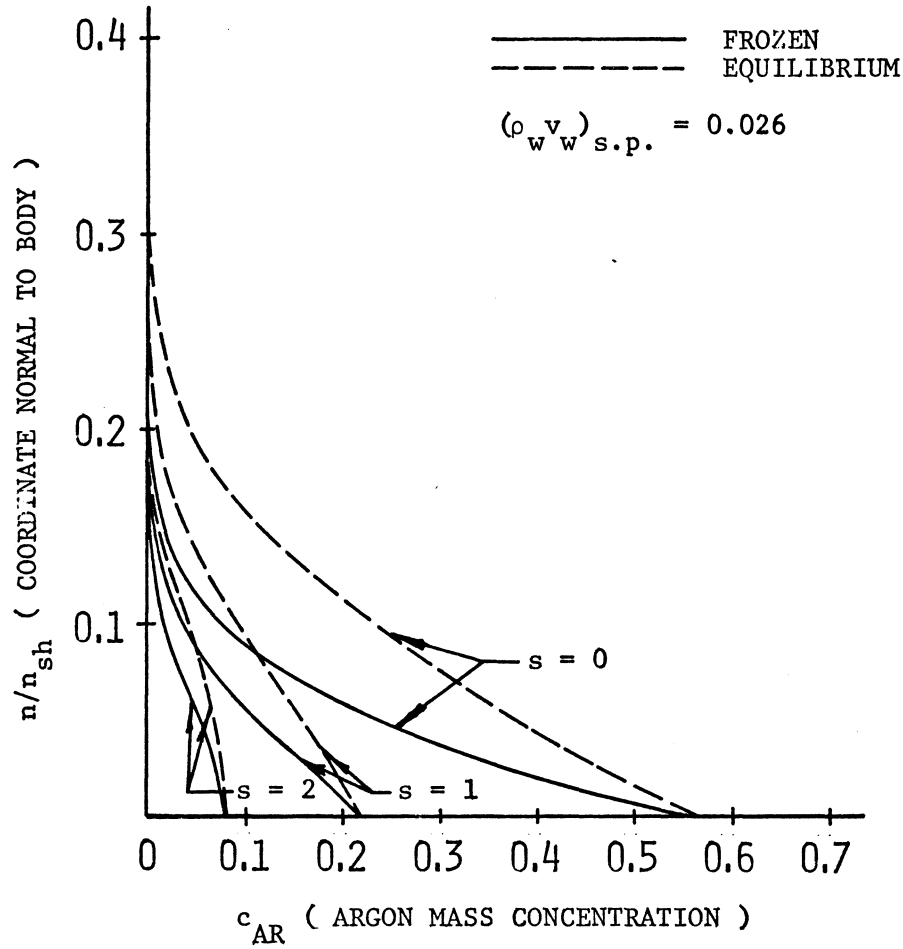

FIGURE 43 COMPARISON OF ARGON MASS CONCENTRATION FOR EQUILIBRIUM AND FROZEN AIR MODELS AT AN ALTITUDE OF 125,000 FT.

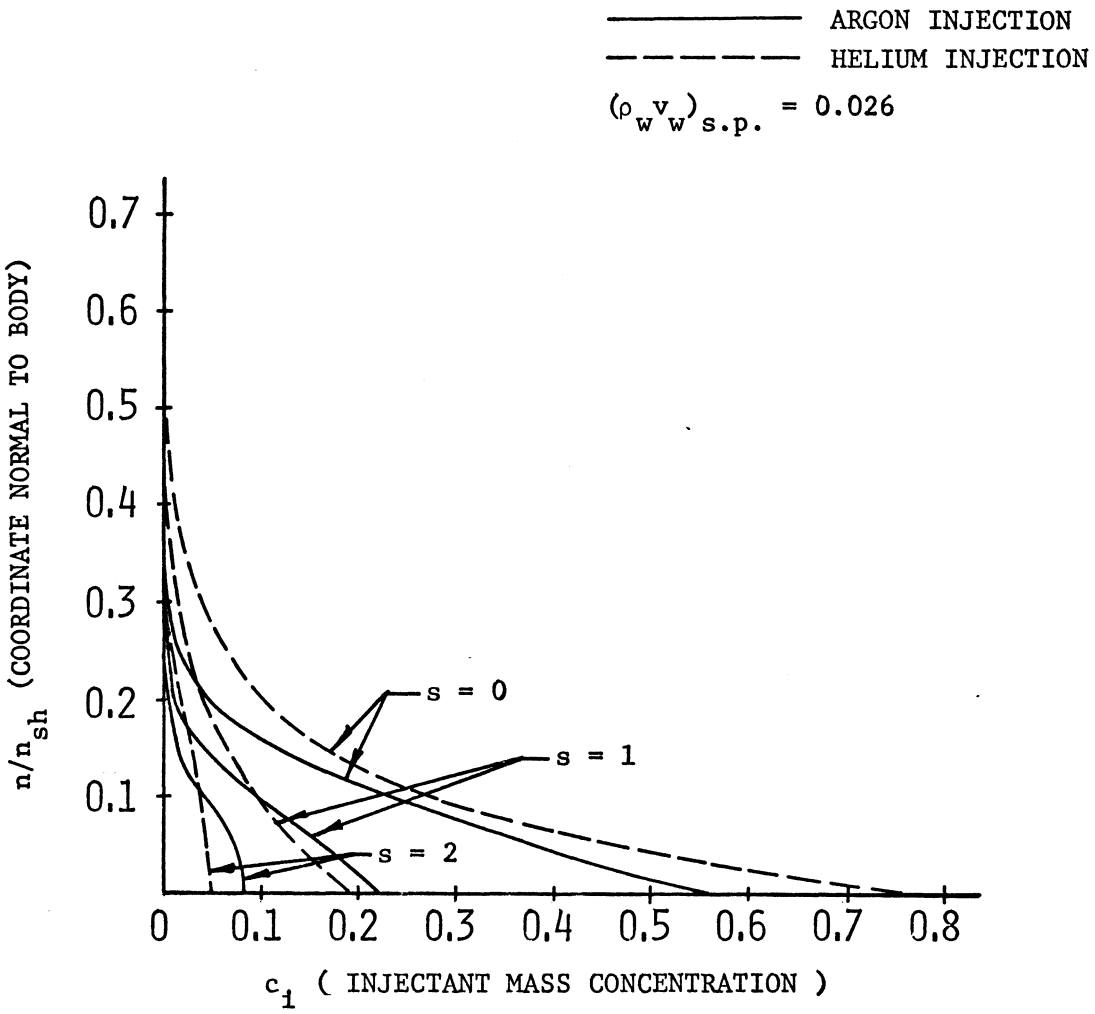

FIGURE 44 COMPARISON OF INJECTANT MASS CONCENTRATION FOR EQUILIBRIUM AIR MODEL AT AN ALTITUDE OF 125,000 FT.

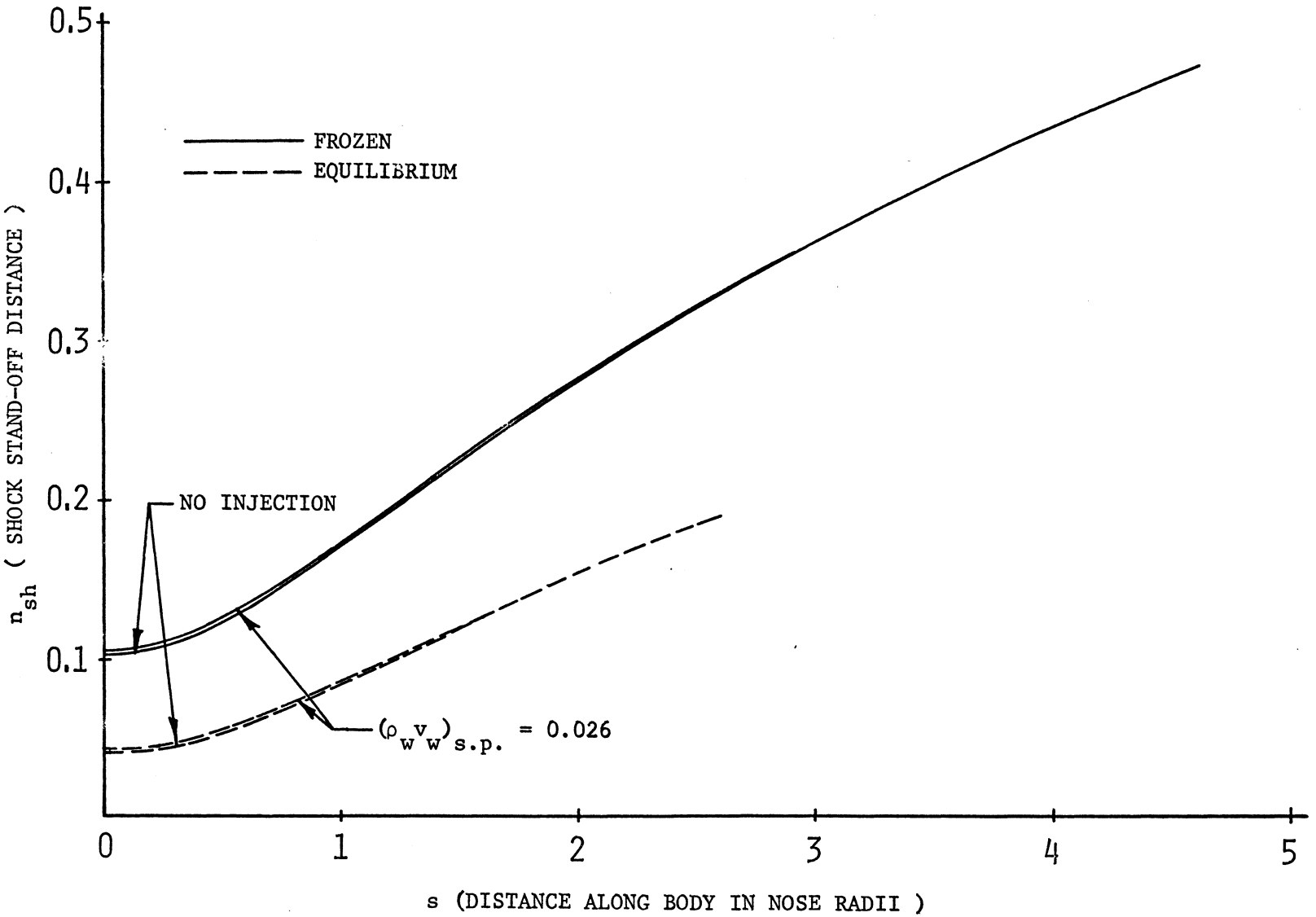

FIGURE 45 COMPARISON OF SHOCK STAND-OFF DISTANCE FOR EQUILIBRIUM AND FROZEN AIR MODELS WITH ARGON INJECTION AT AN ALTITUDE OF 125,000 FT.

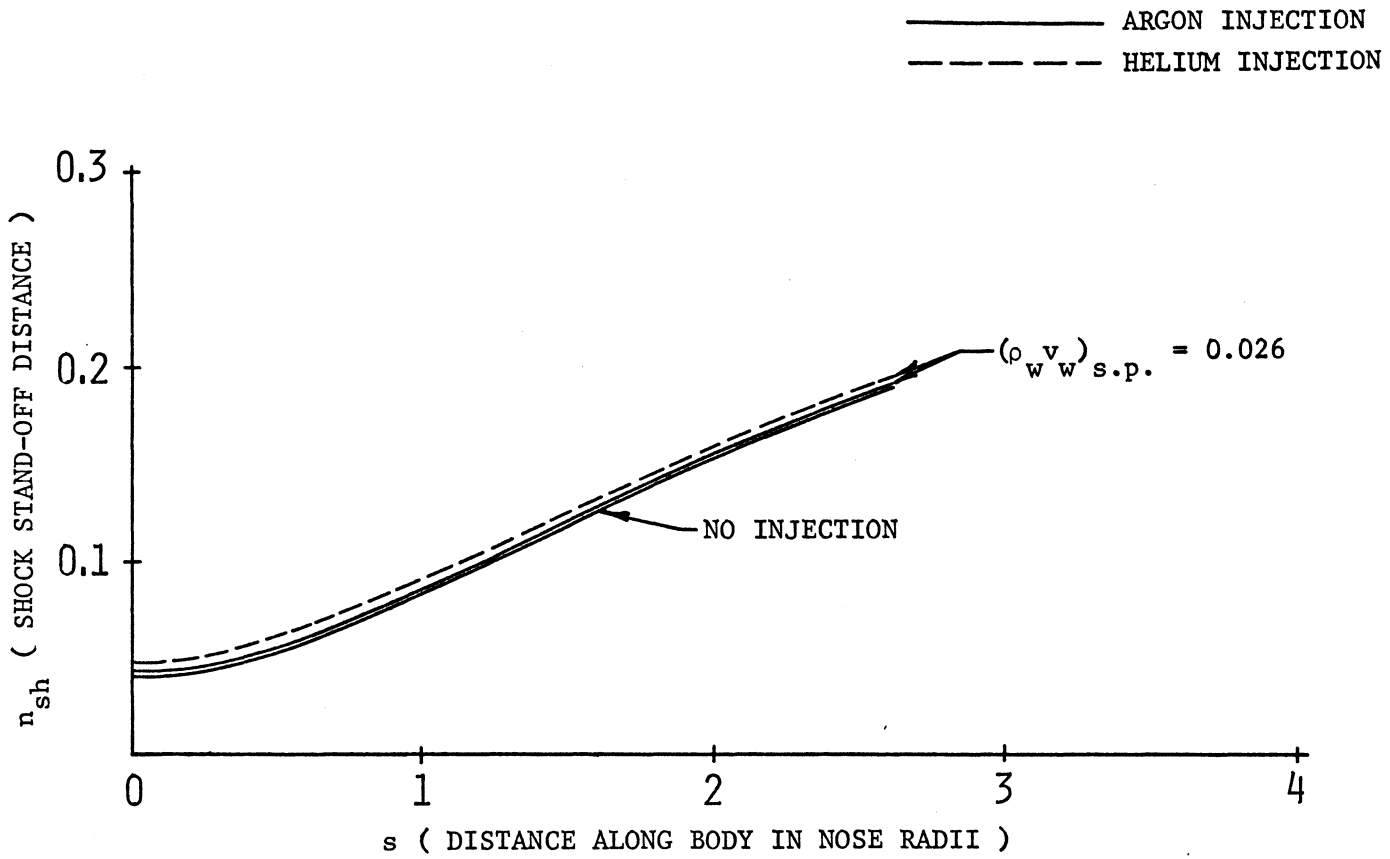

FIGURE 46 COMPARISON OF SHOCK STAND-OFF DISTANCE FOR DIFFERENT INJECTANTS FOR EQUILIBRIUM AIR MODEL AT AN ALTITUDE OF 125,000 FT.

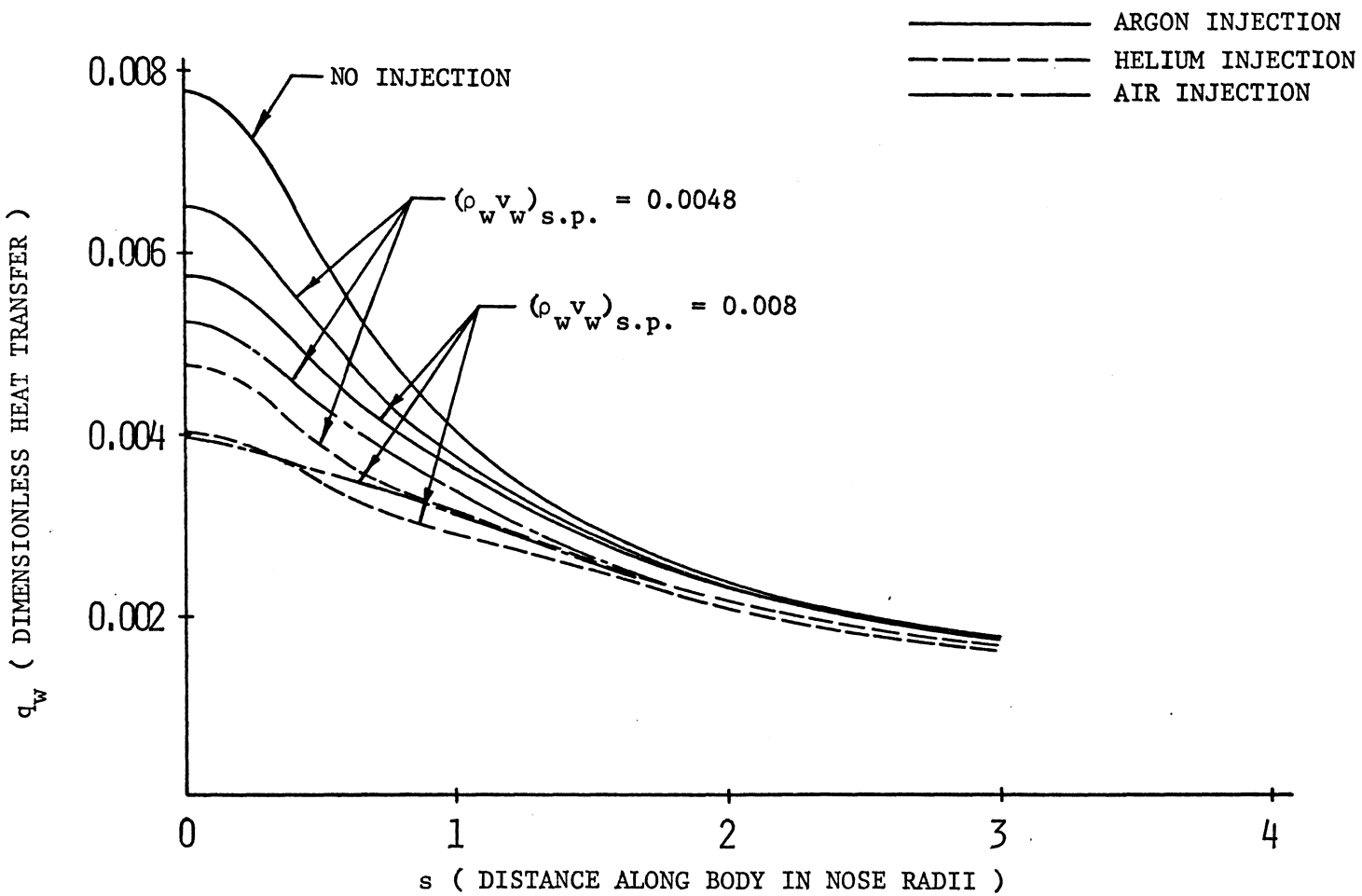

FIGURE 47 COMPARISON OF HEAT TRANSFER FOR DIFFERENT INJECTANTS FOR EQUILIBRIUM AIR MODEL AT AN ALTITUDE OF 100,000 FT.

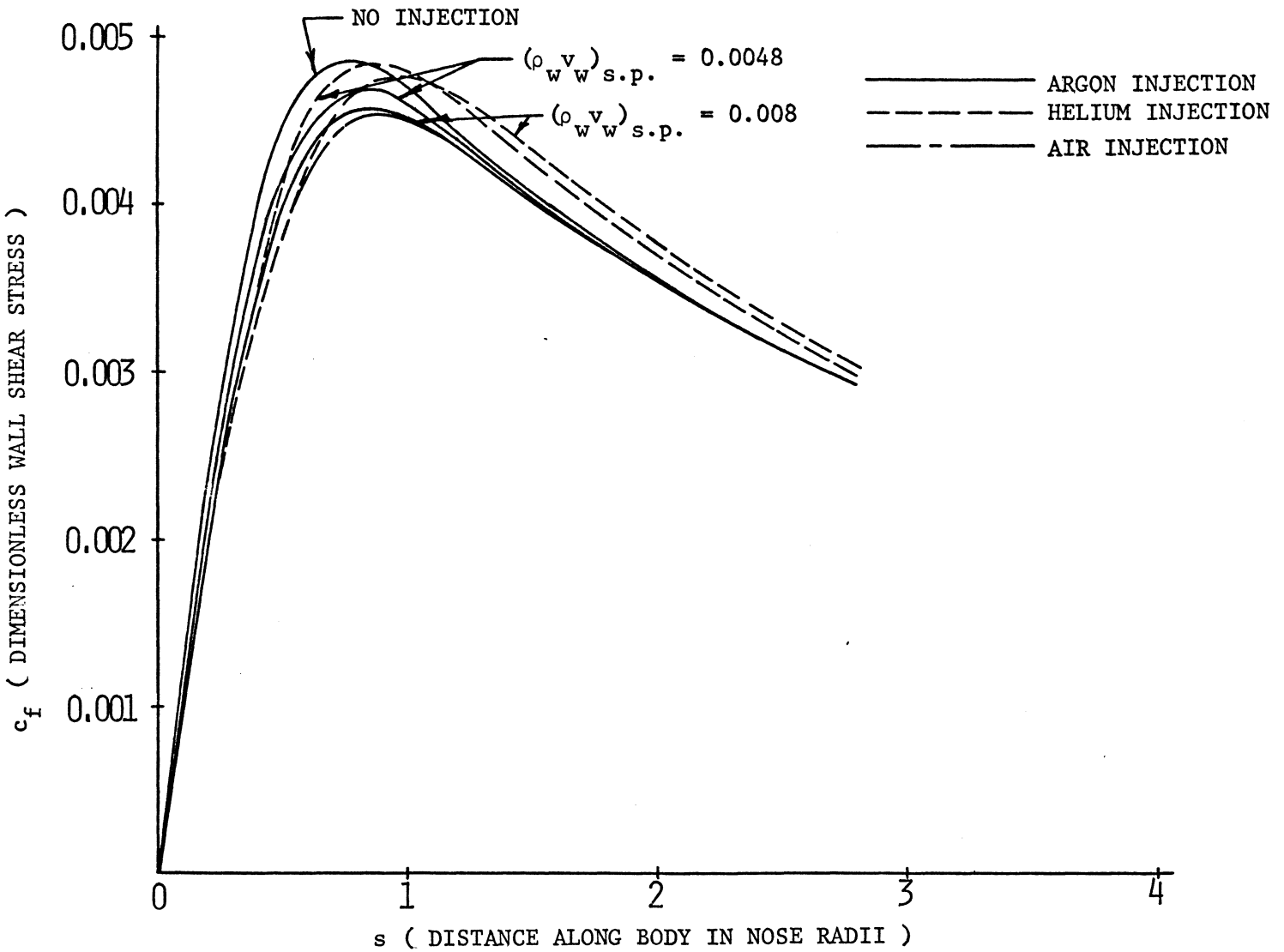

FIGURE 48 COMPARISON OF WALL SHEAR STRESS FOR DIFFERENT INJECTANTS FOR EQUILIBRIUM AIR MODEL AT AN ALTITUDE OF 100,000 FT.

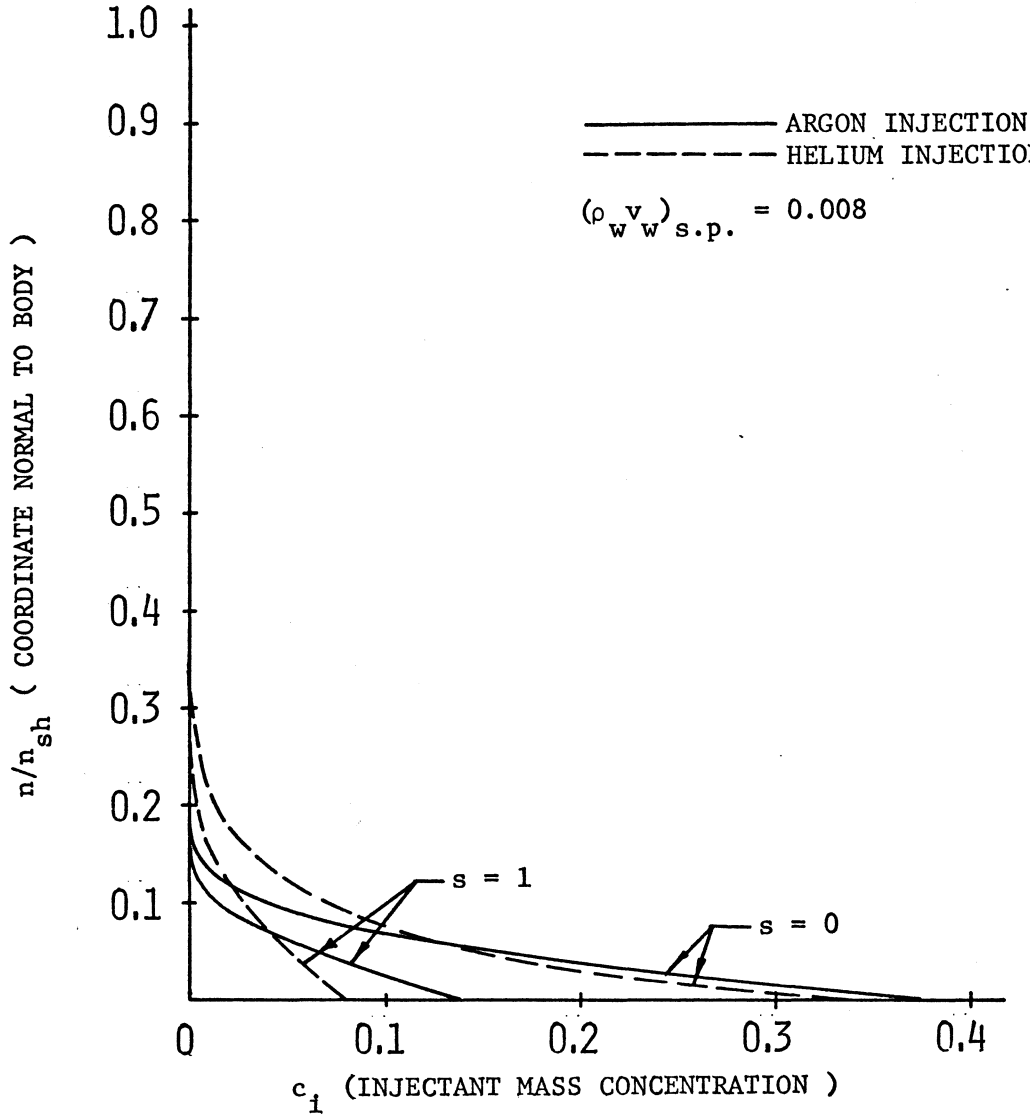

FIGURE 49 COMPARISON OF INJECTANT MASS CONCENTRATION FOR EQUILIBRIUM AIR MODEL AT AN ALTITUDE OF 100,000 FT.

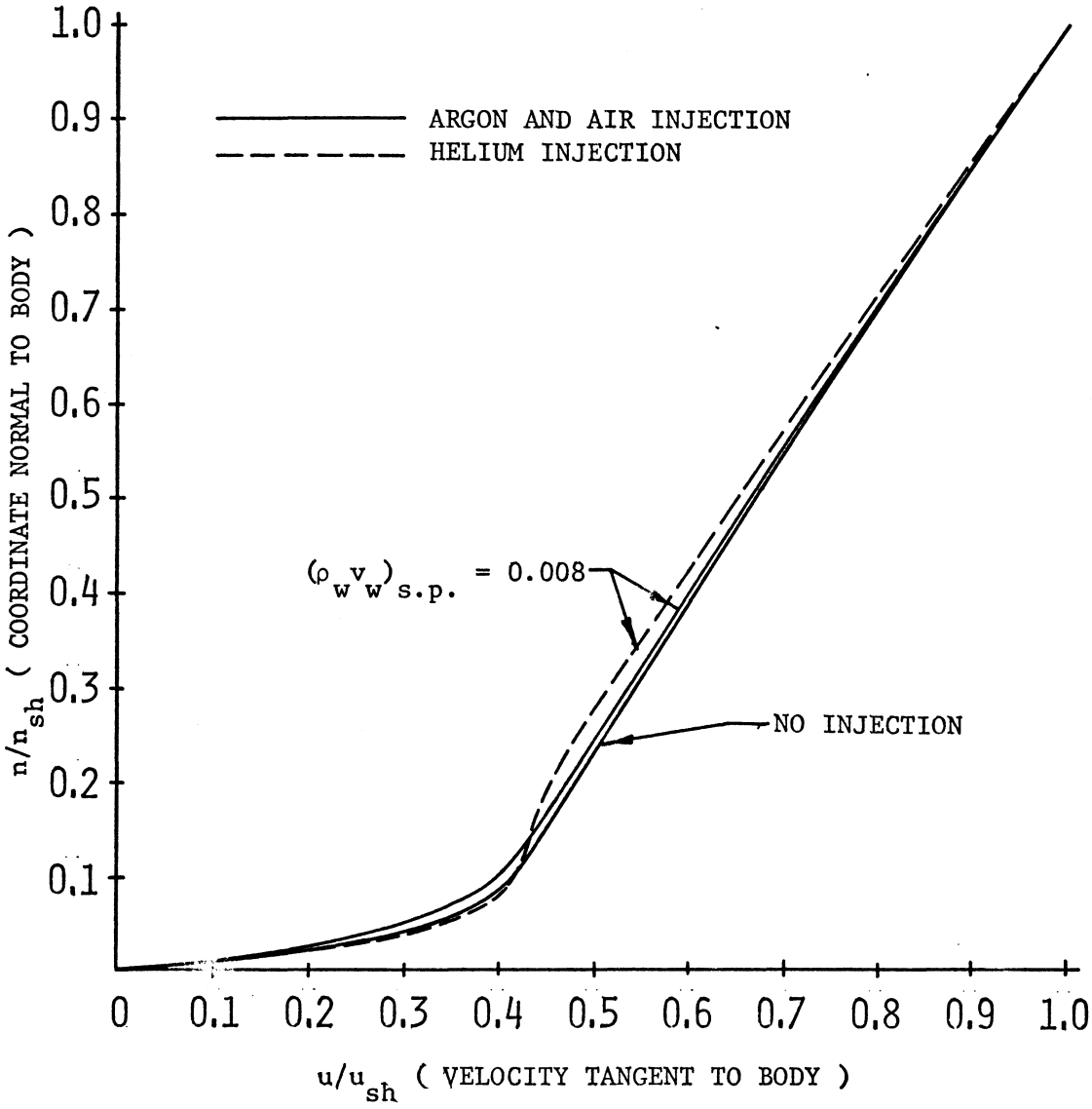

FIGURE 50 VELOCITY PROFILES AT STAGNATION POINT FOR DIFFERENT INJECTANTS FOR EQUILIBRIUM AIR AT AN ALTITUDE OF 100,000 FT.

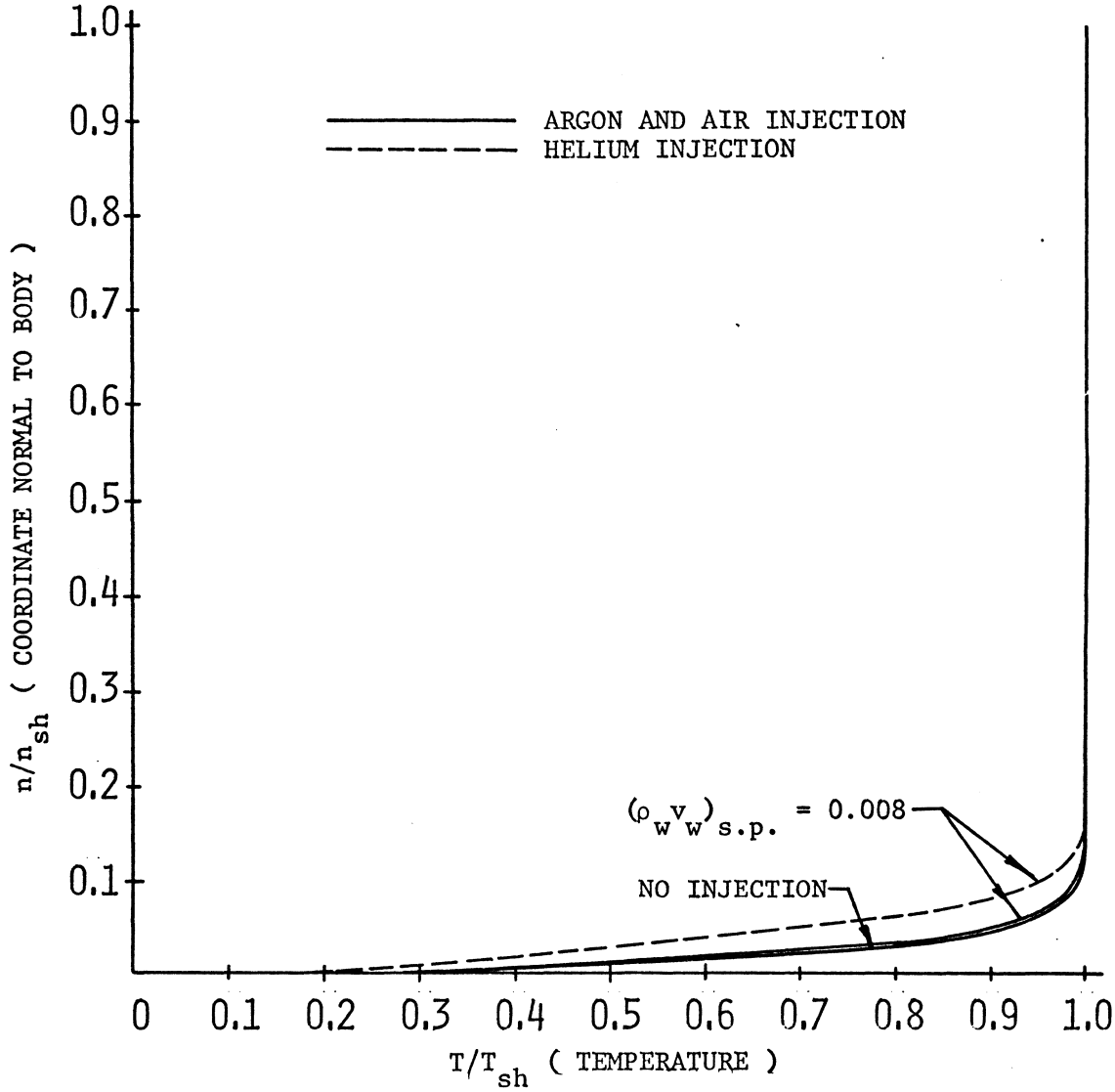

FIGURE 51 TEMPERATURE PROFILES AT STAGNATION POINT FOR DIFFERENT INJECTANTS FOR EQUILIBRIUM AIR MODEL AT AN ALTITUDE OF 100,000 FT.

Attention Patron:

The one-page vita has been removed

from the scanned document

Numerical Solutions to the Viscous Shock-Layer Blunt-Body Problem With Inert Gas Injection

Robert Earl Whitehead

ABSTRACT

A set of laminar hypersonic viscous shock-layer equations are obtained for a non-reacting binary mixture. The equations are valid to second-order in the inverse square root of a Reynolds number for the entire shock layer. A set of slip-flow boundary conditions which include mass transfer at the body surface is derived in a form applicable as boundary conditions for the governing equations. A set of modified Rankine-Hugoniot shock conditions are used as boundary conditions at the shock.

The governing equations are solved using an implicit finite-difference scheme applicable to parabolic differential equations. The governing equations in their full form are parabolic-hyperbolic in nature and approximations are made to put them in total parabolic form allowing solutions to be obtained by marching step-by-step downstream from the stagnation streamline. The approximations are eliminated by iterations and solutions to the complete equations are found.

Flow conditions applicable to re-entry problems are chosen for example solutions. Solutions are found for a hyperboloid asymptotic to a cone of total interior angle of 45°. A free stream velocity of 20,000 fps. is used in every case. Solutions are found for free stream conditions found at altitudes from 300,000 ft. to 100,000 ft.

For the free stream species, two air models are chosen. In one case it is assumed that the reaction rates for the air components in the shock layer are so slow that they are neglected and the air is assumed to be a mixture of oxygen and nitrogen molecules. In the other case, the air is assumed to be in equilibrium at the temperature and pressure at each point in the shock layer and equilibrium air properties are used. Solutions are found with the injection of argon, helium, and air across the body surface. A mass injection distribution that decays exponentially from the stagnation point is used. A variety of total mass injection rates are used.

Comparisons are made of the heat transfer, wall shear stress, and shock stand-off distances for the two air models with different injectants and injection rates. Results show that at altitudes above 250,000 ft. injection is ineffective in reducing heat transfer and wall shear stress. At lower altitudes, relatively small injection rates can cause sizable reductions in heat transfer and wall shear stress. Helium is the most effective of the injectants studied. At sufficiently high injection rates for the distribution used, the stagnation point heat transfer is reduced to an extent that the maximum heat transfer occurs downstream of the stagnation point. In cases where the shock shape and shock stand-off distance are appreciably changed by the injection, the heat transfer and wall shear stress do not recover their no injection values downstream as the injection rate goes to zero back on the body but remains below the no injection values.